

Inaugural dissertation
for
obtaining the doctoral degree
of the
Combined Faculty of Mathematics, Engineering and Natural Sciences
of the
Ruprecht - Karls - University
Heidelberg

Presented by
M.Sc. Zina Maria Uckeley
born in: Marl, Germany
Oral examination: 30.06.2022

The role of GBF1 and GlcCer in UUKV infection

Referees:

Prof. Dr. Oliver T. Fackler

Dr. Pierre-Yves Lozach

Table of content

I. Publications	IV
II. Abbreviations	VI
III. List of figures	IX
IV. List of tables	X
V. Summary	XI
VI. Zusammenfassung	XII
1. Introduction	1
1.1. Arboviruses and epidemiological threats	1
1.2. Phenuiviruses in the order <i>Bunyavirales</i>	5
1.3. Phenuivirus structure and genome organization	7
1.4. Phenuivirus infection cycle	9
1.4.1. UUKV entry.....	10
1.4.2. UUKV replication and egress	13
1.5. Host proteins involved in UUKV infection	14
1.6. GBF1 is involved in infection of various RNA viruses.....	15
1.7. Lipids involved in virus infection	17
1.7.1. The cellular lipidome.....	18
1.7.2. Glucosylceramide plays a role for infection of different viruses	21
1.8. Ticks and tick cell culture.....	22
1.9. UUKV composition varies depending on the producer cells.....	24
1.10. Objectives of this thesis	24
2. Results	26
2.1. Viral particle production and labeling strategies	26
2.1.1. Virus production and concentration from mammalian cells.....	26
2.1.2. Viral particle labeling	29
2.1.3. UUKV production from the tick cell lines IDE-8 and IRE/CTVM-19	32

2.2. Cryo-EM analysis of tick and mammalian cell-derived virions	34
2.3. GBF1 as a proviral host factor of UUKV	38
2.3.1. UUKV glycoproteins interact with GBF1.....	38
2.3.2. Silencing of GBF1 reduces UUKV infection	40
2.3.3. GBF1 promotes infection of various RNA viruses	42
2.3.4. GBF1 is not involved in infection with DNA viruses or retroviruses	44
2.3.5. UUKV replication and viral particle release rely on GBF1.....	45
2.4. GlcCer is required for UUKV binding to target cells.....	49
2.4.1. UUKV infection increases HexCer levels	49
2.4.2. UUKV infection is reduced upon silencing or inhibition of UGCG.....	51
2.4.3. The release of infectious UUKV virions is decreased by PPMP treatment.....	57
2.4.4. GlcCer is incorporated into the UUKV particles	59
2.4.5. UUKV binding is supported by GlcCer present in viral particles	61
2.4.6. Receptors that recognize UUKV through GlcCer remain to be identified	65
2.4.7. TOSV infectivity depends on GlcCer.....	67
2.4.8. GlcCer is involved in TOSV binding	69
2.4.9. GlcCer and RVFV infection	71
3. Discussion	73
3.1. Tick and mammalian cell-derived UUKV particles differ in size.....	74
3.1.1. Tick derived UUKV particles are smaller than mammalian derived virions.....	75
3.1.2. Virus stocks derived from tick cells contain small 25 nm particles.....	77
3.2. GBF1 is a host protein involved in UUKV infection.....	79
3.2.1. A protein MS approach identifies GBF1 as an UUKV interaction partner.....	79
3.2.2. Various RNA viruses depend on GBF1 for infection	79
3.2.3. GBF1 plays a role during UUKV replication and egress	81
3.3. Host-derived GlcCer on the viral envelope promotes UUKV infection.....	83
3.3.1. Lipid MS indicates enriched HexCer in UUKV particles and infected cells.....	83
3.3.2. GlcCer is required for infectivity of progeny UUKV particles.....	85
3.3.3. GlcCer seems to play an ambiguous role for RVFV infection.....	86

3.3.4. GlcCer in the UUKV envelope promotes binding to target cells	87
4. Conclusion.....	92
5. Materials and Methods	94
5.1. Materials	94
5.2. Methods	101
5.2.1. Cells.....	101
5.2.2. Viruses.....	102
5.2.3. Flow cytometry-based assays	105
5.2.4. Cryo-EM imaging of UUKV particles	106
5.2.5. Label-free protein MS	107
5.2.6. Lipid MS.....	108
5.2.7. CLR binding studies	109
5.2.8. Protein and lipid expression analysis	110
5.2.9. Statistical analysis	111
6. Acknowledgements	112
7. References.....	114

I. Publications

First-author publications:

Z. M. Uckeley*, R. Moeller*, L. I. Kühn, E. Nilsson, C. Robens, L. Lasswitz, R. Lindqvist, A. Lenman, V. Passos, Y. Voß, C. Sommerauer, M. Kampmann, C. Goffinet, F. Meissner, A. K. Överby, P.-Y. Lozach, G. Gerold. Quantitative proteomics of Uukuniemi virus-host cell interactions reveals GBF1 as proviral host factor for phleboviruses. *Molecular & Cellular Proteomics*. **18**(12), 2401-2417 (2019), doi:10.1074/mcp.RA119.001631. (Research article) **indicates first authors*

Z. M. Uckeley*, J. Koch*, N. D. Tischler, P. Léger, P.-Y. Lozach. Cell biology of phlebovirus entry. *Virologie*. **23**(3), 176-187 (2019), doi:10.1684/vir.2019.0780. (Review article) **indicates first authors*

J. Koch*, **Z. M. Uckeley***, P. Doldan, M. Stanifer, S. Boulant, P.-Y. Lozach. TMPRSS2 expression dictates the entry route used by SARS-CoV-2 to infect host cells. *The EMBO journal*. **40**(16), e107821 (2021), doi:10.15252/embj.2021107821. (Research article) **indicates first authors*

J. Koch*, **Z. M. Uckeley***, P.-Y. Lozach. SARS-CoV-2 variants as super cell fusers: cause or consequence of COVID-19 severity? *The EMBO journal*. **40**(24), e110041 (2021), doi:10.15252/embj.2021110041. (News & Views article) **indicates first authors*

Z. M. Uckeley, M. Mazelier, C. Lüchtenborg, S. Winter, P. Schad, P. Chlanda, B. Brügger, P.-Y. Lozach. The glycolipid GlcCer recruited into viral envelope facilitates phenuivirus binding to host cells. *Manuscript in preparation 2022* (Research article)

Co-author publications:

F. Woelfl, P. Léger, N. Oreshkova, F. Pahmeier, S. Windhaber, J. Koch, M. Stanifer, G. R. Sosa, **Z. M. Uckeley**, F. A Rey, S. Boulant, J. Kortekaas, P. J. Wichgers Schreur, P.-Y. Lozach. Novel Toscana virus reverse genetics system establishes NSs as an antagonist of type I interferon responses. *Viruses*. **12**(4), 400 (2020), doi:10.3390/v12040400. (Research article)

S. Windhaber, Q. Xin, **Z. M. Uckeley**, J. Koch, M. Obr, C. Garnier, C. Luengo-Guyonnot, M. Duboeuf, F. K. M. Schur, P.-Y. Lozach. The Orthobunyavirus Germiston Enters Host Cells from Late Endosomes. *Journal of Virology*. **96**(5), jvi.02146-21 (2022), doi:10.1128/jvi.02146-21. (Research article)

J. Koch, **Z. M. Uckeley**, P.-Y. Lozach. SARS-CoV-2 uses different entry routes to infect host cells. *Médecine Sciences. In press 2022* (News article)

Scholarships

Attendance of the Workshop “Steppingstone to an academic career in Virology” by the Academy for Clinical and Experimental Virology (ACHIEVE), GfV 2021

Oral conference presentations

17th Workshop Cell Biology of Viral Infections of the German Society for Virology (GfV) - Schöntal, Germany 2018. “Uukuniemi virus relies on glucosylceramide synthase for amplification.”

International Meeting on Arboviruses and their Vectors of the Microbiology Society 2019 - Glasgow, UK. “Quantitative proteomics of Uukuniemi virus - host cell interactions reveals GBF1 as a proviral host factor for phleboviruses.”

19th Workshop Cell Biology of Viral Infections of the German Society for Virology (GfV) - Schöntal, Germany 2021. “Glucosylceramide is required for infectivity of progeny Uukuniemi viral particles.”

ASV 2021, 40th Annual Meeting of the American Society for Virology - virtual event 2021. “Glucosylceramide is required for infectivity of progeny Uukuniemi viral particles.”

II. Abbreviations

Arbovirus	Arthropod-borne virus
Arf	ADP-ribosylation factor
BHK-21 cells	Baby hamster kidney cells
BSL	Bio-safety level
Cas9	CRISPR-associated protein 9
CCHFV	Crimean-Congo hemorrhagic fever orthonavivirus
Cer	Ceramide
CHIKV	Chikungunya virus
Clec	C-type lectin
CLR	C-type lectin receptor
COP	Coat protein complex
CRISPR	Clustered regularly interspaced short palindromic repeats
C-type	Calcium-dependent
DABV	Dabie virus
DAG	Diacylglycerol
DC	Dendritic cell
DC-SIGN	Dendritic cell-specific intercellular adhesion molecule 3-grabbing non-integrin
DENV	Dengue virus
E2 protein	Envelope protein 2
EE	Early endosome
EM	Electron microscopy
Endo H	Endoglycosidase H
ER	Endoplasmic reticulum
ERGIC	ER-Golgi intermediate compartment
ffu	Focus forming units
GalCer	Galactosylceramide
GBA	Glucosylceramidase
GBF1	Golgi-specific brefeldin A-resistance guanine nucleotide exchange factor 1
G _C	Glycoprotein C
GCA	Golgicide A
GEF	Guanine-nucleotide exchange factor
GERV	Germiston virus
GlcCer	Glucosylceramide
G _N	Glycoprotein N
GSL	Glycosphingolipid
HAdV-5	Human adenovirus type 5

HBV	Hepatitis B virus
HCMV	Human cytomegalovirus
HCV	Hepatitis C virus
HEK 293T cells	Human embryonic kidney 293 cells that express the SV40 T-antigen
HeLa cells	Henrietta Lacks cells
HexCer	Hexosylceramide
HIV	Human Immunodeficiency virus
hpi	Hours post infection
HRTV	Heartland virus
IAV	Influenza A virus
KO	Knockout
LACV	La Cross virus
LE	Late endosome
LGTV	Langat virus
L segment	Large segment
L-SIGN	Liver/lymph node cell-specific intercellular adhesion molecule 3-grabbing non-integrin
mBMC	Murine bone marrow cell
mBMDC	Murine bone marrow-derived dendritic cell
Mincle	Macrophage-inducible C-type lectin
MOI	Multiplicity of infection
M segment	Medium segment
MS	Mass spectrometry
NB-DGJ	N-Butyldeoxygalactonojirimycin
NB-DNJ	N-Butyldeoxynojirimycin
NHS ester	N-Hydroxysuccinimide ester
N protein	Nucleoprotein
NSm protein	Nonstructural protein M
NSs protein	Nonstructural protein S
PC	Phosphatidylcholine
PDMP	N-[2-hydroxy-1-(4-morpholinylmethyl)-2-phenylethyl]-decanamide
PE	Phosphatidylethanolamine
PFA	Paraformaldehyde
pfu	Plaque forming units
PI	Phosphatidylinositol
PNGase F	Peptide-N-glycosidase F
PPMP	DL- <i>threo</i> -1-Phenyl-2-palmitoylamino-3-morpholino-1-propanol
PS	Phosphatidylserine

RdRp	RNA-dependent RNA polymerase
RNP	Ribonucleoprotein
RVFV	Rift Valley fever virus
SARS-CoV-2	Severe acute respiratory syndrome coronavirus 2
SDS-PAGE	Sodium dodecyl sulfate polyacrylamide gel electrophoresis
SEM	Standard error of the mean
SFTSV	Severe fever with thrombocytopenia syndrome virus
SFV	Semliki forest virus
siRNA	Small interfering RNA
SM	Sphingomyelin
S segment	Small segment
SVP	Subviral particles
SV40	Simian virus 40
TAG	Triacylglycerol
TOSV	Toscana virus
UGCG	UDP-glucose ceramide glucosyltransferase
UUKV	Uukuniemi virus
VLP	Virus-like particle
VSV	Vesicular stomatitis virus
VSV-G	VSV glycoprotein
wt	Wild type
YFV	Yellow fever virus

III. List of figures

Figure 1. The dual life cycle of arthropod-borne viruses (arboviruses).....	2
Figure 2. Organization of phenuiviral particles.	8
Figure 3. Phenuivirus infection cycle in mammalian cells.....	9
Figure 4. Entry of phenuiviruses into cells.	12
Figure 5. Replication, budding, and release of phenuivirus particles.	13
Figure 6. Cellular functions of GBF1.....	16
Figure 7. Major lipids in plasma membranes.	19
Figure 8. Glucosylceramide (GlcCer) metabolism.....	20
Figure 9. Tick cells grow to high cell densities and in three dimensions.	23
Figure 10. Characterization of arboviral particles.	28
Figure 11. UUKV infection levels can be acquired by flow cytometry.....	29
Figure 12. Atto488 NHS ester labeled UUKV particles are infectious.	31
Figure 13. UUKV production from tick-derived IDE-8 cells.....	33
Figure 14. UUKV particles produced from IDE-8 cells are smaller than BHK-21- derived virions.....	35
Figure 15. Tomography of one IDE-8 cell-derived UUKV particle indicates that the glycoprotein coat forms ordered hexameric multimers.	37
Figure 16. Host proteins interacting with the UUKV glycoproteins are identified by an immunoprecipitation followed by label-free protein mass spectrometry (MS). .	39
Figure 17. GBF1 silencing reduces UUKV infection in A549 cells.....	41
Figure 18. UUKV, TOSV, RVFV, and SFV infection is impaired upon GBF-1 inhibition or silencing.	43
Figure 19. HAdV-5 and HIV-1 do not rely on GBF1 for infection.	44
Figure 20. GBF1 is not involved in UUKV entry.....	46
Figure 21. GBF1 plays a role during UUKV replication and particle release	48
Figure 22. Lipidome analysis of UUKV-infected BHK-21 cells reveals enriched HexCer levels.	50
Figure 23. Silencing of glucosylceramide synthase (UGCG) reduced UUKV infection in BHK-21 cells.....	52
Figure 24. Blocking GlcCer metabolism by inhibiting UGCG decreases HexCer levels after UUKV infection.	54

Figure 25. Inhibition of UGCG reduces UUKV infection levels in BHK-21 and A549 cells.....	56
Figure 26. A lack of GlcCer in the producer cells leads to decreased infectivity of offspring UUKV particles.....	58
Figure 27. Lipidome analysis of UUKV particles reveals enriched HexCer levels.	60
Figure 28. Virus binding of UUKV particles lacking GlcCer is hampered.	62
Figure 29. C6-GlcCer competes with UUKV-Atto488 for binding to BHK-21 and A549 cells.	64
Figure 30. An ELISA-based screen suggests UUKV binding to Mincle.....	66
Figure 31. GlcCer plays a role for TOSV infectivity while it can be omitted for SFV infection.	68
Figure 32. GlcCer plays a role for TOSV and GERV binding to target cells.....	70
Figure 33. The role of GlcCer during RVFV infection remains elusive.	72
Figure 34. GBF1 involvement in UUKV infection.....	82
Figure 35. Potential GlcCer-receptor cell interaction during virus binding.....	90

IV. List of tables

Table 1. Selected viruses in the order <i>Bunyavirales</i>	4
Table 2. Selected protein hits used for silencing screening approach.....	40
Table 3. Small interfering RNAs (siRNAs).....	94
Table 4. List of cell lines and primary cells.	95
Table 5. List of plasmids.....	95
Table 6. List of antibodies.....	96
Table 7. List of viruses.....	97
Table 8. List of reagents and enzymes.....	97
Table 9. List of buffers.	97
Table 10. List of chemicals, media, and kits.	98
Table 11. Lipid MS internal standard master mix ingredients.....	99
Table 12. List of machines.....	100
Table 13. List of software.....	100

V. Summary

During the past decades, highly pathogenic arthropod-borne viruses (arboviruses) have emerged globally, posing a threat to public health. Arboviruses not only replicate in their vertebrate hosts but feature a dual life cycle with a switch to and from their arthropod vector. This switch is difficult to reproduce experimentally, and the link between infectivity and the molecular features acquired by arboviruses in arthropod vectors or mammalian hosts remains elusive. Moreover, only a few host factors have been functionally described for arbovirus infections.

In this thesis, the tick-borne Uukuniemi virus (UUKV) was used as a surrogate system to explore the molecular features of *Phenuiviridae*, a large family of highly pathogenic arboviruses in the order *Bunyvirales*. Label-free proteomic mass spectrometry analysis revealed that GBF1 interacts with the UUKV glycoproteins. Golgicide A-mediated inhibition of GBF1-driven intracellular vesicle trafficking and siRNA-mediated silencing of GBF1 impaired UUKV infection, demonstrating that GBF1 is involved in UUKV replication and egress. GBF1 appeared to be important for a broad range of RNA viruses budding from the endoplasmic reticulum and Golgi networks. Then, lipidomic mass spectrometry analysis indicated that hexosylceramide (HexCer) is enriched in infected cells and in the envelope of UUKV particles. Pharmacological inhibition of the synthesis of the HexCer glucosylceramide (GlcCer) in producer cells resulted in viral progeny with reduced infectivity, likely due to defects in virion binding to target cells. I also found that other bunyaviruses rely on GlcCer for infectious entry. Finally, I established protocols for UUKV production and purification from both tick vector cells and mammalian host cells. Cryo-electron microscopy showed that viral particles were smaller and more heterogenous in size when UUKV was derived from tick cells.

In sum, my thesis allowed the identification of general infection-promoting factors, not only for UUKV, but also for other viruses that bud from the endoplasmic reticulum and Golgi compartments. Strikingly, GlcCer is the first example of a glycolipid mediating virion attachment. My work lays the basis for future studies in virus-receptor interactions and comparative analysis of viral particles produced from their mammalian host and arthropod vector cells. Elucidating these molecular features and related functional processes is paramount to prepare for the emergence of future phenuiviruses and other arboviruses.

VI. Zusammenfassung

Während der letzten Jahrzehnte gewannen hochpathogene, durch Arthropoden übertragene Viren (Arboviren), weltweit an Bedeutung und stellen eine Herausforderung für die Gesundheitswesen vieler Länder dar. Arboviren vermehren sich nicht nur in ihrem Wirt, sondern verfügen über einen doppelten Lebenszyklus, der ihnen einen Wechsel zu und von ihrem jeweiligen Arthropodenvektor ermöglicht. Dieser natürliche Vorgang ist experimentell schwer zu reproduzieren. Darum sind die molekularen Merkmale, welche die Virionen in Arthropoden- oder Säugetierzellen erwerben, und deren mögliche Verbindung zur Infektiosität nach wie vor unklar. Außerdem wurden bisher nur wenige Wirtsfaktoren identifiziert, die an der Infektion mit Arboviren beteiligt sind, und für viele von diesen müssen die Funktionen noch im Detail aufgeklärt werden.

Mit Hilfe hochauflösender markierungsfreier Proteomik und Lipidomik Massenspektrometrie identifizierte ich neue Wirtsfaktoren und Eigenschaften des Uukuniemi Virus (UUKV). Bei diesem Virus handelt es sich um ein Surrogat System für hochpathogene Phenuiviren. Ergebnisse der Proteom Analyse der aus Säugetierzellen gewonnenen Virionen wiesen darauf hin, dass der Golgi-spezifische Brefeldin-A-resistente Guanin-Nukleotid-Austauschfaktor 1 (GBF1) mit den UUKV Glykoproteinen interagierte. Sowohl die durch Golgicide A vermittelte Hemmung des GBF1-gesteuerten intrazellulären Vesikeltransports als auch das durch siRNA vermittelte Silencing von GBF1 reduzierten die UUKV Infektionslevel. Eine eingehende Analyse des viralen Infektionszyklus ergab, dass GBF1 an der UUKV Replikation und dem Virenaustritt beteiligt ist. Außerdem konnte ich durch Lipidom-Analysen nachweisen, dass Hexosylceramid (HexCer) sowohl in infizierten Zellen als auch in der Hülle von UUKV-Partikeln angereichert ist. Die pharmakologische Hemmung der Synthese des HexCer Glucosylceramid (GlcCer) in produzierenden Zellen führte zu einer verminderten Infektiosität von UUKV-Partikeln. Dies könnte durch eine beeinträchtigte Binding des Virus an die Zielzellen verursacht werden. Darüber hinaus etablierte und optimierte ich Protokolle für die Produktion und Aufreinigung von UUKV aus Zeckenzellen. Kryo-Elektronenmikroskopie zeigte, dass die aus Zeckenzellen produzierten Partikel einen kleineren Durchmesser hatten als die aus Säugetierzellen gewonnenen Virionen.

Diese Arbeit bildet die Grundlage für zukünftige vergleichende Studien von Viruspartikeln, die aus Zeckenzellen und solchen, die aus Säugetierzellen stammen.

Ich habe in dieser Arbeit neue Wirtsfaktoren identifiziert, die bei der UUKV-Infektion eine zentrale Rolle spielen. So ist das vom Wirt stammende Lipid GlcCer an der Bindung an die Zielzellen beteiligt und ist damit das erste Beispiel für ein Glykolipid, das die Anheftung des Virions vermittelt. Generell könnten sowohl GBF1 als auch GlcCer bei Viren beteiligt sein, die aus dem Endoplasmatischen Retikulum und dem Golgi-Apparat knospen. Die mechanistische Grundlage dieser Prozesse wird in künftigen Studien von entscheidender Bedeutung sein. Vor allem therapeutische Ansätze könnten sich diese Wirkungsweise zu Nutze machen, um auf mögliche künftige Ausbrüche von Arboviren besser vorbereitet zu sein.

1. Introduction

1.1. Arboviruses and epidemiological threats

Viruses are obligate intracellular parasites encoded by genetic material (DNA or RNA) and hijack cellular factors of the host to replicate and produce progeny. Viruses can pose a severe threat to global health as recently proven by the severe acute respiratory syndrome coronavirus 2 (SARS-CoV-2) pandemic that began in 2020. Arthropod-borne viruses (arboviruses) constitute a supergroup of viruses with worldwide distribution, that share the dependence on arthropod vectors for transmission to vertebrate hosts. Some arboviruses which are causing diseases in humans or domestic animals are regarded as potential pandemic threats such as Chikungunya virus (CHIKV), Crimean-Congo hemorrhagic fever orthonavivirus (CCHFV), Rift Valley fever virus (RVFV), and yellow fever virus (YFV) (1–4).

Vertebrate-specific arboviruses possess two life cycles including amplification in their arthropod vector (e.g., tick, mosquito, and sandfly) and in their vertebrate host (e.g., hamster, sheep, and human) with constant transmissions between vector and host (Figure 1). Arboviruses establish a persist infection in the arthropod vector and are then transmitted upon feeding on vertebrates (5, 6). In turn, arthropods can also get infected during a blood meal from a viremic host. Moreover, transovarial transmissions occur from the parent to the offspring in arthropods. Transmissions between vertebrates were also described, for example, via aerosols or blood contact (7). Arboviruses are believed to initially have been “insect viruses” before they were transmitted to vertebrates. Hence, arthropods and arboviruses could have co-evolved, resulting in asymptomatic and persistent infections, while vertebrates frequently get severely sick upon exposure to arboviruses (8, 9).

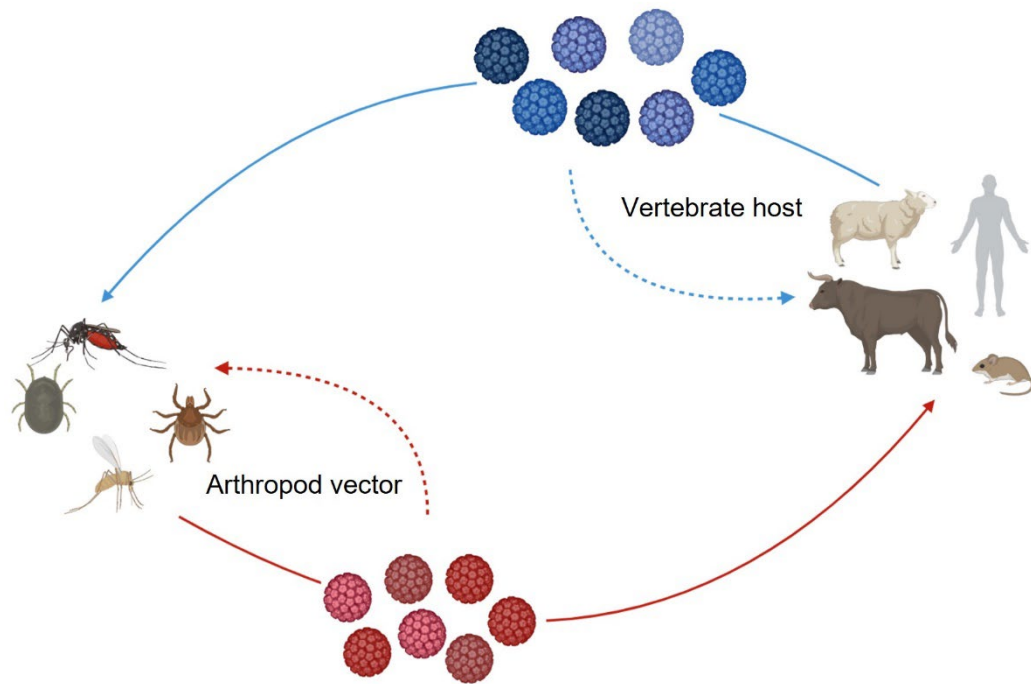


Figure 1. The dual life cycle of arthropod-borne viruses (arboviruses).

Arbovirus amplification takes place in their arthropod vectors and their vertebrate hosts, and the life cycles include a host switch with transmission between vector and host through bloodmeal as reviewed in (9). Furthermore, transmissions from vertebrate to vertebrate occur via aerosols or direct blood contact. For arthropods transovarial transmission from parent to offspring has been described. The figure was created using BioRender.

In general, zoonosis is defined as an infection transmitted from animals to humans. Such cross-species spillover events often lead to the infection of dead-end hosts that do not allow sustained transmission of the pathogen. Hence, dead-end hosts do not contribute to a stable transmission cycle. Yet, if the new host is capable to further transmit the virus, a new virus can be established in a population (e.g., SARS-CoV-2). Many arboviruses are regarded as emerging or reemerging pathogens. This means that they are causative agents of new or previously unrecognized infections. Emerging viruses can possess an expanded host range, and/or previously unknown diseases develop after infection with a known virus. An example for an emerging virus with an expanded host range that was previously known but then discovered to cause neuronal birth defects such as microcephaly, is Zika virus (ZIKV).

As infection of vertebrates occurs mainly via the vector saliva which is introduced into the skin dermis during an arthropod blood meal, dermal macrophages and dendritic cells (DCs) at the anatomical site are among the first

target cells of many arboviruses (9, 10). However, various arboviruses do not solely rely on vector transmission but they can also be transmitted between vertebrates, for example via aerosols, direct blood contact, vertical transmission, blood transfusion, or organ donation (6, 11). Due to a broad host and tissue specificity, arboviruses allow for zoonotic transmissions. Nonetheless, humans are regarded as a dead-end host for many arboviruses (12, 13). Because of deforestation and humans populating previously uninhabited land, sylvatic arbovirus transmission cycles between arthropods and wild animals get increasingly disturbed. Thus, this leads to humans getting exposed to arboviral vectors and the viruses they carry (14, 15). Additionally, globalization and increased travelling lead to the spread of arboviral diseases to new geographical regions. Global warming simultaneously facilitates the geographical expansion of vectors and viruses (16, 17).

Arboviruses are a super group of viruses harboring different viral families, such as among others, *Phenuiviridae*, *Peribunyaviridae*, *Nairoviridae*, *Flaviviridae*, and *Togaviridae*, all sharing the dual life cycle in vectors and hosts. Many different arthropods transmit viruses and other pathogens to vertebrate hosts, but mosquitoes, sandflies, and ticks are responsible for most arboviral diseases in humans.

Examples of mosquito-borne arboviruses are CHIKV, YFV, ZIKV, West Nile virus (WNV), and Dengue virus (DENV). DENV is a flavivirus which was designated as a primary international public health concern by the World Health Organization (WHO) because of a dramatic geographic spread in recent years. It causes several hundred-million infections each year, increasing substantially in the past two decades. In addition, another arbovirus spread rapidly during the last two decades: outbreaks of the alphavirus CHIKV occurred in Kenya (2004) and India (2005), before travelers introduced CHIKV into many European and American countries (18). Symptoms range from rashes, digestive abnormalities, and headaches to fever and muscle and joint pain. Semliki forest virus (SFV) is an alphavirus closely related to CHIKV but allows handling in biosafety level (BSL)-2 conditions due to low pathogenicity in humans. Thus, SFV is frequently used as a surrogate to study more pathogenic mosquito-borne alphaviruses (19). Germiston virus (GERV) is another mosquito-borne arbovirus that is employed as a surrogate system for a closely related and more pathogenic virus, namely, La Crosse virus (LACV) (20, 21). GERV and LACV are bunyaviruses belonging to the genus *Orthobunyavirus* in the family

of *Peribunyaviridae* (Table 1). LACV is present in North America and is regarded as the major causative agent of pediatric encephalitis (22).

CCHFV, Heartland virus (HRTV), and Dabie virus (DABV) are examples of tick-borne arboviruses in the order *Bunyavirales*. CCHFV belongs to the *Nairoviridae* family (Table 1). This virus is classified as a BSL-4 pathogen and causes infections mainly in Eastern Europe, Asia, and Africa (23–25). Natural hosts are wild and domestic animals such as cattle, goats, and sheep. Human infections mainly occur via tick bites or contact with blood of infected animals. Symptoms of CCHFV infection include headache, joint pain, high fever, changes in sensory perception, and bleeding. Depending on the outbreak and study, the fatality rate of hospitalized patients was reported to be between 9% and 50% as reviewed by (26). Other emerging tick-borne arboviruses in the order *Bunyavirales* that causes seasonal infections are HRTV and DABV, previously referred to as severe fever with thrombocytopenia syndrome virus (SFTSV). They belong to the family *Phenuiviridae*. DABV has a wide host range including goats, sheep, dogs, and chickens and can cause diarrhea, fever, multiple organ failure, and thrombocytopenia in humans (27, 28).

Table 1. Selected viruses in the order *Bunyavirales*.

Virus species	Vector	Virus family	Virus genus
CCHFV	Ticks	<i>Nairoviridae</i>	<i>Orthonairovirus</i>
LACV	Mosquitoes	<i>Peribunyaviridae</i>	<i>Orthobunyavirus</i>
GERV	Mosquitoes	<i>Peribunyaviridae</i>	<i>Orthobunyavirus</i>
DABV	Ticks	<i>Phenuiviridae</i>	<i>Bandavirus</i>
HRTV	Ticks	<i>Phenuiviridae</i>	<i>Bandavirus</i>
RVFV	Mosquitoes	<i>Phenuiviridae</i>	<i>Phlebovirus</i>
TOSV	Sandflies	<i>Phenuiviridae</i>	<i>Phlebovirus</i>
UUKV	Ticks	<i>Phenuiviridae</i>	<i>Uukuvirus</i>

1.2. Phenuiviruses in the order *Bunyavirales*

The international committee on taxonomy of viruses (ICTV) designed a system of grouping a virus into an order, family, and genus based on genome organization, replication strategy, and morphology (29). The order *Bunyavirales* consists of twelve virus families. Among them, *Phenuiviridae* are of particular importance. They include more than 100 identified members in 19 genera, many of which are emerging pathogens in both, humans and livestock. Phenuiviruses are transmitted by both, insects and arachnids such as the tick-borne phenuivirus DABV and the non-pathogenic relative Uukuniemi virus (UUKV). Within the virus family *Phenuiviridae*, arboviruses in the genus *Phlebovirus* are mostly transmitted by sandflies such as Toscana virus (TOSV). RVFV belongs to the *Phlebovirus* genus but is an exception as it is reported to be transmitted by mosquitoes. UUKV was moved from this genus into the newly formed genus *Uukuvirus* in 2019 (30, 31). The main reasons for the relocation of UUKV to the new genus were that the transmission vectors of UUKV are ticks that are arachnids and not insects. Moreover, UUKV does not code for the non-structural protein NSm which is encoded by phleboviruses.

Another classification system is the Baltimore scheme which assigns classes based on replication strategy. Phenuiviruses possess a single stranded segmented RNA genome with mostly negative polarity and hence belong to group V of this system (32).

Many bunyaviruses can cause severe diseases in livestock and humans posing a global threat to agricultural productivity and public health. Globalization and climate change lead to the spread of vectors and viruses to new geographical locations. Hence, many bunyaviruses are considered as emerging pathogens (33, 34). UUKV was the main focus of my thesis. It is a frequently used surrogate for many highly pathogenic tick-borne bunyaviruses such as CCHFV and DABV. Moreover, I employed the closely related sandfly-borne TOSV and the mosquito-borne RVFV to test whether my findings were specific to UUKV or shared within the same viral family of *Phenuiviridae*. UUKV, TOSV, and RVFV are all transmitted by different arthropods (ticks, sandflies, and mosquitoes, respectively) allowing to assess whether the arthropod vector influences the utilization of mammalian host factors.

RVFV is a phlebovirus most commonly present in animals such as cattle, sheep, and goats in sub-Saharan Africa. Transmission to humans can occur upon

mosquito bites, contact with animal blood, or via aerosols, mainly causing a mild disease with symptoms including headache, fever, and muscle pain (35–37). RVFV infection can cause liver manifestations, loss of sight, meningoencephalitis, and hemorrhagic fever in severe cases. Reports of case fatalities vary greatly between different outbreaks and studies but are estimated to be generally below 1%. However, in cases where hemorrhagic fever has manifested, fatality rates are as high as 50% (38–40).

TOSV is transmitted by sandflies and is endemic in Southern Europe and Northern Africa. Recent studies revealed high seroprevalence of the virus in Italy, but primarily flu-like symptoms seem to be misdiagnosed frequently (41–44). Complications of TOSV infection include neuronal symptoms. Furthermore, TOSV infections are the leading cause of meningitis or encephalitis in Southern Europe in summer. However, no public awareness is drawn to this neglected and understudied arbovirus (45, 46).

UUKV is a tick-borne phenuivirus isolated from *Ixodes ricinus* ticks, small rodents, and birds in Central and Eastern Europe and Scandinavia. Moreover, antibodies against UUKV were detected in cows (47–49). UUKV is closely related to highly pathogenic phenuiviruses such as DABV, HRTV, and RVFV, while UUKV infection is not associated with human diseases (30, 50, 51). Hence, UUKV has been used as a model arbovirus for decades. Studying UUKV infection led to many findings, which were later confirmed also for more pathogenic phenuiviruses (52, 53).

1.3. Phenuivirus structure and genome organization

Viruses in the family *Phenuiviridae* are roughly spherical and approximately 80-160 nm in diameter (54, 55). Phenuiviruses possess a tri-segmented single-stranded RNA genome surrounded by a host-derived lipid bilayer embedding the viral glycoproteins G_N and G_C (Figure 2 A). The three RNA segments of negative or ambisense polarity were named based on their respective sizes: large (L), medium (M), and small (S) (Figure 2 B).

The L segment encodes the RNA-dependent RNA polymerase (RdRp) which is required for transcription of the viral RNA and replication. The M segment codes for a glycoprotein precursor protein which is processed at the endoplasmic reticulum (ER) and the Golgi apparatus. In dipteran-borne phenuiviruses, the M segment additionally codes for the non-structural NSm protein. The functions of NSm remain largely uncharacterized. However, for RVFV, it was shown that it inhibits apoptosis in infected cells while it does not play a crucial role in viral replication (56, 57). The S segment has an ambisense polarity encoding the nucleoprotein (N protein) in negative-sense and the non-structural protein NSs in positive-sense. The N protein and the RdRp bind to the RNA segments forming ribonucleoprotein (RNP) complexes which constitutes the minimal necessary replicative elements for genomic viral replication processes (58).

Yet, phenuiviruses do not seem to rely on NSs for replication in mammalian cell culture models, but rather for escaping innate immunity *in vivo*. The NSs protein of RVFV typically forms cytosolic *punctae* and nuclear filaments in infected cells, which have recently been described to be amyloidogenic (59). The fibrilization of RVFV NSs into amyloid fibrils appears to be crucial for inhibiting interferon- β expression and protein kinase R function and, in turn, counteracting the innate immune response in infected cells (60–62).

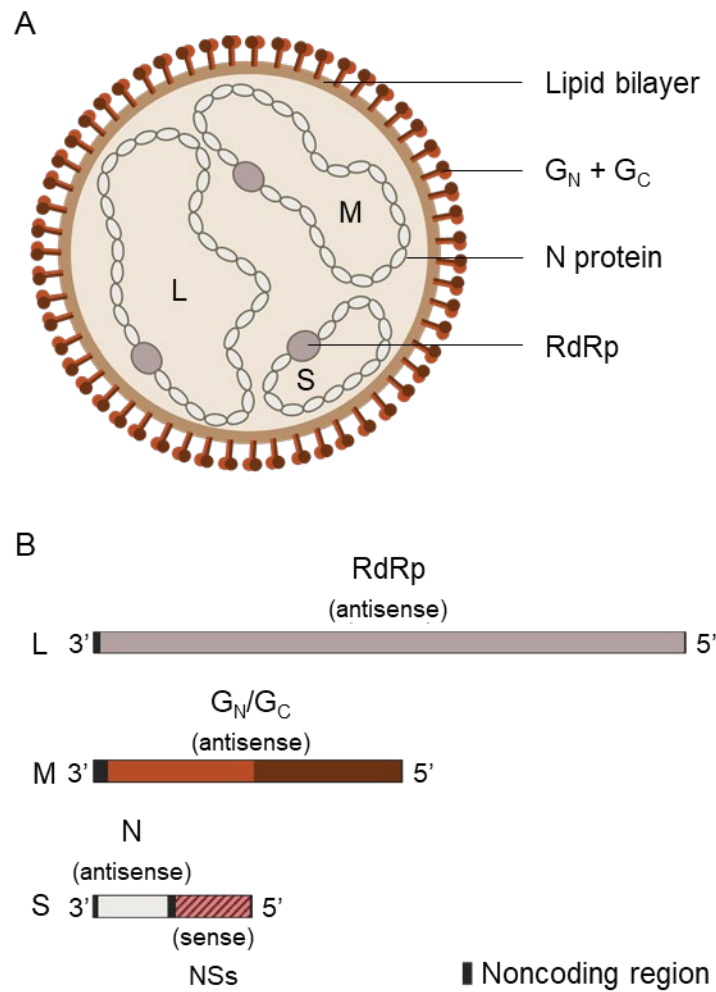


Figure 2. Organization of phenuiviral particles.

(A) As other phenuiviruses, UUKV particles have a diameter of about 100 nm and are roughly spherical. The tri-segmented single-stranded RNA genome is accompanied by the ribonucleoprotein (RNP) complex consisting of nucleoprotein (N protein) and RNA-dependent RNA polymerase (RdRp). Virions are enveloped by a host-derived lipid bilayer with transmembrane viral glycoprotein (G_N and G_C) protrusions arranged in a T-12 icosahedral lattice. Figure 2 A was adapted from Uckeley, Koch, et al. 2019 (63). (B) Three RNA segments code for all viral proteins: the large (L) segment encodes the RdRp, the medium (M) segment codes for the viral glycoproteins G_N and G_C , and the small (S) segment encodes the N protein and the non-structural protein NSs in an ambisense strategy.

1.4. Phenuivirus infection cycle

The UUKV life cycle was generally investigated and described in mammalian cells (30, 58). In contrast, tick cell biology remains poorly understood, and virus infection in tick cells has not been characterized on molecular levels. The first step of phenuivirus infection is entry, including virus attachment, internalization, intracellular trafficking, and fusion with the endosomal membrane to release the viral genome. Subsequently, phenuiviruses replicate in the cytoplasm and bud through intracellular compartments, leaving the cell in vesicles (Figure 3). The individual steps of the UUKV infection cycle will be explained in more detail in the following sections.

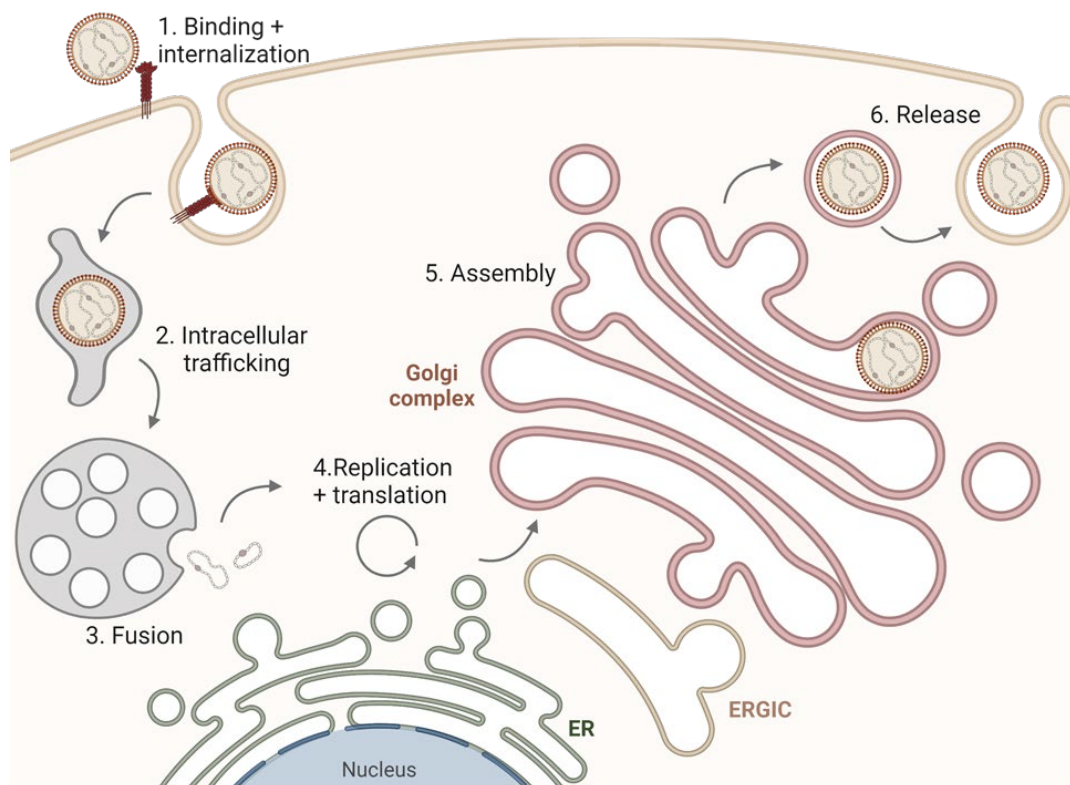


Figure 3. Phenuivirus infection cycle in mammalian cells.

Phenuiviruses entry starts with binding to the target cell. Virions enter via the endocytic route and fuse from late endosomes. Replication and translation occur in the cytoplasm and viral particles assemble at the endoplasmic reticulum (ER), ER-Golgi intermediate compartments (ERGIC), and Golgi compartments. Budding of viral particles through the Golgi apparatus is followed by virion release by exocytosis. The figure was illustrated using BioRender.

1.4.1. UUKV entry

Virus attachment to target cells usually occurs through interactions between the surface proteins decorating viral particles and host cell receptors, such as proteins, glycans, or lipids (Figure 4/1). The C-type lectin receptor (CLR) dendritic cell-specific intercellular adhesion molecule-3-grabbing non-integrin (DC-SIGN) is a primary entry receptor for UUKV and the closely related phleboviruses TOSV and RVFV (52). It was shown that DC-SIGN not only mediates the attachment of these viruses to cells but is also involved in endocytic internalization. In addition, cells that could previously not be infected with UUKV were rendered permissive upon DC-SIGN expression suggesting that this CLR is sufficient to mediate UUKV infectious entry (52, 64).

Liver-specific intercellular adhesion molecule-3-grabbing non-integrin (L-SIGN) acts as an attachment factor (also referred to as co-receptor) for UUKV, TOSV, and RVFV, meaning it promotes infection by binding to the virus without playing a direct role for virus uptake (53). DC-SIGN and L-SIGN share high sequence homology with main differences in the cytosolic tails and internalization motifs (65, 66). These findings further highlight the complexity of virus-receptor mechanisms beyond interactions between particles and the receptor ectodomain. Strikingly, DC-SIGN is for example expressed on dermal DCs, which are present at the anatomical site of phenuivirus transmission and belong to the primary target cells. L-SIGN is expressed in epithelial liver cells, in line with the hepatotropism of many phenuiviruses (30).

However, cells such as the lung epithelial cell line A549, the fibroblastic cells baby hamster kidney (BHK)-21, and the cervical carcinoma epithelial cells Henrietta Lacks (HeLa) that do not express these CLRs are permissive to infection with UUKV, proving that there are more yet unknown receptors that the virus can use. Furthermore, for the phleboviruses RVFV and TOSV, heparan sulfate facilitates attachment via electrostatic interactions (67–69). Recently, low-density lipoprotein (LDL) receptor-related protein 1 (Lrp1) was described to be important for RVFV entry via an interaction with G_N (70).

Phenuivirus binding to the target cell is followed by receptor-mediated endocytosis (Figure 4/2) and intracellular trafficking (Figure 4/3) to the site of fusion and release of the viral genome into the host cell (Figure 4/4). Clathrin-mediated endocytosis was suggested as the internalization pathway for DABV, while the uptake mechanisms of UUKV and RVFV remain less characterized (71, 72). UUKV

infects cells even when clathrin is silenced, suggesting that UUKV can use another uptake mechanism (64). For RVFV, three possible internalization routes (clathrin-mediated endocytosis, caveolin-mediated endocytosis, or micropinocytosis) were proposed in three independent studies using various RVFV strains and different cell types (67, 73, 74).

Upon internalization, phenuiviruses traffic within endosomal compartments. Endosomes mature from early endosomes (EE) to late endosomes (LE) and then fuse with lysosomes. Driven by vacuolar-type H⁺-ATPases (vATPases), the pH in the endosomal lumen steadily decreases from roughly pH 6.8-6.0 in EE, about pH 6.0-5.0 in LE, down to pH 4.5 in lysosomes (75). For UUKV, it was shown that viral particles travel in EEs, LEs, and endolysosomal compartments (64). Acid-dependent penetration of the viral genome into the cytosol is triggered after reaching optimal conditions for fusion of the viral and the endosomal membrane. Phenuiviral fusion with the endosomal membrane is mediated by the glycoprotein G_C and can be triggered by specific environmental factors such as a pH drop, ion concentrations, and/or availability of host proteases (76). It was demonstrated that acidification is sufficient to trigger UUKV fusion, which typically occurs at pH ~5.4, compatible with a penetration from late endosomes/endolysosomes where intraluminal pH varies from 4.5 to 6.0 (Figure 4). This makes UUKV a late-penetrating virus (30, 77). Neutralization of the endosomal pH using vATPase inhibitors or weak lysosomotropic bases impaired UUKV and RVFV from fusion with the endosomal membrane (64, 78). In addition, it was described that UUKV depends on an intact microtubule network for efficient entry (64).

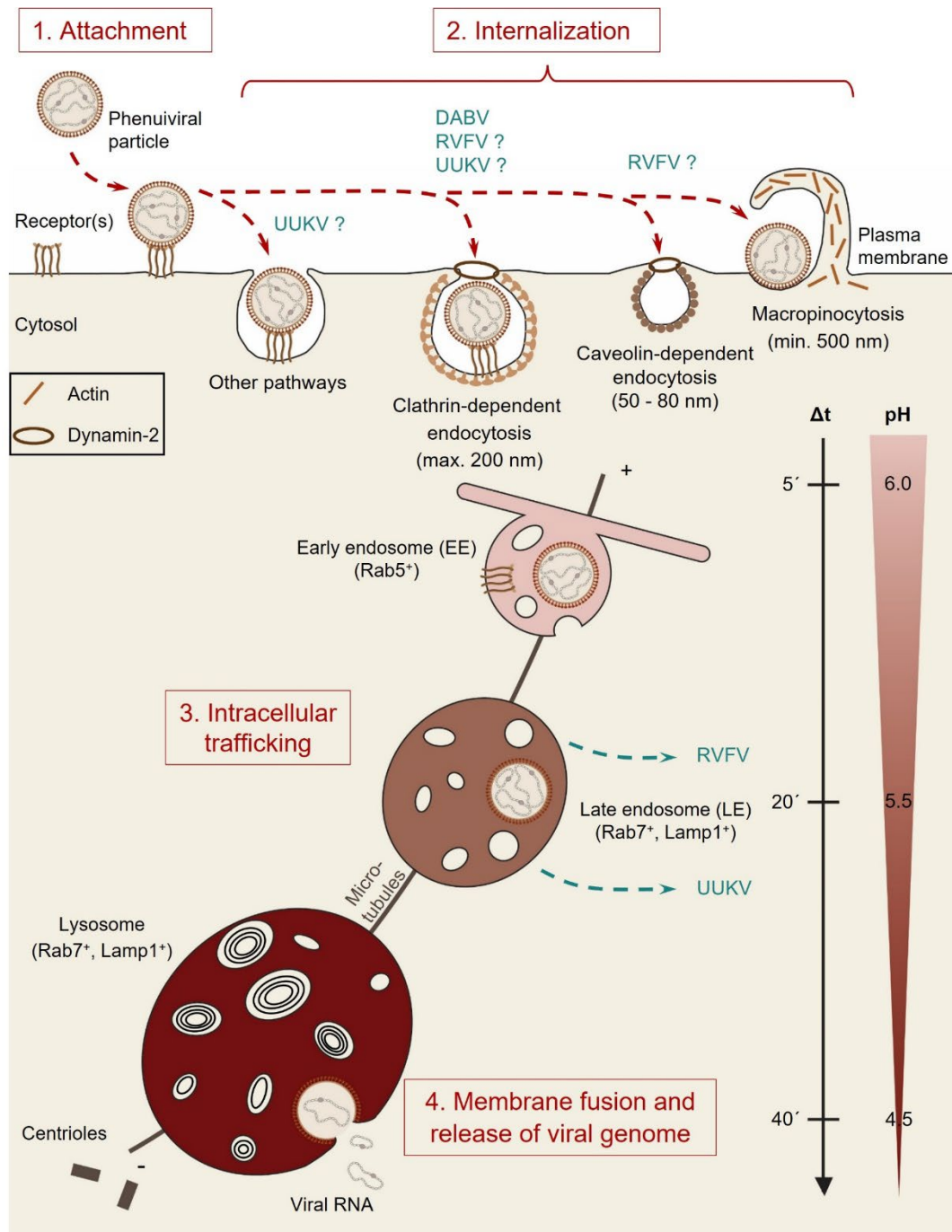


Figure 4. Entry of phenuiviruses into cells.

After binding (1.), phenuiviruses can use different uptake pathways (2.) including clathrin- and caveolin- dependent endocytosis, micropinocytosis, and clathrin-independent pathways. Viruses are trafficked along the endocytic route (3.) and fuse once the endosomal environmental conditions are considered optimal for the individual virus (4.). Adapted from Uckeley, Koch, et al. 2019 (63).

1.4.2. UUKV replication and egress

Upon acid-activated fusion and penetration, the viral RNA segments are released into the cytoplasm, where replication of the viral genome driven by viral RNPs (vRNPs) takes place. RNPs generally consist of N proteins and the RdRp. The RdRp synthesizes complementary RNA (cRNA) strands which are then bound by N proteins and RdRp to form complementary RNPs (cRNPs). These are in turn used as a template to synthesize more vRNPs.

Initial protein synthesis occurs at the ER, and the viral glycoproteins G_N and G_C are cleaved from the precursor, folded, and matured at ER, ER-Golgi intermediate compartments (ERGIC), and Golgi apparatus (79). The exact mechanisms of glycoproteins maturation remain poorly documented. vRNPs and the glycoproteins assemble to form phenuiviral particles budding from ER, ERGIC, and Golgi compartments where they acquire their lipid envelope (80–83). Assembled virus particles are believed to be released via exocytosis (Figure 5).

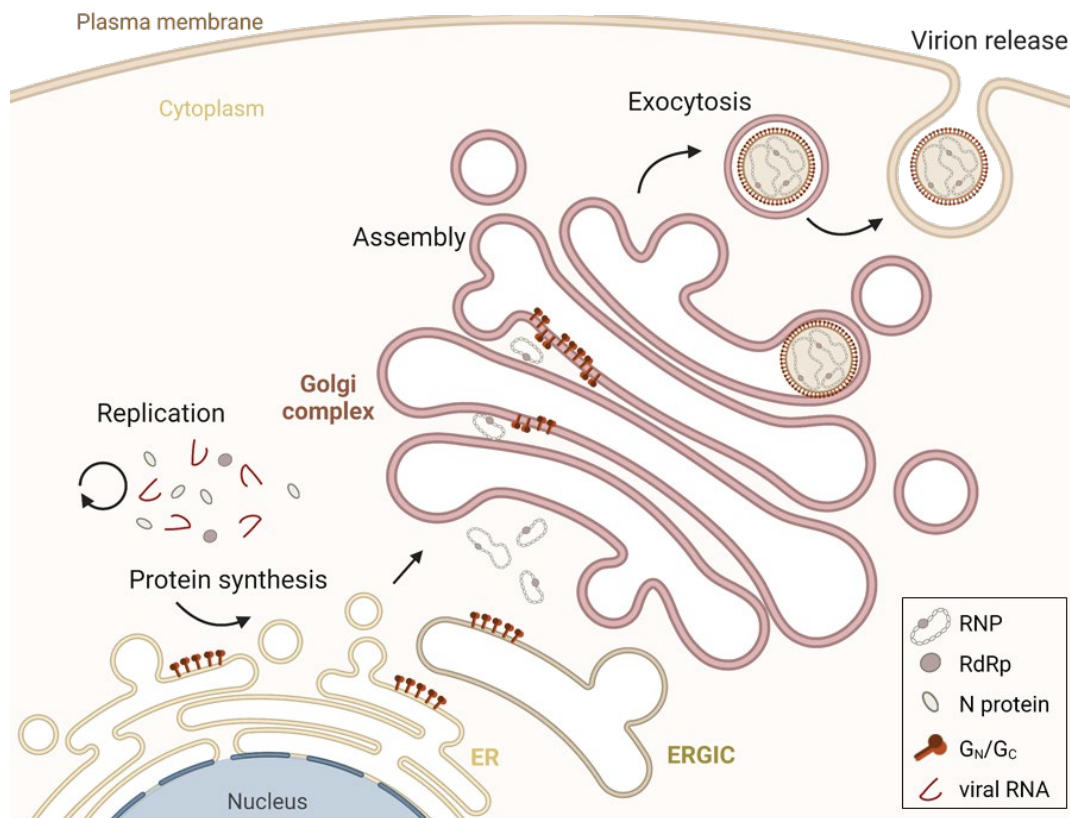


Figure 5. Replication, budding, and release of phenuivirus particles.

Phenuivirus replication takes place exclusively in the cytoplasm. Upon viral protein synthesis at the ER, phenuivirus assembly takes place at ER, ERGIC, and Golgi compartments. After assembly, phenuiviruses acquire their lipid bilayer by budding through ERGIC/Golgi compartments. Virions are trafficked to the plasma membrane in

vesicles, leaving the cells via exocytosis. Phenuivirus replication and egress was reviewed by (58, 84). The figure was created with BioRender.

1.5. Host proteins involved in UUKV infection

Although especially assembly and egress of UUKV infection remain poorly understood processes, some distinct host factors playing a crucial role during viral infection have been characterized. As mentioned in the previous section (1.4.1.), UUKV particles employ the CLR DC-SIGN and L-SIGN to bind to target cells. Moreover, UUKV was shown to colocalize with Rab5⁺ EE, Rab7⁺ LE, and lysosome associated membrane protein type 1 (LAMP-1)⁺ endolysosomes, while trafficking along the endosomal route (52). Rab5 is a small guanosine triphosphate hydrolase protein (GTPase) present in EEs and involved in further endosomal maturation. Rab7 is mainly present in LEs and was described to play a role in endosomal trafficking and maturation, while LAMP-1 is a frequently used marker for lysosomes (85). Furthermore, the vesicle soluble *N*-ethylmaleimide-sensitive factor attachment protein receptor (v-SNARE) protein vesicle-associated membrane protein 3 (VAMP-3), which is present in recycling endosomes, is required for UUKV to reach the optimal endosomal compartment for fusion and subsequent viral genome penetration into the cytosol (86). My group has recently found that the small GTPase Rab11a involved in trafficking of recycling endosomes and the autophagic factor Atg7 were associated with infection-promoting functions during UUKV infection (87). Both host factors facilitate endosomal transport of UUKV particles from the plasma membrane to late endosomes where the viral glycoproteins induce fusion. Together, these studies suggest that UUKV uses a complex, non-classical intracellular trafficking pathway to enter cells. Many UUKV host factors, especially during virus replication and the release of progeny virus particles, still remain to be identified.

1.6. GBF1 is involved in infection of various RNA viruses

Previously, Golgi-specific brefeldin A-resistance guanine nucleotide exchange factor 1 (GBF1) was demonstrated to be involved in the replication of enveloped viruses such as DENV, hepatitis C virus (HCV), human coronavirus 229E (hCoV 229E), vesicular stomatitis virus (VSV), and YFV (88–90). GBF1 is a guanine exchange factor (GEF) for members of the adenosine diphosphate (ADP)-ribosylation factor (Arf) GTPases. It is resident at the *cis*-Golgi, and additionally present in the ERGIC and lipid droplets, already indicating its wide variety of functions (Figure 6). GBF1 possesses a membrane-bound and a cytosolic state. By activating Arf1, GBF1 regulates coat protein I (COPI) dependent retrograde Golgi–ER trafficking. GBF1, Arf1, and COPI also play a role in lipid droplet metabolism. Moreover, in a COPI-independent manner, GBF1 and Arf1 are involved in clathrin-independent endocytosis and recruitment of the dynein receptor golgin160 to the Golgi apparatus (91).

The positive sense RNA viruses DENV, HCV, human coronavirus 299E (hCoV 299E), and YFV share a dependence on the formation of replication complexes. Replication complexes serve as protective viral factories within the crowded cytosol. Apart from influencing retrograde COPI trafficking, GBF1 also seems to be involved in the generation of these replication organelles (88–90). Furthermore, GBF1 was described as a proviral factor for the non-enveloped viruses Coxsackievirus B (CVB) and hepatitis E virus (HEV). Also in case of HEV, GBF1 was suggested to play a role in the generation of replication complexes (92, 93). For CVB, it was proposed that active GBF1 is important for efficient replication, while the exact function of GBF1 in this mechanism requires further investigation. Interestingly, also the non-enveloped poliovirus interacts with GBF1, but it does not rely on its GEF activity for RNA replication. It remains elusive by which mechanism GBF1 affects poliovirus infection (94, 95). GBF1 thus appears as an important factor for replication, assembly, and egress of viruses budding from ER, ERGIC, and Golgi compartments. However, the role of GBF1 was not yet characterized for phenuiviruses.

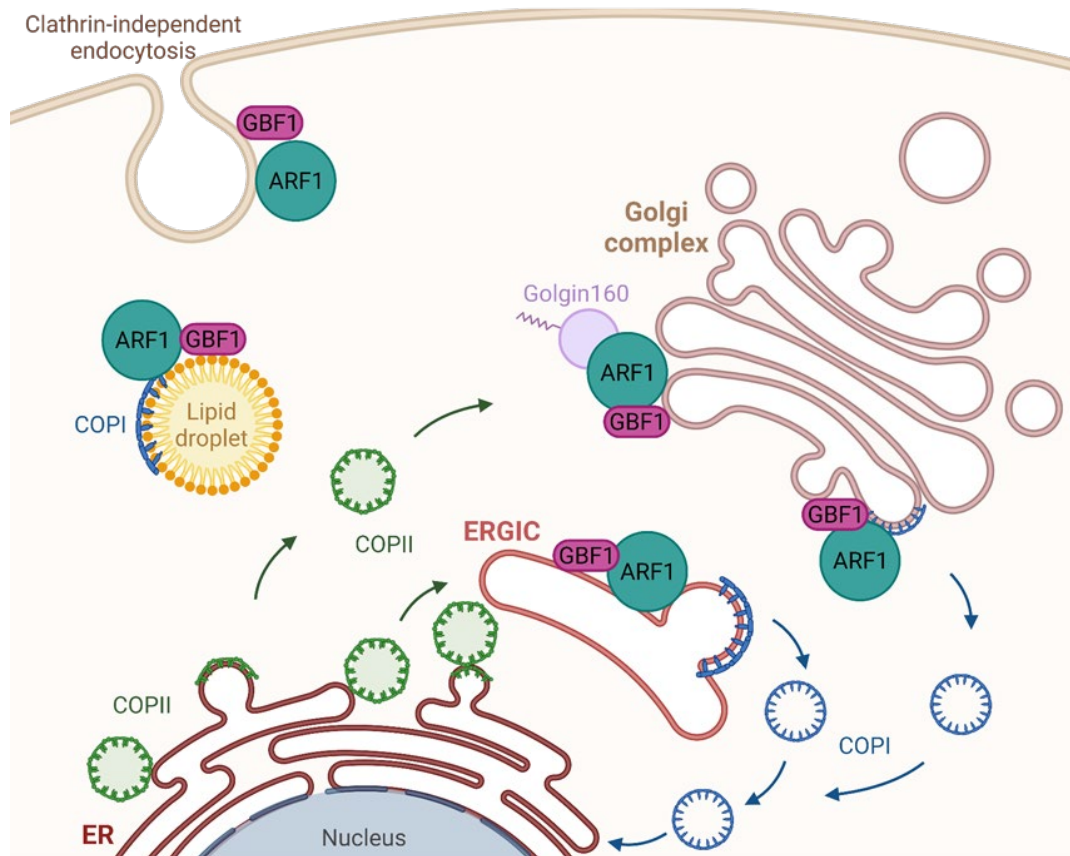


Figure 6. Cellular functions of GBF1.

GBF1 is localized at *cis*-Golgi, ERGIC, and lipid droplets, where it activates Arf1. GBF1 and Arf1 recruit COPI to form vesicles. COPI vesicles mediate retrograde transport from the Golgi and ERGIC back to the ER. GBF1 and Arf1 are also involved in clathrin-independent endocytosis and recruitment of the dynein receptor golgin160 to Golgi membranes. The multifaceted roles of GBF1 were reviewed in (91). The figure was created with BioRender.

1.7. Lipids involved in virus infection

As obligatory intracellular parasites, viruses strongly rely on the host machinery and interactions with several cellular factors to promote viral infection (96–98). Apart from the extensively described virus-host protein interactions, literature increasingly identifies different host cell lipids involved in viral entry, replication, and egress (99, 100). For example, lipids in the host cell membrane can facilitate virus binding. Simian virus 40 (SV40) was demonstrated to bind to the ganglioside GM1 on the plasma membrane, facilitating uptake and intracellular trafficking during infection (101). The protein coat of non-enveloped polyomaviruses can interact with glycosphingolipids (GSLs) such as GT1b, GD1a, and GD1b on the cell membrane, which are suggested to play a role in virus trafficking to the ER (101, 102).

Influenza A virus (IAV), Ebola virus (EBOV), SARS-CoV-2, and human immunodeficiency virus (HIV)-1 were reported to rely on lipid microdomains on host cells for virus entry. Lipid microdomains are platforms of highly ordered lipid structures on plasma membranes hypothesized to be involved in various cellular functions. Hydrophobic residues of the IAV hemagglutinin (HA) interact with lipid microdomains playing a role in virus attachment (103). Furthermore, interactions of the EBOV glycoproteins with cholesterol were suggested to facilitate fusion and virus entry (104). The importance of cholesterol-rich lipid rafts for SARS-CoV-2 entry was indicated by employing SARS-CoV-2 spike-expressing pseudoviruses (105). Similarly, HIV-1 utilizes cholesterol in lipid microdomains as an attachment factor during virus entry (106–108). Regarding phenuiviruses, cholesterol was suggested to be involved in RVFV entry and fusion (109). In addition, Bitto et al. revealed that the phospholipid bis(monoacylglycero)phosphate (BMP), which is present in late endosomal membranes, facilitates UUKV fusion (110).

Over the past decades, it has been shown that some viruses use phosphatidylserine (PS) in the viral envelope as a co-factor to bind the plasma membrane of the target cell (111–115). PS is a lipid that is usually exclusively present at the inner leaflet of the plasma membrane. Its localization to the outer leaflet occurs in dying cells resulting in rapid phagocytosis. Viruses, such as CHIKV, DENV, EBOV, and HIV-1 use this mechanism for uptake into target cells.

Enveloped viruses acquire their lipid bilayer from the producer cells. The lipid composition of the viral envelope generally resembles that of the cell organelle

membranes from which viruses usually bud, *i.e.*, ER, ERGIC, Golgi apparatus, or plasma membrane. A lipid composition analysis of Semliki forest virus (SFV) and VSV which both bud from the plasma membrane, indicated that the lipidome of the viral envelope and the plasma membrane are very similar (116–118). In contrast, several studies found that specific lipids were enriched or reduced in the virus envelope compared to the host cell. For instance, the vaccinia virus (VACV) envelope possesses more PS than the host cell, while the human cytomegalovirus (hCMV) envelope is enriched in phosphatidylethanolamine (PE) and constitutes less PS than its producer cells (119, 120). IAV infection enriched sphingolipids and cholesterol in the apical membranes and the viral particles, while glycerophospholipids were reduced (121). For HIV-1, it was described that its envelope is enriched in phosphatidylinositol-4,5-bisphosphate (PIP₂), sphingomyelin (SM), cholesterol, and PS, while phosphatidylcholine (PC) and ceramide (Cer) were reduced (122).

HIV-1 egress has been suggested to rely on interactions between viral proteins with lipid microdomains on the inner leaflet of the plasma membrane. This process involves interactions of the viral Gag protein with PIP₂, eventually leading to budding and release of virions from the plasma membrane (123, 124).

1.7.1. The cellular lipidome

The plasma membrane of mammalian cells is a lipid bilayer consisting of more than 100 different lipids from three major classes, namely glycerophospholipids, sphingolipids, and sterols (Figure 7) (125). The majority of membrane lipids are amphiphilic, meaning they possess a hydrophobic and a hydrophilic part enabling spontaneous self-organization into a lipid bilayer in aqueous solutions (126, 127). PC, PE, PS, and phosphatidylinositol (PI) are examples for glycerophospholipids sharing a common glycerol backbone. Cholesterol, the predominant sterol in the membrane, is important for membrane integrity and stability, and is a precursor for a vast number of hormones and signaling molecules (128, 129). Sphingolipids comprise Cer, SM, and GSL. Cer is a precursor for SM-, and GSL-metabolism (130). GSLs are important for many cellular processes, for instance, they are involved in cell growth, development, and differentiation (131, 132).

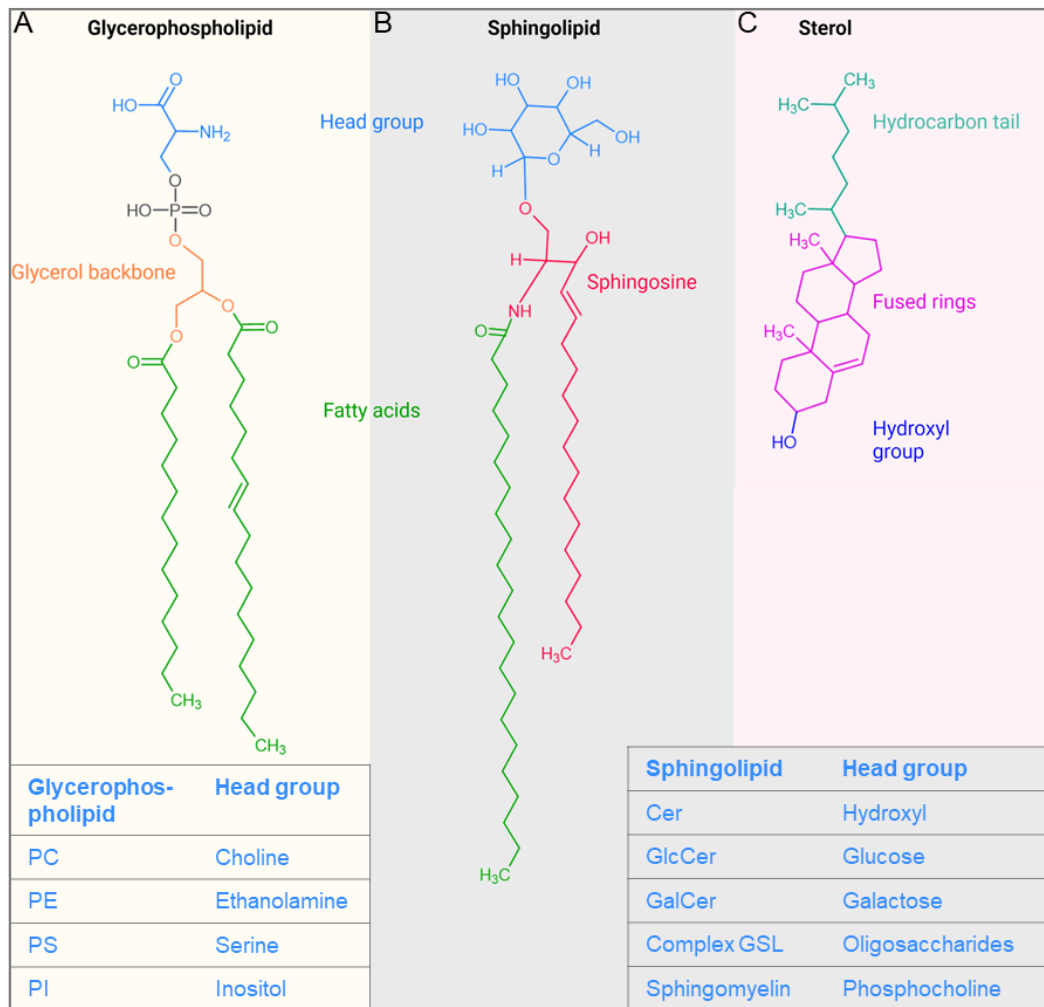


Figure 7. Major lipids in plasma membranes.

Glycerophospholipids, sphingolipids, and sterols are the main three lipid classes present in the plasma membrane. (A) Glycerophospholipids possess a glycerol backbone with fatty acids and different head groups as exemplified in the yellow box. Phosphatidic acid is indicated in grey. (B) Sphingolipids have a common sphingosine backbone, a fatty acid chain, and a head group that differs as indicated in the grey box. (C) The major sterol in mammals is cholesterol which possesses a hydrocarbon tail linked to fused rings with a hydroxyl group. The figure was prepared using ChemSketch (Advanced Chemistry Development, ACD/Labs) and BioRender. Cer, ceramide; GalCer, galactosylceramide; GlcCer, glucosylceramide; GSL, glycosphingolipid; PC, phosphatidylcholine; PE, phosphatidylethanolamine; PS, phosphatidylserine; PI, phosphatidylinositol

Glucosyl- and galactosylceramide (GlcCer, GalCer) are hexosylceramides (HexCers) that serve as the main precursors for complex GSLs (133). The conversion of Cer to GlcCer is catalyzed by UDP-glucose ceramide glucosyltransferase (UGCG) which is abundant on the cytosolic side of the Golgi apparatus (Figure 8). GlcCer is then further metabolized by the stepwise addition of

glycans in the Golgi lumen (133, 134). Degradation of GlcCer is mediated by glucosylceramidase (GBA) resulting in glucose and Cer (135, 136). On the other hand, GalCer is metabolized by GalCer synthases, enzymes which are present mostly in the ER of neuronal and renal cells (137). GalCer synthases are limited to only some tissues. In contrast, UGCG, the enzyme metabolizing GlcCer, is present in most tissues and cell types (133, 137). While GlcCer serves as the precursor for more than 300 different GSLs, GalCer can only be synthesized to a few of them (138).

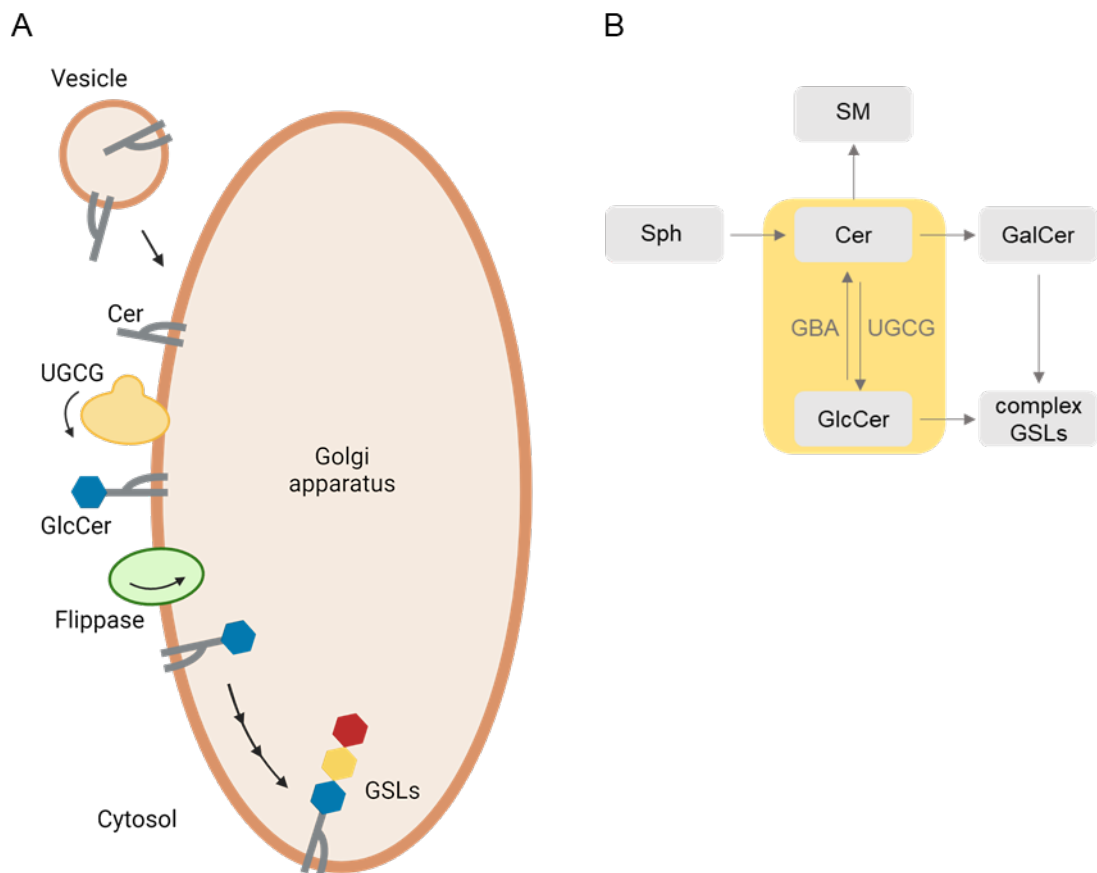


Figure 8. Glucosylceramide (GlcCer) metabolism.

(A) UDP-glucose ceramide glucosyltransferase (UGCG) synthesizes GlcCer from ceramide (Cer) at the Golgi apparatus. GlcCer is translocated into the Golgi lumen and complex glycosphingolipids (GSLs) are metabolized by a stepwise addition of glycans. The figure 8 A was generated using BioRender. (B) Cer is synthesized by acylation of sphingosine (Sph) and represents the precursor of sphingomyelin (SM) and GSL metabolism. As reviewed by (138), the hexosylceramides (HexCer) GlcCer and galactosylceramide (GalCer) serve as a source for more complex GSLs. GlcCer is metabolized to more than 300 different GSLs, while in contrast GalCer serves as a precursor for only few GSLs. The enzyme glucosylceramidase (GBA) degrades GlcCer into Cer and glucose.

1.7.2. Glucosylceramide plays a role for infection of different viruses

Recently, several studies suggested that UGCG can influence virus infection. IAV infection relies on GBA and UGCG activity, proposing that highly regulated homeostatic GlcCer levels are required for efficient IAV infection (139–141). The IAV lipidome was already analyzed earlier and did not reveal significantly increased HexCer in infected cells or the virions. However, it seemed like Hex2Cer levels were enriched in viral particles (121). In addition, UGCG was shown to play a role during infection with SARS-CoV-2. In this study, pharmacological inhibition of UGCG in target cells reduced the production of infectious SARS-CoV-2 particles (142). Concerning phenuiviruses, Drake et al. silenced and inhibited UGCG leading to decreased DABV infection levels. They suggested a role of UGCG during viral entry but also demonstrated that the production of infectious DABV particles was hampered in UGCG depleted cells. Moreover, they assessed DABV binding and internalization into cells that were silenced for UGCG which resulted in no difference in the binding or internalization capacity (143). GlcCer or UGCG seem to be involved in the infection of unrelated viruses possibly indicating that also other viruses rely on GlcCer and/or UGCG.

1.8. Ticks and tick cell culture

My PhD project mainly focused on UUKV which is a tick-borne arbovirus. To understand whether the producer cells influence virus morphology, molecular traits, and thus, infection of target cells, I was interested in comparing UUKV produced from tick and mammalian cells. While some mosquito cells are commercially available and start being used in arboviral laboratories, tick cells remain largely uncharacterized.

Ticks are ectoparasitic arachnids that feed on blood. They have eight legs, a body, and mouthparts. The tick life cycle comprises developmental stages starting from eggs, larvae, and nymphs, leading to adults. They molt between each developmental stage while being able to survive prolonged periods between feeds. Ticks have giant genomes of 1,000-7,000 Mb. Hard (*Ixodidae* family) and soft (*Argasidae* family) ticks can be distinguished by the presence of a hard shield behind the mouthparts. Ticks are associated with different diseases (144, 145). They can directly damage the skin at the feeding site which may lead to secondary infections. Furthermore, ticks can transmit diverse pathogens such as viruses, bacteria, and protozoa. Tick-borne viruses include, for example, tick-borne encephalitis virus (TBEV), CCHFV, DABV, HRTV, and UUKV (146). Nevertheless, ticks remain poorly studied at the level of molecular biology.

Tick cell cultures are hard to establish and hence only rarely used in laboratories, which explains the little knowledge about tick cell biological mechanisms. My collaboration partner Lesley Bell-Sakyi (Tick Cell Biobank Liverpool) established various tick cell lines from different tick strains, for which eggs, larvae, or nymphs served as the starting material (147–149). To get a primary culture from eggs, surface sterilized engorged female ticks lay their eggs and once developing embryos become visible, the eggs were again surface-sterilized. Subsequently, the eggshells were gently crushed and filtered out to release embryos. Tissues were then incubated in complete medium at 28°C with a weekly medium change. On average, it took 1-7 years until the cells were stably growing. Established cell lines are not clonal but comprise more than one cell type. They are not strongly adherent and grow in three dimensions (Figure 9). Moreover, the cells grow slowly with high cell densities (10^6 - 10^7 cells/ml) and do not require regular subculturing (147). Instead, one medium change per week is sufficient to keep them growing. Cryopreservation is only possible for a few cell lines and cells might need

several months after thawing until they grow adequately to be expanded and used for experiments (148).

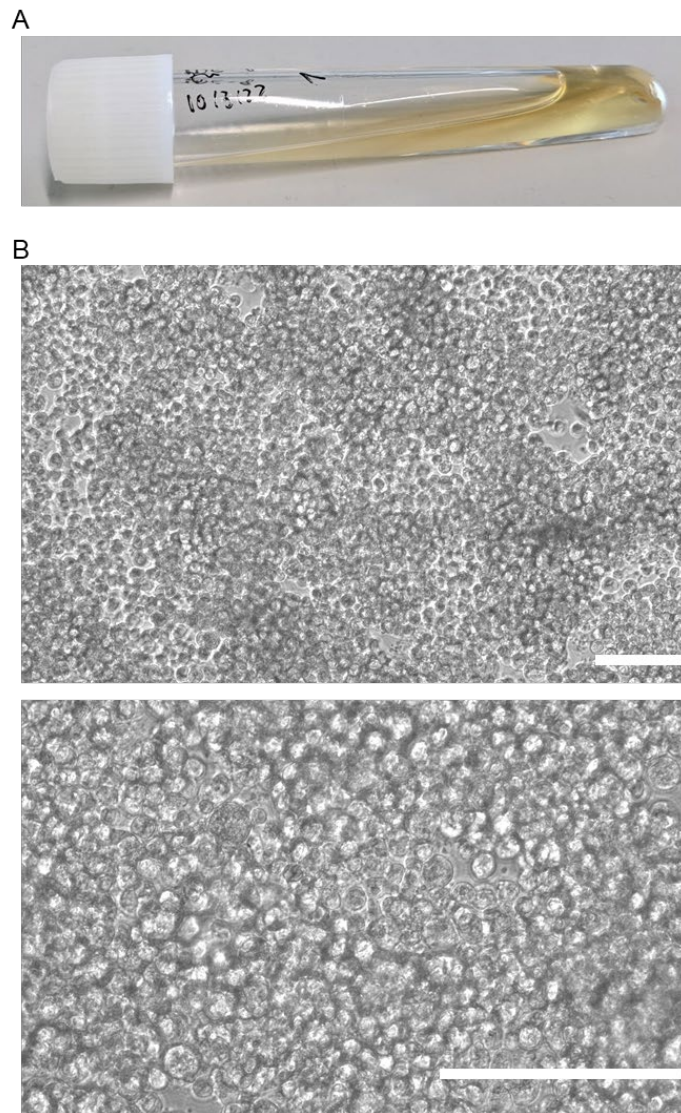


Figure 9. Tick cells grow to high cell densities and in three dimensions.

The tick cell lines were grown at 28°C and a weekly medium change was performed. Tick cells were cultured in flat-bottom glass tubes (A) at high cell densities of about 10^6 - 10^7 cells/ml. (B) Brightfield images show that tick cells grow in three dimensions. The scale bars correspond to 100 μ m.

1.9. UUKV composition varies depending on the producer cells

Arboviral infection of vertebrate hosts is usually caused by transmission from an infected vector during a blood meal. Thus, in a real-life scenario, virus particles infecting a vertebrate host are usually produced in arthropods where they acquire their molecular and morphological characteristics. Nevertheless, most laboratory studies are performed on arboviruses produced from mammalian cells. My group previously compared UUKV particles derived from mammalian versus tick cells and demonstrated that virions differ in *N*-glycosylation patterns of the viral glycoproteins (150). The amount of the viral proteins N, G_N, and G_C also appeared to differ upon whether the virus was produced from tick or mammalian cells. UUKV particles produced in BHK-21 (mammalian) cells were less infectious and possessed lower ratios of glycoproteins amount compared to N protein amount (150). These results clearly highlight molecular and functional distinctions between viruses produced in their arthropod vector cells and their mammalian host cells. This work further supports the importance of studying the arboviral vector-host switch as well as the molecular and morphological diversity between virions derived from different producer cells (*i.e.*, arthropod versus mammalian cells) to understand the differences in infectivity.

1.10. Objectives of this thesis

UUKV is closely related to highly pathogenic phenuiviruses and has been proven useful as a surrogate to investigate various aspects of arboviral infections. The use of UUKV led to significant advances in deciphering the particle structure and the infection cycle of phenuiviruses (52, 54, 64, 86, 151–153).

The project of my PhD thesis is organized around three main objectives: First, I aimed to follow up on the work of Magalie Mazelier, a former PhD student in my group who revealed molecular differences between UUKV particles derived from tick and mammalian cells (150). Here, morphological distinctions of tick and mammalian cell-derived UUKV particles were assessed by cryo-electron microscopy (cryo-EM). Secondly, I aimed to investigate cellular interaction partners of UUKV in a proteomic mass spectrometry (MS) approach, contributing to a better understanding of the virus life cycle in mammalian cells. Thirdly, to shed light on the lipid composition of infected mammalian cells and virions, lipid MS was performed. Using UUKV, one can expect to obtain deeper knowledge of cellular host factors and molecular

determinants important for transmission, infection, and spread of phenuiviruses. These results may lead to the identification of new specific anti-viral drug targets or could lay the groundwork for the development of vaccines against phenuiviruses and other arboviruses with a significant burden on society.

Therefore, I have developed and optimized protocols to study UUKV derived from BHK-21 cells, including among others, virus production and purification to implement label-free protein and lipid MS approaches. The proteomic analysis was achieved in collaboration with the team of Gisa Gerold (TWINCORE Hannover). After co-immunoprecipitation of the UUKV glycoproteins G_N and G_C with host cellular proteins, proteomic MS analysis identified GBF1 as a cellular protein interacting with the UUKV glycoproteins. I used different molecular and cellular approaches to determine the role of GBF1 in the UUKV infection cycle, from virus binding and penetration to replication and egress. Next, through a collaboration with the group of Britta Brügger (BZH Heidelberg), I determined the lipidomes of UUKV-infected BHK-21 cells and the virions and revealed that GlcCer is an important component of the UUKV envelope. In this part of my PhD project, I aimed to characterize the role of GlcCer for UUKV infection and demonstrated its functional importance for UUKV entry into host cells. Of note, the last two years of my PhD project overlapped with the coronavirus disease 2019 (COVID-19) pandemics. Together with my colleague Jana Koch, I got the opportunity to work on the cell entry of the novel coronavirus SARS-CoV-2. This work will not be described here as it is not part of my initial PhD project, but it was published in 2021 (154).

2. Results

2.1. Viral particle production and labeling strategies

2.1.1. Virus production and concentration from mammalian cells

In this thesis, my primary virus model was UUKV, a phenuivirus that is a frequently used surrogate for highly pathogenic phenuiviruses and other tick-borne bunyaviruses. To expand the study to other phenuiviruses important for human health, I additionally included the closely related TOSV and RVFV, and the more distant relative GERV, a bunyavirus belonging to the family of *Peribunyaviridae*. Furthermore, in some experiments, I used the togavirus SFV as a control. SFV is an early penetrating arbovirus that buds from the cell membrane. Prior to being used in routine for my investigation, production, purification, characterization, and titration protocols for these viruses needed to be established or optimized. Moreover, immunofluorescent staining and labeling of viral particles for flow cytometry acquisition and determination of binding or infection levels was optimized for the above-mentioned viruses. RVFV, GERV, and SFV are routinely produced from the epithelial African green monkey kidney cell line Vero E6. In contrast, UUKV can only be produced from the fibroblastic BHK-21 cells. For the lipidomic approaches, it was essential to produce all viruses from the same cell line to allow the comparison of the lipid compositions (155). Additionally, BHK-21 cells support growth in a serum-free medium for several days leading to less lipid and proteins contaminations advantageous for OMICS analyses.

Therefore, I optimized the production of the viruses in BHK-21 cells. During the production of virus particles, no serum was added to BHK-21 cells enabling easier purification of the produced virus stocks. Virus particles were then semi-purified and concentrated via ultracentrifugation through a sucrose cushion. The viral proteins were separated by sodium dodecyl sulfate polyacrylamide gel electrophoresis (SDS-PAGE) and characterized by Coomassie blue staining. UUKV glycoproteins G_N and G_C were localized at 65 kDa and 60 kDa respectively, while the nucleoprotein N was observable at 28 kDa (Figure 10 A). RVFV Δ NSs green fluorescent protein (GFP), a BSL-2 compatible mutant of the highly pathogenic RVFV, revealed the proteins G_N and G_C at 49 kDa and slightly below, while the N protein was at 28 kDa (Figure 10 B). For TOSV, the glycoproteins were visible as one band of the size 45 kDa and the N protein was detectable at about 28 kDa (Figure 10 C). In case of the alphavirus SFV, the viral capsid C (35 kDa) and the

envelope proteins E1 (45 kDa) and E2 slightly lower were visible on the SDS-PAGE gel (Figure 10 D). For the orthobunyavirus GERV bands at 28 kDa (N), 35 kDa (G_N), and 98 kDa (G_C) were detected (Figure 10 E). UUKV and RVFV Δ NSs GFP were titrated by focus forming units (ffu) assays on BHK-21 cells, while for TOSV, RVFV wt, GERV, and SFV plaque forming units (pfu) titration assays were performed on BHK-21 cells. All viruses could be produced to high titers (Figure 10 F) allowing virus labeling. Using the titers obtained on BHK-21 cells, the multiplicity of infection (MOI) was calculated.

Infection of cells with all viruses mentioned above could be detected by flow cytometry following immunostaining of infected cells. Figure 11 A represents an example of UUKV infection of A549 cells. It shows the gating strategy used for all following infection assays, if not stated differently. The fraction of UUKV-infected cells was detected by an immunofluorescent antibody raised against the UUKV N protein (8B11A3, in-house) followed by flow cytometry acquisition. Since RVFV Δ NSs GFP expressed GFP instead of NSs, infection levels were determined based on directly measured GFP fluorescence expression instead of immunostaining.

To observe the replication kinetic of UUKV and to determine the suitable MOIs for different time frames, BHK-21 and A549 cells were infected with UUKV at an MOI of 0.1 and 0.5, respectively. Cells were then fixed after different time points to analyze infection levels by flow cytometry (Figure 11 B). In BHK-21 and A549 cells, the number of infected cells increased significantly after 8 h. While in A549 cells infection peaked at 24 hours post infection (hpi) with about 20% of infected cells, the proportion of UUKV-infected BHK-21 cells was still increasing until 48 hpi.

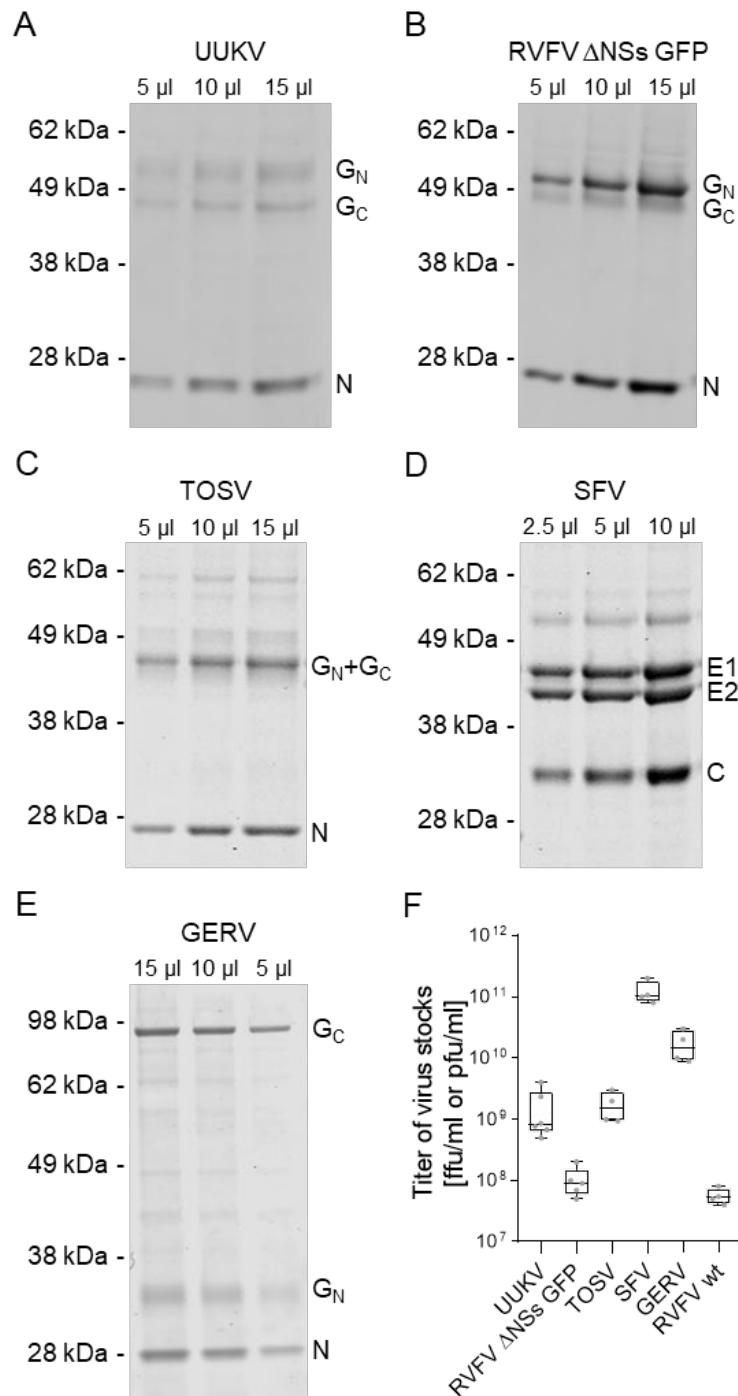


Figure 10. Characterization of arboviral particles.

(A-E) After production from BHK-21 cells, virus particles were semi-purified and concentrated by ultracentrifugation through a 25% sucrose cushion. UUKV (A), RVFV Δ NSs GFP (B), TOSV (C), SFV (D), and GERV (E) viral proteins were separated by SDS-PAGE and visualized by Coomassie blue staining. For all bunyaviruses, the glycoproteins G_N and G_C , and the nucleoprotein N were visible, while for SFV the envelope proteins E1 and E2, and the capsid protein C were observable. (F) Titers after semi-purification were determined by plaque forming units (pfu) (TOSV, GERV, SFV) or focus forming units (ffu) (UUKV, RVFV Δ NSs GFP) titration assay on BHK-21 cells. RVFV wt was not semi-purified, instead the infectious supernatant from producer cells was cleared of cell debris by centrifugation and then titrated by a pfu titration assay on BHK-21 cells. All data points and the median are depicted.

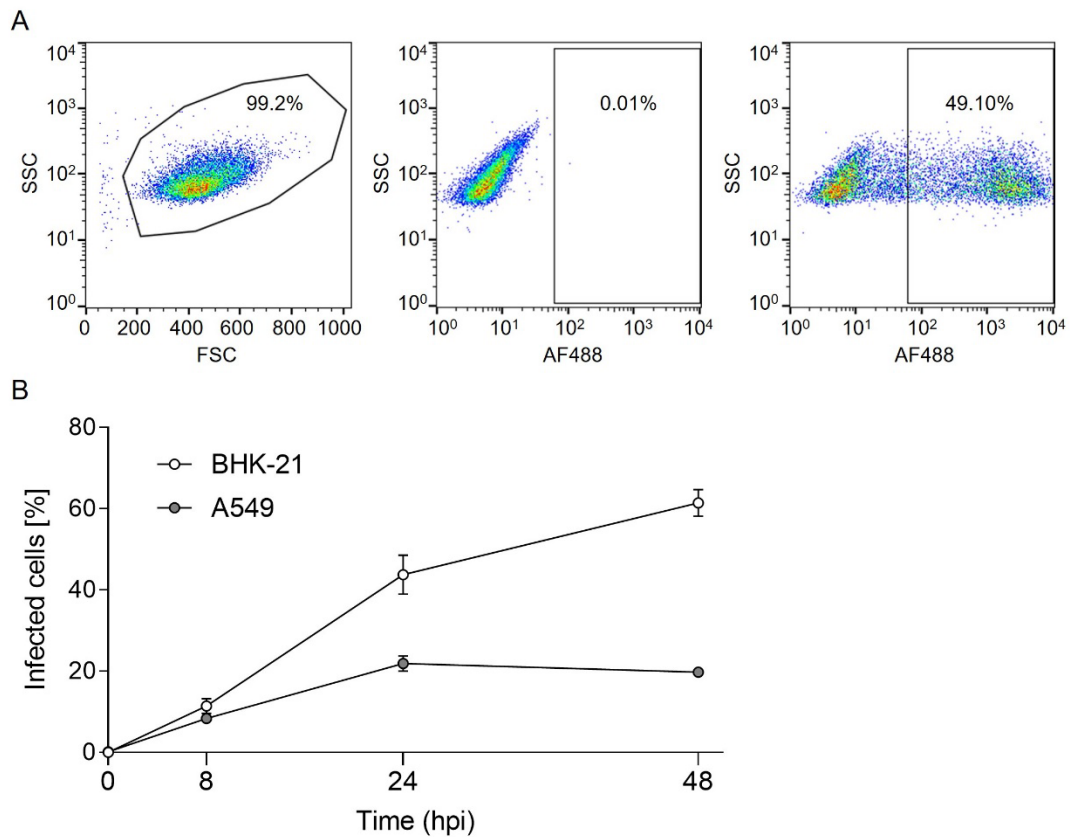


Figure 11. UUKV infection levels can be acquired by flow cytometry.

(A) Representative gating strategy for UUKV infection of A549 cells starting with a cell gate in the forward scatter (FSC) side scatter (SSC) plot. Then, Alexa Fluor (AF) 488 positive (infected) and negative (not infected) cells were distinguished based on their fluorescent signal. (B) A549 and BHK-21 cells were infected with UUKV at a multiplicity of infection (MOI) of 0.5 and 0.1, respectively. Infection was monitored over time by flow cytometry after immunofluorescent staining of the viral N protein in cells.

2.1.2. Viral particle labeling

After establishing production, concentration, titration, and flow cytometry-based infection assays for the viruses, I aimed to fluorescently label viral particles. To this end, I labeled the viral glycoproteins with amine-reactive Alexa Fluor (AF)488 and Atto488 N-Hydroxysuccinimide (NHS) esters. Fluorescent labeling of viral glycoproteins enables visualization of the virions during viral entry. For instance, fluorescently labeled virus particle binding, internalization, and trafficking can be analyzed and quantified by flow cytometric and microscopic approaches. Previously, my group established labeling protocols for the envelope glycoproteins of phleboviruses (156), which I used and adapted in this thesis to label UUKV, RVFV Δ NSs GFP, TOSV, GERV, and SFV.

In order to label viral particles with specific molecular ratios of viral glycoproteins to dye, the viral glycoproteins were semi-quantified. Three different volumes of a virus preparation and a serial dilution of bovine serum albumin (BSA) were separated by SDS-PAGE (Figure 12 A). By employing BSA as a reference scale after Coomassie blue staining, the concentration of glycoproteins in a virus preparation was estimated (Figure 12 B). Approximately 100 μ g of glycoproteins G_N and G_C or E1 and E2 were labeled using AF488 or Atto488 NHS ester. The molecular ratios of viral glycoprotein to AF488 or Atto488 NHS ester were determined for each virus so that the best balance between infectivity and fluorescence signal brightness of viral particles was obtained. For this purpose, multiple molecular ratios were tested, and labeled particles were analyzed for infectivity and fluorescence emission. I aimed to prevent a drop in infectivity superior to 1 log, while preserving a fluorescence labeling detectable by flow cytometry and microscopy. The optimal ratios were 1:2 for UUKV, RVFV Δ NSs GFP, and TOSV, 1:3 for GERV, and 1:30 for SFV.

Upon purification using a sucrose gradient, a visible band containing virus particles was extracted (Figure 12 C). AF488- or Atto488 labeling of viral glycoproteins resulted in a milky green band (left), while unlabeled purified virions were visible in a milky white band (right). Excess of the AF488 or Atto488 NHS ester was concentrated on top of the sucrose gradient. Labeled UUKV particles were again characterized for the structural proteins N, G_N , and G_C by Coomassie blue staining after SDS-PAGE (Figure 12 D). The infectious titer of labeled or unlabeled purified UUKV particles was determined by a ffu titration assay (Figure 12 E). In sum, glycoprotein labeling using NHS esters was successful and labeled viral particles were visible by immunofluorescence microscopy (data not shown). The labeling did not impair the infectivity of viral particles and the fluorescence was high enough for detection and the subsequent entry experiments.

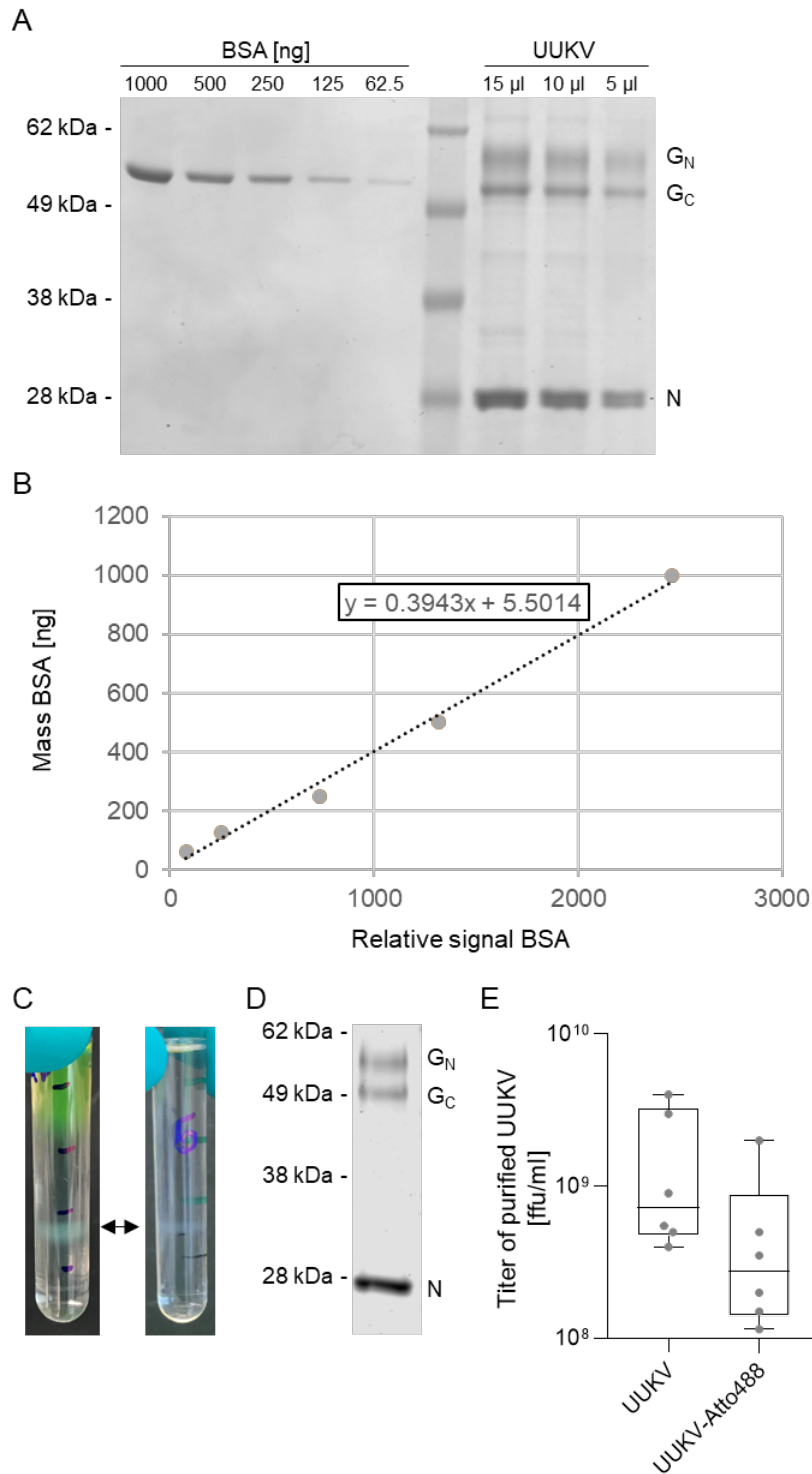


Figure 12. Atto488 NHS ester labeled UUKV particles are infectious.

(A) On an SDS-PAGE gel, Coomassie blue stained viral glycoproteins were semi-quantified using a serial dilution of BSA. (B) Viral protein concentration was determined from the relative signals by a BSA standard curve obtained from the relative signals for the BSA serial dilution. (C) After labeling of the UUKV glycoproteins with AF488 or Atto488 NHS esters, the labeled virions were purified through a sucrose gradient via ultracentrifugation. The colored band marked with the arrow contained the labeled UUKV particles and was extracted. (D) Labeled virus stocks were characterized on a Coomassie gel after sucrose gradient purification. (E) UUKV-Atto488 was titrated in a ffu titration assay. The graph shows all data points and the median.

2.1.3. UUKV production from the tick cell lines IDE-8 and IRE/CTVM-19

As mentioned above, UUKV possesses different molecular characteristics (viral protein ratio, infectivity, *N*-glycosylation) depending on whether the virus is produced from tick or mammalian cells (150). Hence, I aimed to optimize the protocol previously employed by Mazelier et al. to produce and purify UUKV from tick cells in high quantities. IDE-8 (*Ixodes scapularis*) and IRE/CTVM-19 (*Ixodes ricinus*) tick cells showed viral permissiveness at very low MOIs and produced infectious UUKV particles (Figure 13 A). These data were consistent with other arboviruses such as RVFV, Bunyamwera virus (BUNV), and DENV in their arthropod vector-derived mosquito cells (157–159). I observed a persistent infection process for UUKV-infected tick cells, which could be continuously kept in culture while producing viral particles for at least twelve weeks.

In contrast to mammalian cells that could produce the virus in a much shorter period of time, I added fetal bovine serum (FBS) to the tick cells while producing UUKV as the cells started dying once serum was omitted. After semi-purification through a sucrose cushion, this led to additional biological material in the viral stocks detectable by additional bands after Coomassie blue staining (Figure 13 B). The SDS-PAGE analysis of the viral proteins G_N , G_C , and *N* confirmed the previously described results by Mazelier et al. indicating that tick cell-derived UUKV particles possess more glycoproteins in relation to *N* compared to mammalian cell-derived UUKV particles (Figure 13 B). In order to reduce the FBS concentration in the viral preparation and thereby removing the additional bands detected in the gel, I further purified UUKV virions over a sucrose gradient. This resulted in a cleaner pattern of viral proteins without further contaminant bands after SDS-PAGE and Coomassie blue staining (Figure 13 C).

I could also confirm by western blotting that the in-house prepared polyclonal rabbit anti-UUKV (U2) antibody targeted not only the BHK-21 cell-derived, but also the IDE-8 cell-derived structural viral proteins G_N , G_C , and *N* (Figure 13 D). Sucrose gradient-purified UUKV produced from IDE-8 cells reproducibly revealed a titer of 10^8 - 10^9 ffu/ml for individual productions (Figure 13 E). Overall, the tick cell lines IRE/CTVM-19 and IDE-8 both supported persistent UUKV infection. In this part, in addition to mammalian cells, I established protocols to produce UUKV stocks from tick cells with high titers and high purity, important for subsequent experimental procedures such as OMICS analyses and cryo-EM.

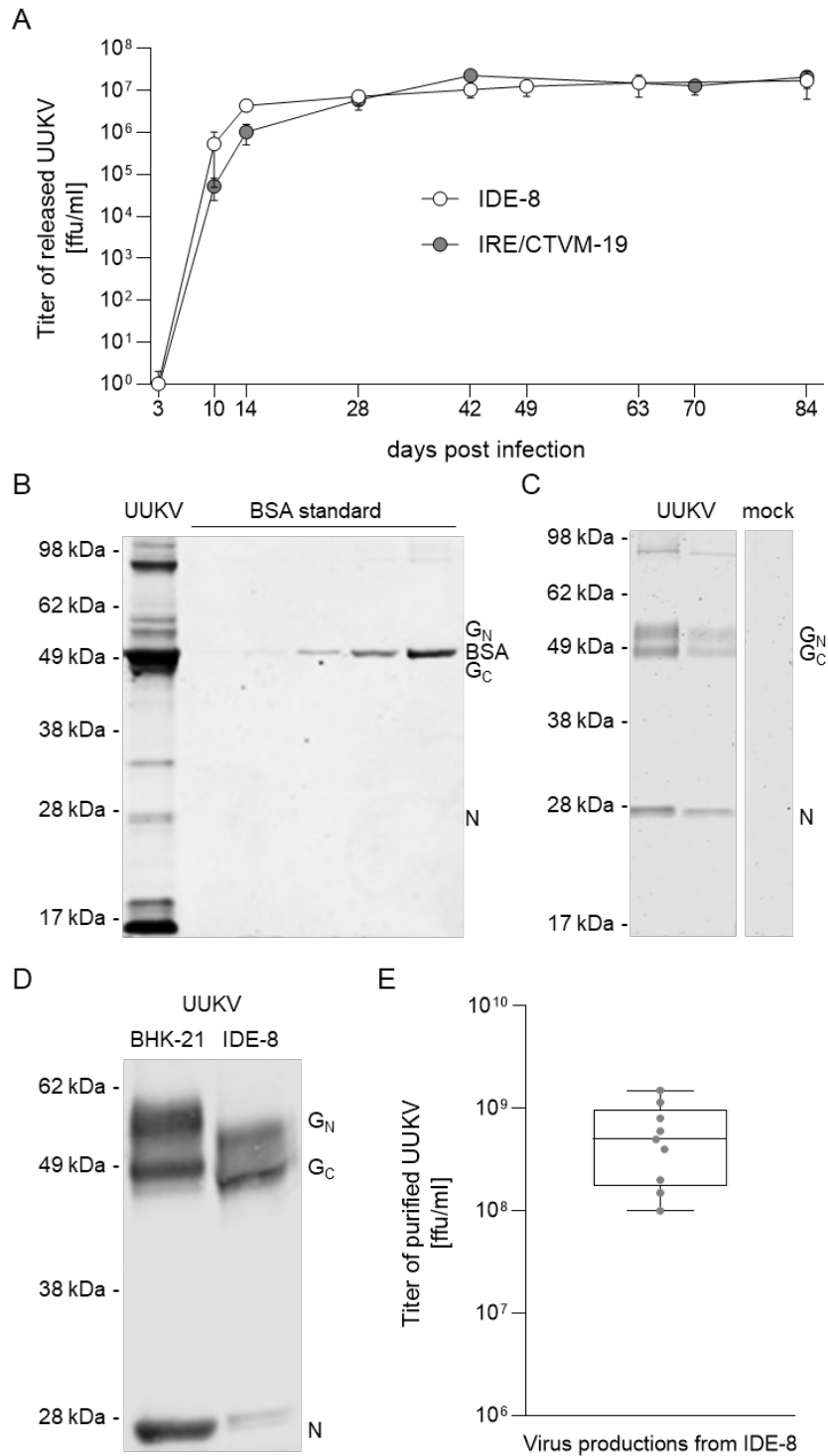


Figure 13. UUKV production from tick-derived IDE-8 cells.

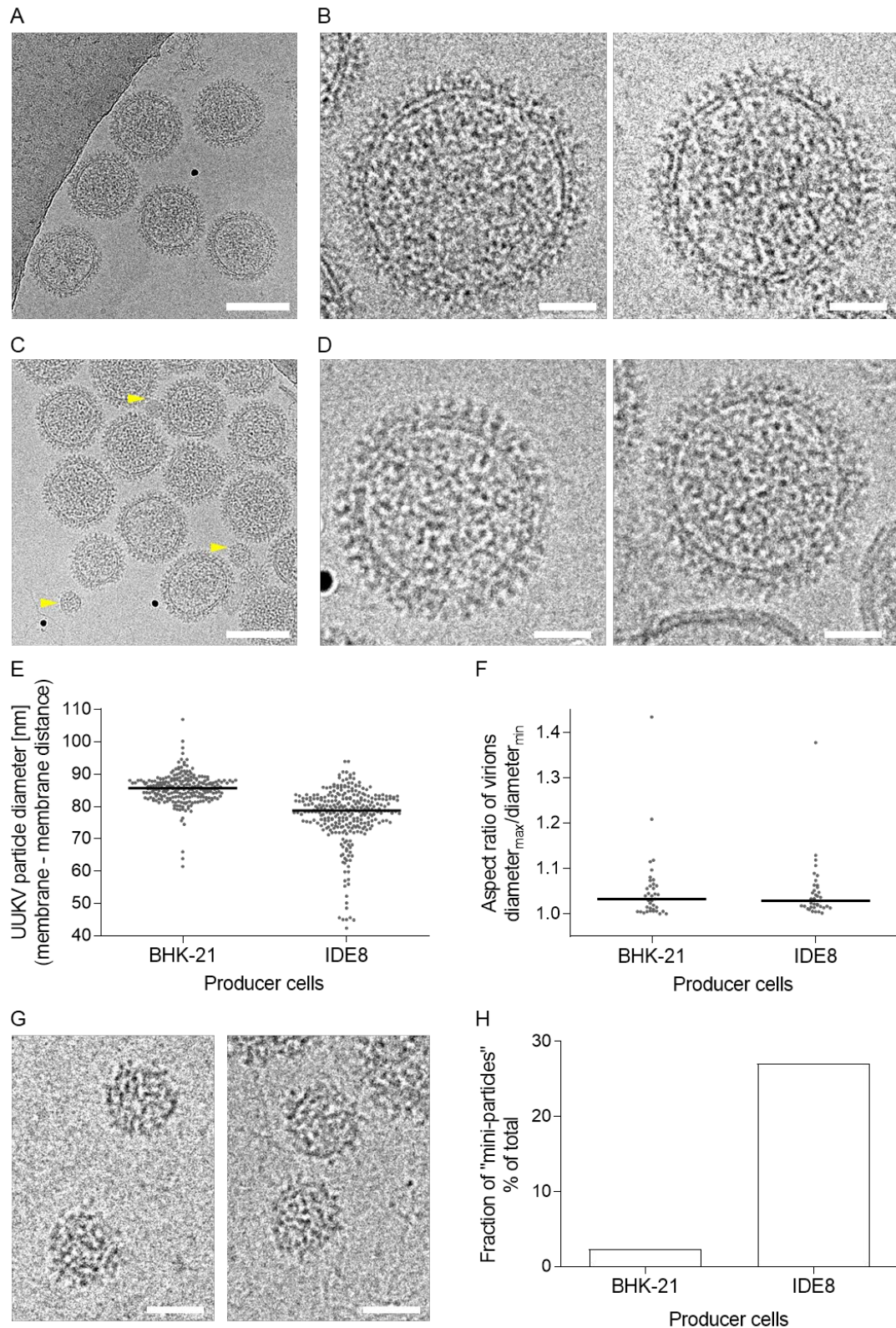
(A) The tick cell lines IDE-8 and IRE/CTVM-19 were infected with UUKV at an MOI of 0.001 and the supernatant was harvested at the indicated days post infection. The infectious supernatant was titrated on BHK-21 cells to assess production of infectious viral particles from the tick cells. (B) UUKV produced from IDE-8 cells was semi-purified through a 25% sucrose cushion and structural viral proteins were visualized by Coomassie blue staining. (C) UUKV produced from IDE-8 cells and semi-purified was then further purified over a sucrose gradient. A milky band containing the virions was extracted and assessed by Coomassie blue staining. Two individual productions and purifications are depicted. Additionally, the supernatant from uninfected cells was purified simultaneously (mock). (D)

Western blotting using the U2 antibody targeting the UUKV proteins G_N, G_C, and N was tested for BHK-21 and IDE-8 cell-derived UUKV particles. (E) Titers of sucrose gradient-purified UUKV stocks were determined on BHK-21 cells. The median is represented and the titers of nine distinct productions are shown as individual data points.

2.2. Cryo-EM analysis of tick and mammalian cell-derived virions

In collaboration with Martin Obr from the Florian Schur group (IST Austria), cryo-EM imaging of fixed purified UUKV particles derived from either mammalian- or arthropod cells was performed (Figure 14 A-D). In line with the above-mentioned increased glycoprotein to nucleoprotein ratio, it appeared that IDE-8 cell-derived virions were more densely decorated with glycoproteins. UUKV particles originating from IDE-8 tick cells exhibited a larger diversity in diameter and were on average smaller in size (Figure 14 E). The diameter was measured from membrane to membrane. UUKV produced in IDE-8 cells had a diameter median of 79 nm, while BHK-21 cell-derived virions were 86 nm in diameter. UUKV particle sphericity was explored by determining the aspect ratio of the longest and shortest membrane to membrane distance of each UUKV particle. The aspect ratios were similar regardless of the origin of producer cells and UUKV particles presented a roughly spherical shape (Figure 14 F).

The viral preparation obtained from IDE-8 cells also contained particles with very small diameters of around 25 nm membrane to membrane distance, hereafter referred to as “mini-particles” (Figure 14 G). They possessed luminal densities which could correspond to nucleic acids and glycoproteins were visible on the particle surface. As the mini-particles were distinct in size and mostly present in the samples obtained from tick cells, they were not included for the particle size quantifications but instead quantified separately (Figure 14 H).



derived UUKV particles. The scale bars correspond to 100 nm (C) and 20 nm (D). Yellow arrows (C) indicate “mini-particles” of approximately 25 nm diameter. (E) Quantification of UUKV particle diameter measured from membrane to membrane along the shortest and longest axes ($n > 120$ virions per sample from one experiment). Individual measurements and the median are depicted. (F) The sphericity of virions was determined by calculating the aspect ratio of the long and short axes of 37 UUKV particles per sample. (G-H) Particles with a diameter of around 25 nm were observed predominantly in IDE-8 cell-derived viral stocks. (G) Representative 2D projection images of mini-particles derived from IDE-8 cells. The scale bar corresponds to 20 nm. (H) The proportion of “mini-particles” from the total amount of particles isolated in a single UUKV preparation in percent.

The glycoprotein coat appears to form a highly ordered lattice on the envelope of IDE-8 cell-derived UUKV particles (Figure 15 A, B). Preliminary subtomogram averaging of glycoproteins of a single virion (~80 nm) produced from IDE-8 cells indicated a hexameric motif with a central cavity on the surface of an UUKV particle (Figure 15 C). This suggested an icosahedron-like arrangement of the viral glycoproteins, reminiscent of the hexameric protrusions found on RVFV particles (160, 161). Further work will be required to determine the exact symmetry and to get representative high-detail structures of virions. In summary, UUKV particles produced in BHK-21 and IDE-8 cells revealed distinct morphological features that remain to be characterized for functional implications in the infectious entry.

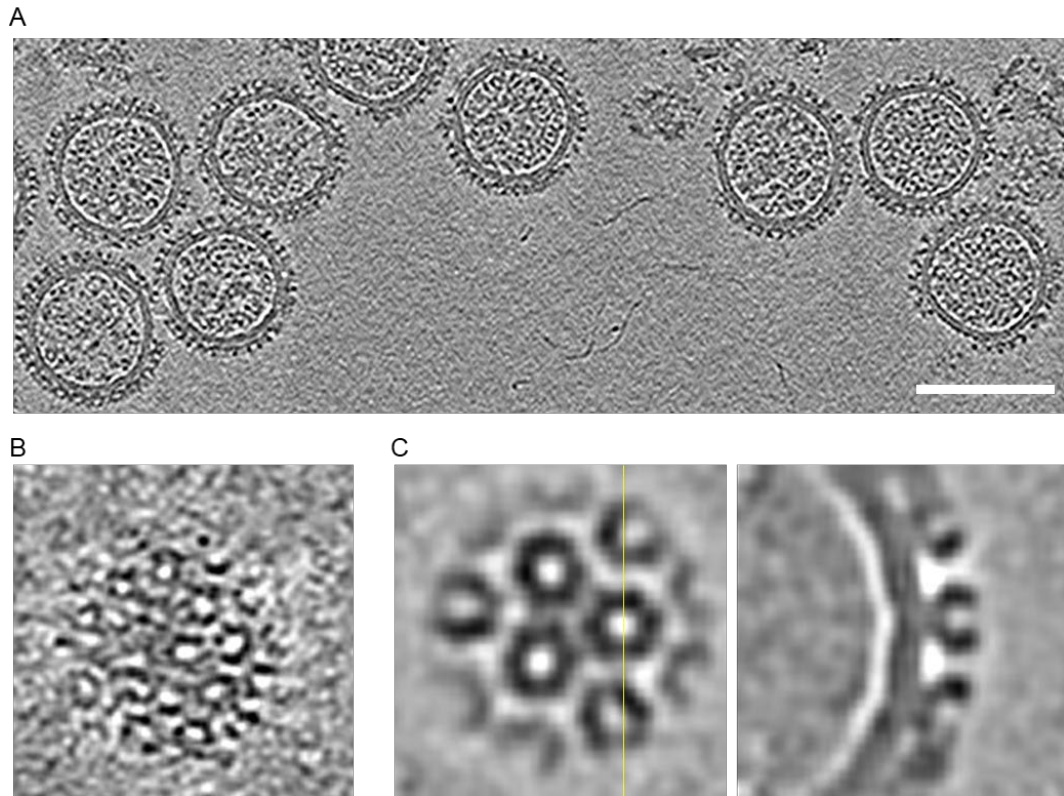


Figure 15. Tomography of one IDE-8 cell-derived UUKV particle indicates that the glycoprotein coat forms ordered hexameric multimers.

(A) A representative slice through a tomogram of IDE-8 cell-derived UUKV particles. The scale bar corresponds to 100 nm. (B) A near-to-surface slice through a tomogram showing the surface of an UUKV particle produced in IDE-8 cells. (C) Subtomogram average of extracted glycoproteins from a single virion. A cross-sectional slice revealing the lattice of densely packed hexameric glycoproteins and a side view along the glycoprotein shell as indicated by the yellow line are depicted. Cryo-electron tomography and subtomogram averaging was performed by Martin Obr (Schur group, IST Austria).

2.3. GBF1 as a proviral host factor of UUKV

As I aimed to decipher the UUKV infection cycle in more detail, the next step was to explore host factors crucial for UUKV infection in mammalian cells. To this end, I focused on BHK-21 cell derived virions in all following experiments. The overarching aim will be to perform similar approaches for UUKV particles produced in tick cells in future projects with the ultimate goal to compare the results with those presented in my PhD thesis. In this section, host proteins interacting with the UUKV glycoproteins were identified in a proteomic MS screening assay performed in collaboration with Gisa Gerold and Lars Kühn (TWINCORE Hannover).

2.3.1. UUKV glycoproteins interact with GBF1

My collaborators carried out UUKV G_N/G_C affinity purification and subsequent label-free MS analysis to identify interaction partners of the viral glycoproteins. The flow of the experiments is depicted in Figure 16 A. Briefly, UUKV was bound to cells, immunoprecipitations with G_N/G_C were performed, and samples were digested and analyzed via liquid chromatography tandem MS (LC-MS/MS). The label-free quantification by delayed normalization and maximal peptide ratio extraction (MaxLFQ) algorithm was applied to compare biological quadruplicates and to evaluate the specificity of the UUKV G_N/G_C interactions (162).

Employing a threshold of Welch's t-test significance, 39 host proteins were shown to be significantly enriched, including the structural UUKV proteins G_N , G_C , N, and L (Figure 16 B). These 39 hits were analyzed by Gene Ontology category cellular component (GOCC) term analysis revealing that 77% of G_N/G_C co-purified and enriched host proteins were membrane annotated (Figure 16 C). Molecular network enrichment analysis using the Ingenuity Pathway Analysis software package (Qiagen) determined "Cellular Assembly and Organization" as the most abundant network. Hence, nine membrane-associated host proteins linked with this network (GBF1, Golgi phosphoprotein 3 (GOLPH3), Golgi phosphoprotein 3 like (GOLPH3L), methionyl-tRNA synthetase (MARS), SEL1L ERAD E3 ligase adaptor subunit (SEL1L), surfeit 4 (SURF4), transportin 3 (TNPO3), trafficking protein particle complex 2 like (TRAPPC2L), and voltage dependent anion channel 2 (VDAC2)) and three proteins with the highest significance in the "Cellular Assembly and Organization" network (endoplasmic reticulum lectin 1 (ERLEC1), HEAT repeat containing 3 (HEATR3), and serum amyloid A like 1 (SAAL1)) were selected for

functional characterization during UUKV infection (Figure 16 D). The results of the Welch's t-test for the viral and the selected proteins are shown in table 2.

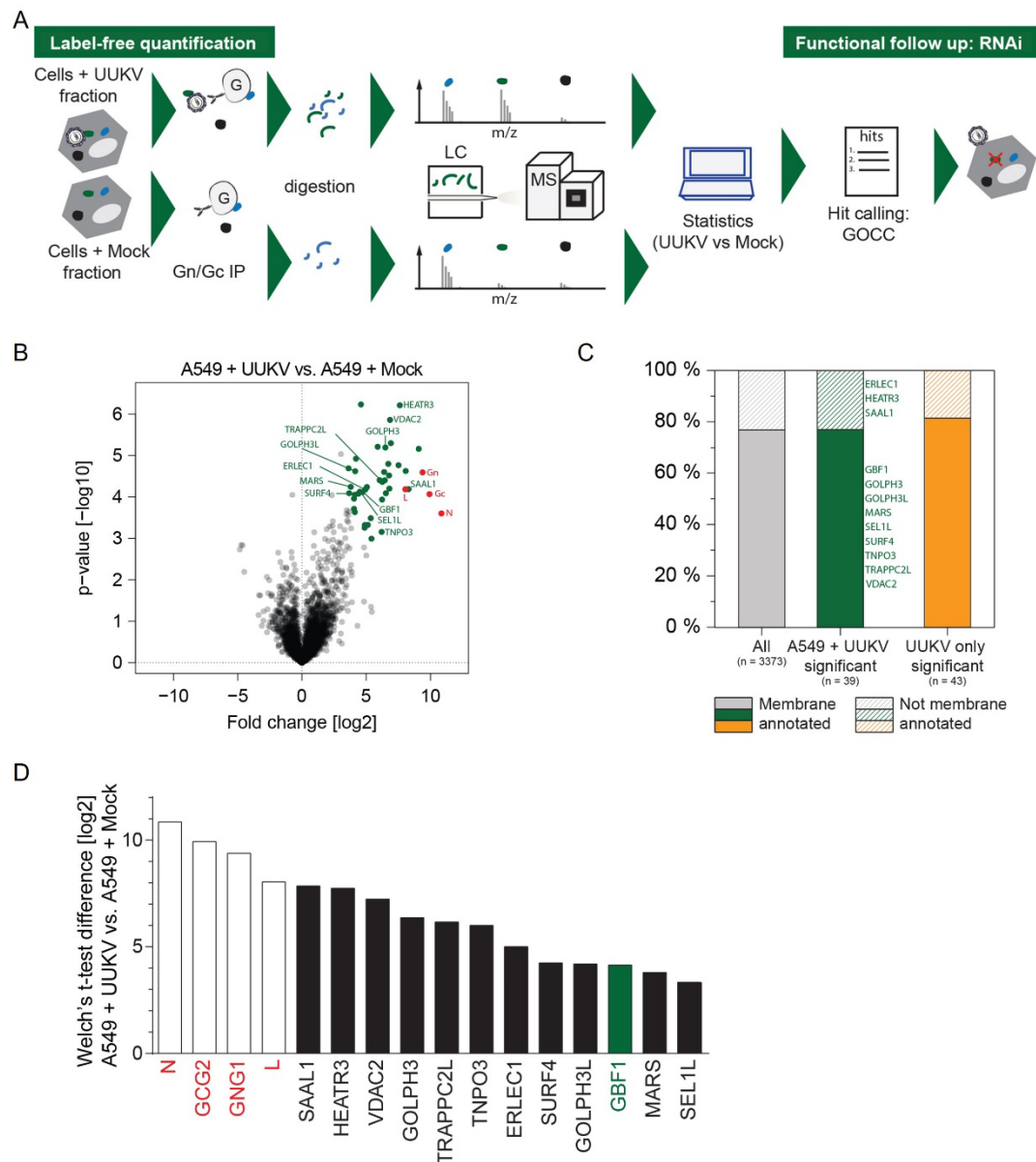


Figure 16. Host proteins interacting with the UUKV glycoproteins are identified by an immunoprecipitation followed by label-free protein mass spectrometry (MS).

Data was jointly obtained in four individual experiments by Gisa Gerold and Lars Kühn (TWINCORE Hannover). (A) Schematic workflow of UUKV host factor detection. (B) A volcano scatterplot revealed 39 proteins that interacted with the UUKV G_N/G_C proteins. All significantly enriched host factors were depicted in green, while the viral proteins G_N , G_C , N , and $RdRp$ (L) were represented in red. (C) Gene Ontology category cellular component (GOCC) term analysis was performed determining that most identified host factors were membrane annotated. (D) Twelve host proteins were chosen for follow up analysis by a small interfering RNA (siRNA) screening approach. The figure was modified from Uckeley, Moeller, et al. 2019 (163).

Table 2. Selected protein hits used for silencing screening approach.

Gene names	Welch's t-test difference	Welch's t-test p-value	Welch's t-test p-value [-log10]
UUKV N	10.86	2.49E-04	3.60
UUKV G_C	9.93	8.54E-05	4.07
UUKV G_N	9.39	2.54E-05	4.59
UUKV RdRp	8.05	6.50E-05	4.19
SAAL1	8.30	6.46E-05	4.19
HEATR3	7.62	6.12E-07	6.21
VDAC2	6.86	1.38E-06	5.86
GOLPH3	6.49	6.39E-06	5.19
TRAPPC2L	6.26	4.33E-05	4.36
TNPO3	6.20	7.70E-04	3.16
ERLEC1	4.94	6.57E-05	4.18
GBF1	4.73	7.57E-05	4.12
SEL1L	4.50	7.50E-05	4.12
SURF4	4.39	8.37E-05	4.08
GOLPH3L	4.14	2.39E-05	4.62
MARS	3.80	5.70E-05	4.24

2.3.2. Silencing of GBF1 reduces UUKV infection

After MS analysis of host factors immunoprecipitated with UUKV G_N/G_C, the role of the twelve proteins ERLEC1, GBF1, GOLPH3, GOLPH3L, HEATR3, MARS, SAAL1, SEL1L, SURF4, TNOP3, TRAPPC2L, and VDAC2 for UUKV infection was further evaluated. A549 cells were first silenced for each of the identified host factors, using two non-overlapping small interfering RNAs (siRNAs) per protein (for the complete siRNA list, see table 3). Infection levels were determined 8 hpi, to limit infection to a single infectious cycle. After immunostaining using an antibody raised against the UUKV N protein, the samples were acquired by flow cytometry as described previously (2.1.1.). Independently of the used siRNA, GBF1 silencing resulted in 50% decreased UUKV infection (Figure 17 A). Additionally, a third non-overlapping siRNA targeting GBF1 was included in western blot experiments which confirmed that silencing of this factor was efficient using each of the GBF1-specific siRNAs (Figure 17 B). Comparing the infection rates in GBF1-silenced and control siRNA transfected cells, a significant reduction of UUKV infection was observed (Figure 17 C). Furthermore, MARS silencing with one of the two applied siRNAs led to decreased UUKV infection (Figure 17 A). ERLEC1 and SEL1L silencing seemed to increase UUKV infection levels marginally (Figure 17 A). It would be interesting to

follow up on the involvement of these proteins in UUKV infection by validating silencing of MARS, ERLEC1, and SEL1L by western blotting and possibly testing the impact of silencing on UUKV infection by using more siRNAs. Collectively, from the siRNA screen, GBF1 appeared as a promising candidate playing a crucial role in UUKV infection.

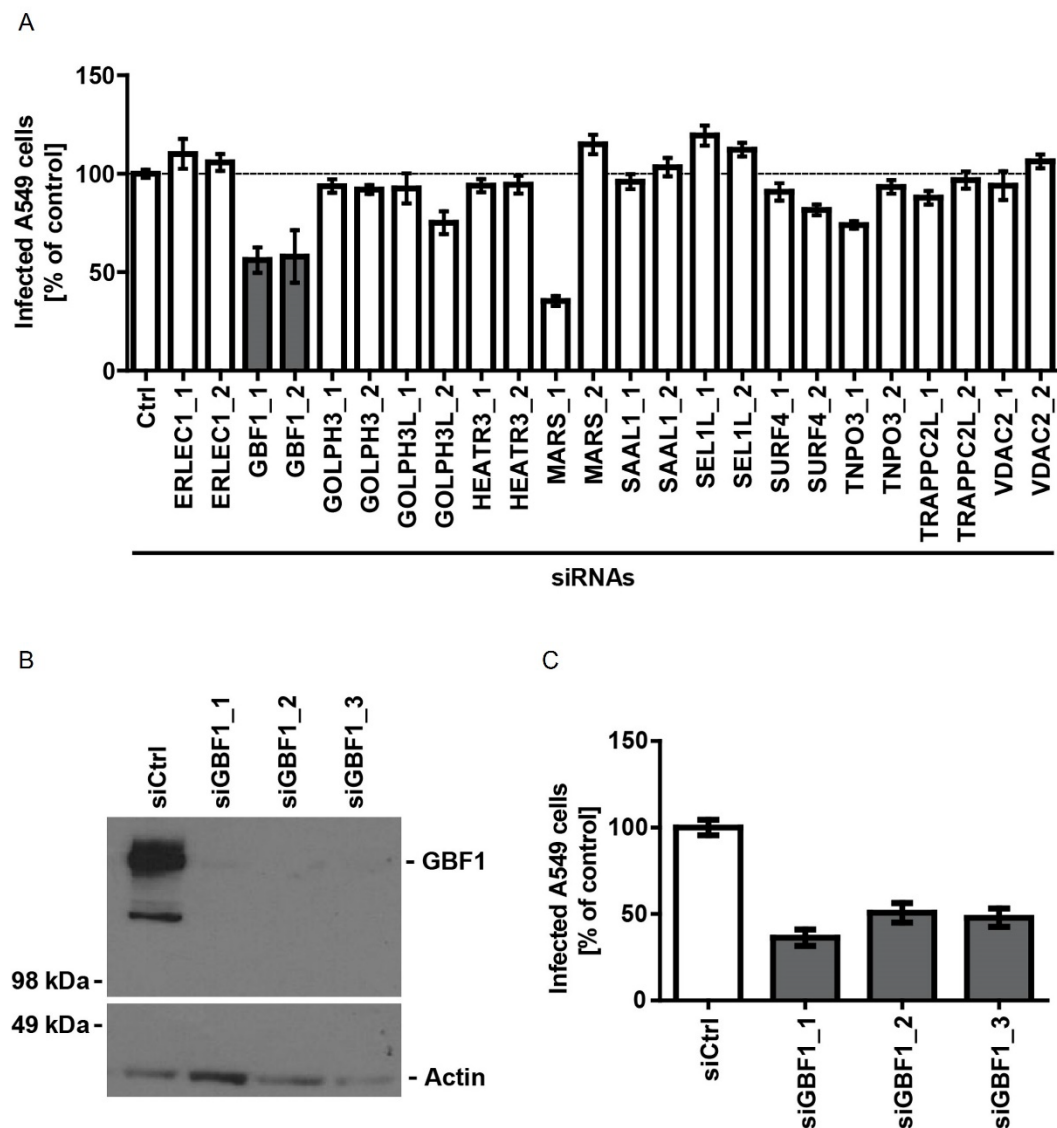


Figure 17. GBF1 silencing reduces UUKV infection in A549 cells.

(A) A549 cells were silenced for twelve potential host factors with each two siRNAs and UUKV infection (MOI ~1) was monitored 8 hpi by flow cytometry. Data was obtained by the bachelor student Claudia Robens. (B) GBF1 silencing was confirmed by western blotting. The experiment was jointly conducted with the rotation student Yannik Voß. (C) UUKV infection reduction was validated in GBF1-silenced A549 using three different siRNAs. Experiments were performed with the rotation student Christian Sommerauer. The figure was published in Uckeley, Moeller, et al. 2019 (163).

2.3.3. GBF1 promotes infection of various RNA viruses

After proving the importance of GBF1 for UUKV infection, I sought to assess whether the host factor also plays a role for other phenuiviruses. Thus, A549 cells silenced for GBF1 were infected with the closely related phenuiviruses RVFV Δ NSs GFP and TOSV. While TOSV infection was monitored by immunofluorescent antibody staining of the structural proteins, infection with RVFV Δ NSs GFP was directly monitored by GFP expression levels. Silencing led to ~ 50% decreased infection for both tested viruses (Figure 18 A, B). The dependence of the positive-stranded RNA togavirus SFV on GBF1 was confirmed after detecting ~ 30% reduced infection levels after GBF1 silencing (Figure 18 C). SFV-infected A549 cells were stained using a primary antibody raised against the viral envelope protein E2.

Golgicide A (GCA), an inhibitor of GBF1-mediated intracellular vesicle trafficking, was used to determine dependency of viral infection on GBF1 activity by a complementary approach. In addition to UUKV infection of A549 cell, I also infected GCA-treated BHK-21 cells to account for cell-type specific artifacts. GCA inhibition of GBF1-dependent vesicle trafficking reduced UUKV infection in both cell lines (Figure 18 D). TOSV infection of A549 cells in the continuous presence of the drug was reduced by ~ 50% (Figure 18 E), while SFV infection levels were decreased by ~ 20% (Figure 18 F). To summarize the results, GBF1 seems to promote the infection of several RNA viruses that all replicate exclusively in the cytoplasm.

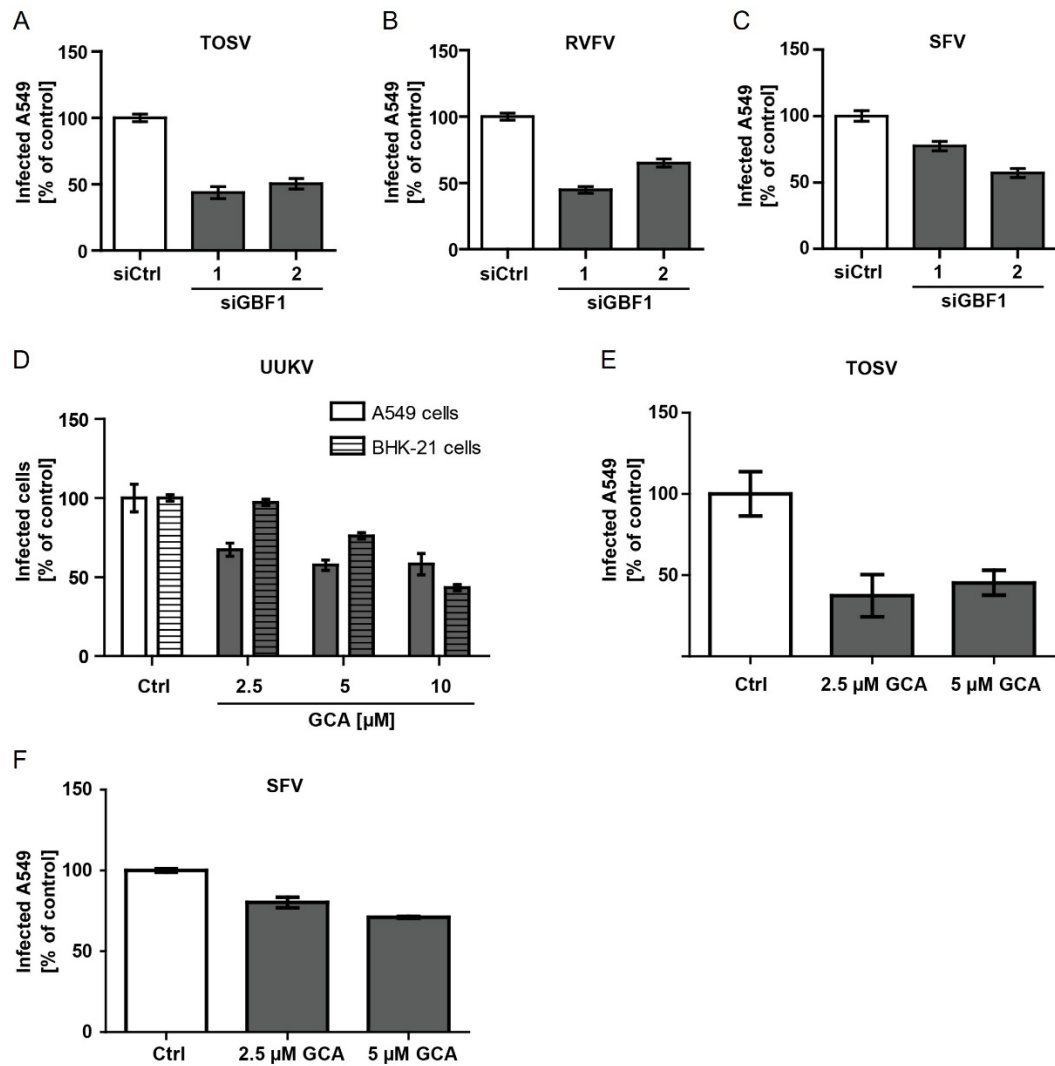


Figure 18. UUKV, TOSV, RVFV, and SFV infection is impaired upon GBF-1 inhibition or silencing.

(A, B, C) A549 cells were silenced for GBF1 by two non-overlapping siRNAs. The effect of GBF1 silencing was assessed on TOSV (A, MOI ~ 2), RVFV Δ NSs GFP (B, MOI ~ 3), and SFV (C, MOI ~ 25) infection. Cells were harvested 8 hpi, fixed in 4% PFA, and acquired after immunofluorescent staining by flow cytometry. Indicated MOIs correspond to titers determined on BHK-21 cells. The results were jointly produced with the rotation students Christian Sommerauer and Martin Kampmann. (D) GBF1 in A549 and BHK-21 cells was inhibited by GCA at the indicated concentrations and UUKV infection levels were monitored by flow cytometry. (E-F) GCA treatment of A549 cells was followed by TOSV (E) and SFV (F) infection and infection levels were explored by flow cytometry. The data was obtained together with the rotation student Martin Kampmann. The figure was adapted from Uckeley, Moeller, et al. 2019 (163).

2.3.4. GBF1 is not involved in infection with DNA viruses or retroviruses

As all arboviruses which were tested in Figure 18 replicate in the cytoplasm, the role of GBF1 for viruses replicating inside the nucleus was further investigated. To assess the GBF1 involvement in the DNA virus human adenovirus type 5 (HAdV-5) infection process, GBF1 was knocked-out (KO) using the clustered regularly interspaced short palindromic repeats (CRISPR)/CRISPR-associated protein 9 (Cas9) system. By flow cytometry no difference of HAdV-5 infection in HEK 293T cells could be detected upon GBF1 KO (Figure 19 A). Moreover, the role of GBF1 was also examined for infection with the retrovirus HIV-1. Analysis of GCA-treated TZM-bl cells indicated an unaltered secretion of infectious HIV-1 particles (Figure 19 B). The reverse transcriptase inhibitor efavirenz inhibited productive HIV-1 infection and served as a positive control.

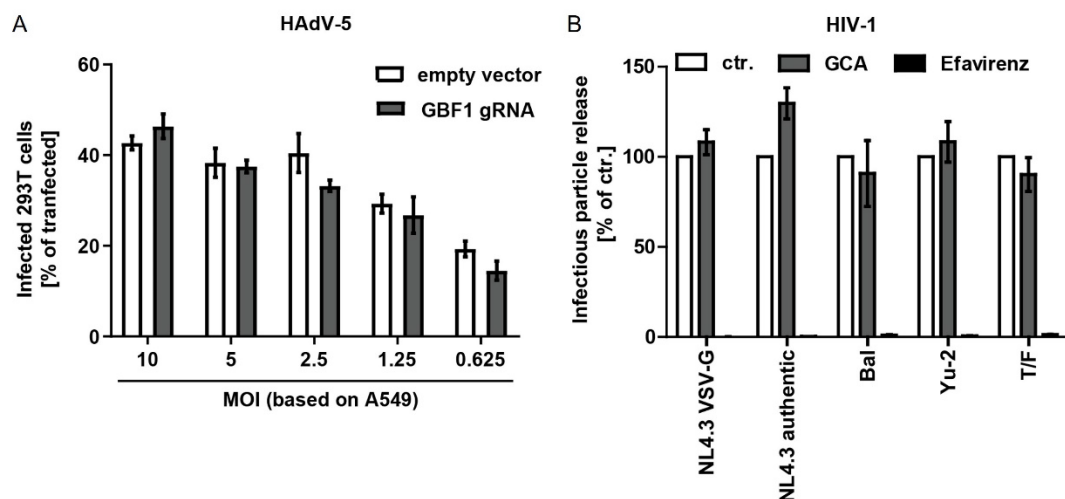


Figure 19. HAdV-5 and HIV-1 do not rely on GBF1 for infection.

(A) The effect of GBF1 knockout in HEK293T cells was investigated for HAdV-5 infection. As a negative control, an empty vector was transfected. Infection levels were quantified by flow cytometry 48 hpi. The experiments were performed by Annasara Lenman (TWINCORE Hannover). (B) VSV-G-pseudotyped HIV-1 NL4.3 GFP (NL4.3 VSV-G), HIV-1 NL4.3 (NL4.3 authentic), HIV-1 Bal strain (Bal), HIV-1 isolate Yu-2 (Yu-2), and the transmitted/founder strain CHO.77t (T/F) were employed to infect TZM-bl cells for 48 h. TZM-bl cells were treated with GCA (2.5 μ M), with efavirenz (20 nM), or with the solvent DMSO as a negative control. Infectious particle release from drug-treated cells was assessed by flow cytometry. Results were produced by Vania Passos (TWINCORE Hannover). The figure was adapted from Uckeley, Moeller, et al. 2019 (163).

2.3.5. UUKV replication and viral particle release rely on GBF1

I previously showed that GBF1 is important for the phenuiruses UUKV, RVFV, and TOSV, as well as for the togavirus SFV. In order to further elucidate which step of UUKV infection is influenced by GBF1, GBF1 was silenced in target cells and specifically analyzed different individual infection steps, namely virus entry, replication, and egress (Figure 3). UUKV particles were fluorescently labeled with AF488 (UUKV-AF488) as described in section 2.1.2. and bound to A549 cells on ice to prevent internalization (64). After 2 h unbound virions were washed away, and UUKV-AF488 particles bound to target cells were monitored by flow cytometry. No difference in binding capacity was revealed upon GBF1 silencing in target cells (Figure 20 A).

Following the entry route of UUKV, uptake of the virus into the siRNA-treated A549 cells was assessed next. After UUKV-AF488 binding on ice, A549 cells were incubated at 37°C to allow virus endocytosis (52, 64). Afterwards trypan blue was used to quench AF488 signal on the outside of the cell. This enabled to discriminate between bound and internalized UUKV particles by a flow cytometry-based assay (Figure 20 B). As trypan blue is not cell permeable, the fluorescent signal of already internalized labeled virions did not change. I calculated the fraction of internalized UUKV particles from the total bound particles showing that the uptake of UUKV into A549 cells remained unaltered upon GBF1 silencing (Figure 20 C).

To delineate the effect of GBF1 during endocytic trafficking and fusion, I performed an assay where viral fusion was forced at the plasma membrane by adding a low pH buffer. Thereby endocytic trafficking was bypassed. Additionally, endosomal fusion of UUKV was inhibited by applying 50 mM NH₄Cl which prevents acidification of endosomes during maturation. Uncoupling trafficking of UUKV particles in the endosomes from infection did not change the effect of GCA, suggesting that GBF1 was not involved in UUKV trafficking (Figure 20 D).

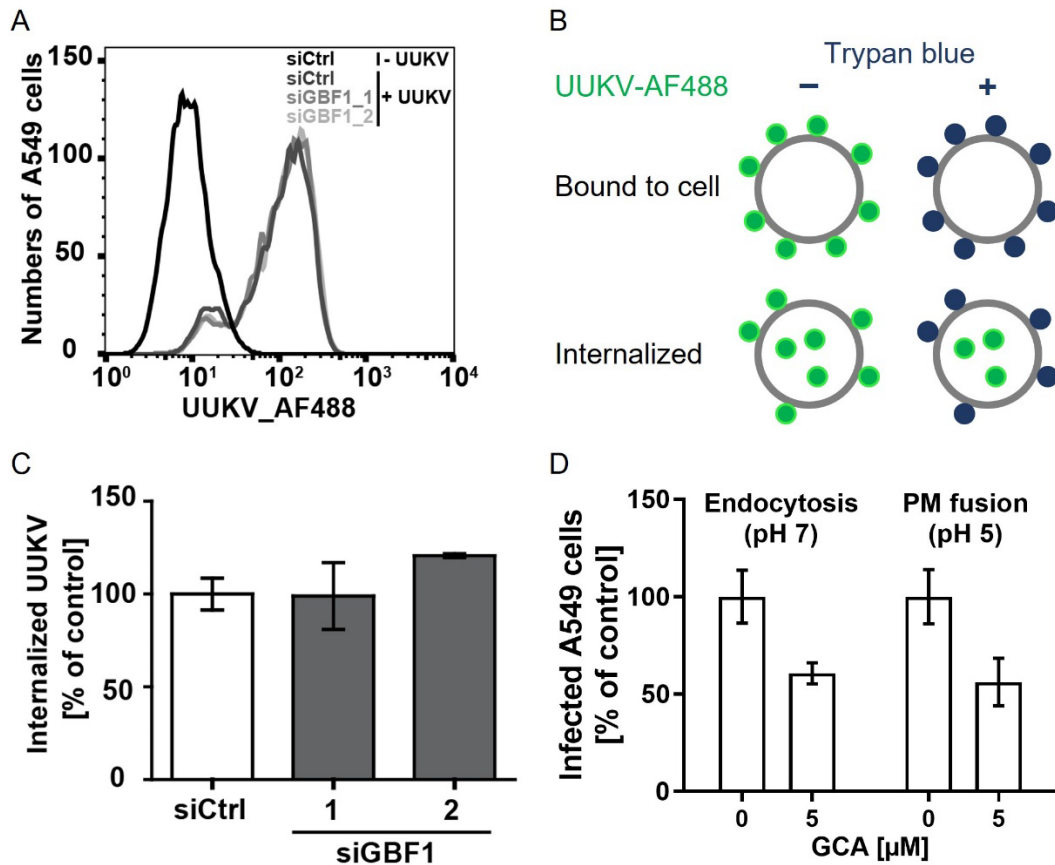


Figure 20. GBF1 is not involved in UUKV entry.

(A) Fluorescently labeled UUKV (UUKV-AF488) was bound to GBF1-silenced A549 cells on ice for 2 h and virus binding was assessed by flow cytometry. Data was obtained by the bachelor student Claudia Robens. (B, C) After binding to GBF1-silenced A549 cells, UUKV-AF488 internalization was enabled for 30 min at 37°C. Trypan blue was applied to quench fluorescence on the cell surface (*i.e.*, cell surface-bound UUKV-AF488), while the fluorescent signal of internalized particles was not quenched. (C) Using the mean fluorescence intensities of each sample \pm trypan blue, the fraction of internalized virions was calculated. (D) To assess the role of GBF1 in trafficking and fusion of UUKV, virus trafficking across the endocytic route was bypassed by low pH treatment. Applying a buffer with pH 5 to virus particles bound to the plasma membrane (PM) for 90 s at 37°C, leads to rapid UUKV fusion directly at the plasma membrane. Adding of NH₄Cl prevents endosomal acidification and thereby hampers UUKV fusion from late endosomal compartments (64). Results were normalized to treatment with 0 μ M GCA and values indicate means \pm SEM from two independent infection assays. The figures 20 A and C were published in Uckeley, Moeller, et al. 2019 (163).

To assess whether GCA treatment hampers UUKV replication, I developed a minigenome system as a replication model. Based on the previously published reverse genetics system for UUKV (150), BHK-21 cells were transfected with two plasmids containing the full length anti-genomic RNA segments S or L of UUKV under the control of the cellular Pol I promoter (Figure 21 A). Segment S encoded the nucleoprotein N and was genetically engineered to express GFP instead of the non-structural NSs protein (Figure 21 B) and the L segment coded for the RdRp. The M segment was omitted as it encodes the glycoproteins important for viral assembly and propagation (30). As the RdRp and the N protein are crucial for viral replication, expression plasmids coding for the RdRp and the nucleoprotein N under the control of a CMV promoter were co-transfected to initiate transcription and replication (Figure 21 A). Thereby, transcription and replication of the anti-genomic UUKV RNAs into messenger RNAs (mRNAs) could be monitored by GFP expression using flow cytometry in this assay. No GFP signal was detected in the absence of the RdRp expression plasmid, confirming the assay's specificity to monitor UUKV replication exclusively. In BHK-21 cells treated with 10 μ M GCA, the GFP signal decreased by \sim 3-fold compared to the solvent control (Figure 21 C).

To evaluate the role of GBF1 for UUKV particle assembly and release, a UUKV virus-like particle (VLP) assay was adapted to solely focus on assembly and release, without the influence of viral replication. Expression plasmids for the glycoproteins and the N protein were transfected into BHK-21 cells, and GCA was added 24 h post transfection (hpt) to inhibit GBF1 activity. After \sim 17 h GCA treatment, the UUKV glycoproteins present inside the cells (cell lysates) versus outside the cells (released into supernatant) were evaluated by western blot analysis (Figure 21 D). In GCA-treated cell, less glycoproteins were released compared to solvent-treated cells. Taken together, these assays revealed that GBF1 did not play a role for UUKV entry but rather in UUKV replication, assembly, and egress.

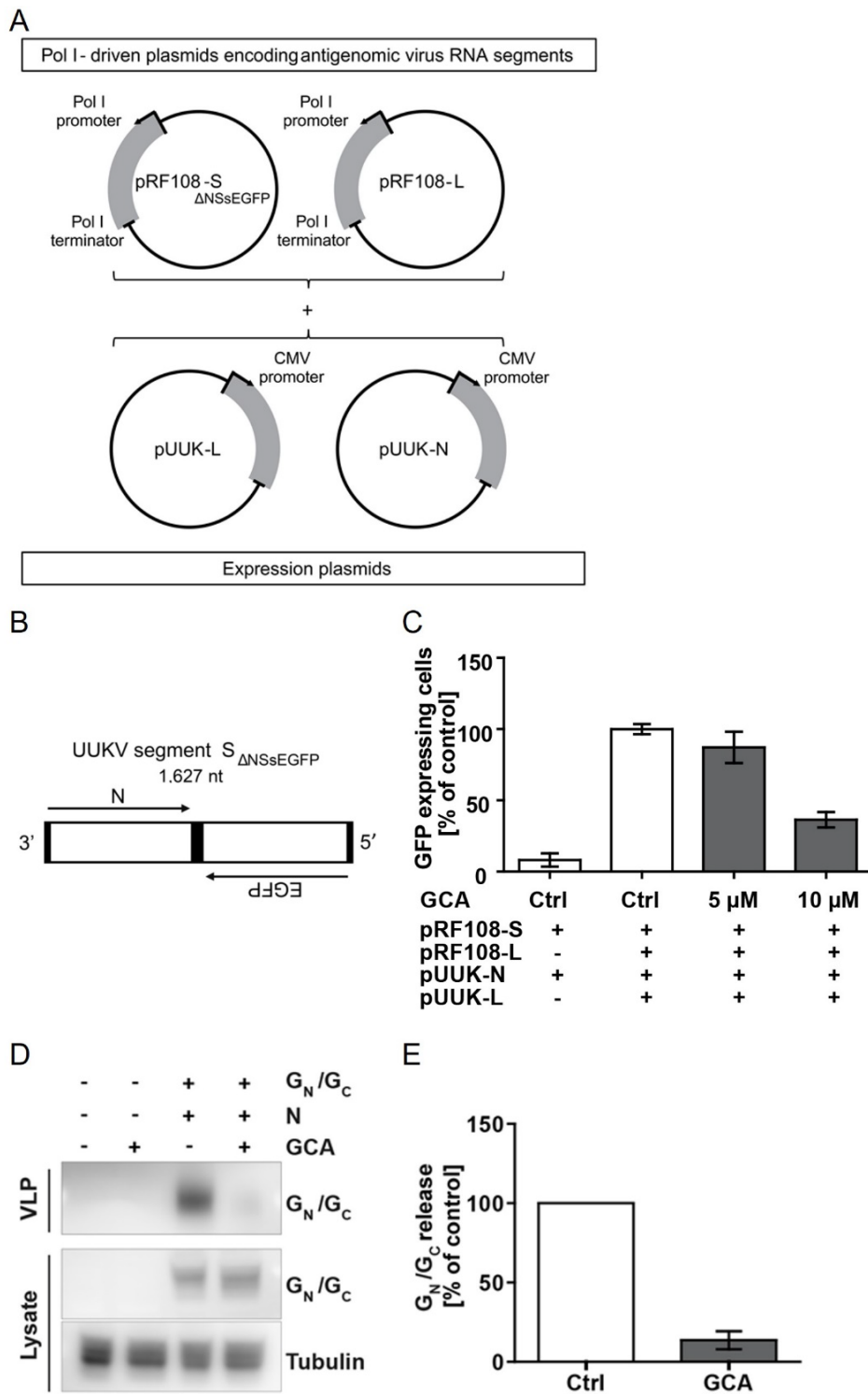


Figure 21. GBF1 plays a role during UUKV replication and particle release

(A) The previously published reverse genetics system for UUKV (150) was adapted to obtain a replication model for UUKV. (B) The UUKV RNA segment S was depleted of NSs and GFP was introduced to enable a simple readout for replication. (C) The adapted reverse genetics system from (A) was employed to assess UUKV replication in the presence and absence of GCA. (D) Western blot analysis monitored UUKV glycoproteins inside cell lysates and released into the cytoplasm after 10 μ M GCA treatment. (E) UUKV glycoprotein release from (D) was quantified. (D-E) Experiments were performed by Emma Nilsson (Overby group, Umeå University). The figure was adapted from Uckeley, Moeller, et al. 2019 (163).

2.4. GlcCer is required for UUKV binding to target cells

2.4.1. UUKV infection increases HexCer levels

As mentioned in the introduction (1.7.), besides host proteins, lipids in enveloped viruses and target cells can also play a role during viral infections. The above characterized host factor for UUKV, GBF1, is present in the Golgi network where UUKV buds and acquires its host-derived lipid envelope (82, 91). From these observations, we sought to investigate the lipidome of mammalian cell-derived UUKV particles and of UUKV-infected BHK-21 cells by lipid MS through a collaboration with Britta Brügger (BZH Heidelberg).

The lipid expression of uninfected BHK-21 cells was compared to UUKV-infected cells and to complete virions (Figure 22 A). BHK-21 cells were infected with UUKV at an MOI of 0.1 for 48 h to ensure several infectious rounds as one round of UUKV infection takes roughly 7 h in BHK-21 cells (64). Uninfected and infected cells were then scraped off in methanol (MeOH) and total cell lysates were analyzed by lipid MS without further membrane fractionation. The phospholipids PC, PE, PS, PI, phosphatidylglycerol (PG), phosphatidic acid (PA), and lysophosphatidylcholine (LPC) had similar expression levels in UUKV-infected and not infected cells. The levels of cholesterol, SM, and the neutral lipids cholesteryl ester (CE), diacylglycerol (DAG), and triacylglycerol (TAG) also did not change upon UUKV infection.

Comparing HexCer levels in UUKV-infected to uninfected BHK-21 cells, I observed a ~ 5-fold enrichment in infected cells (Figure 22 A). Due to their structural similarities, in the lipid MS analysis, the HexCers GlcCer and GalCer could not be distinguished. They are both lipid intermediates that are further metabolized to complex GSLs. The enrichment of HexCer after UUKV infection was of particular significance, as the neighboring intermediates in this pathway, namely Cer upstream and dihexosylceramide (Hex2Cer) downstream were not altered upon infection (Figure 8, Figure 22 A).

Exploring the lipidome of UUKV-infected BHK-21 cells (Figure 22 B), I could show that with ~ 83%, phospholipids together with LPC and SM made up the biggest fraction of lipids present in the infected cells. Cholesterol constituted to ~ 10% of the cellular lipidome, while neutral lipids accounted for ~ 4%. Cer and Hex2Cer remained below 1% in UUKV-infected BHK-21 cells, while HexCer was increased to ~ 3%. Collectively, these data demonstrate an upregulation of HexCer in BHK-21

cells upon UUKV infection, suggesting that UUKV infection interferes with the GSL metabolism pathway.

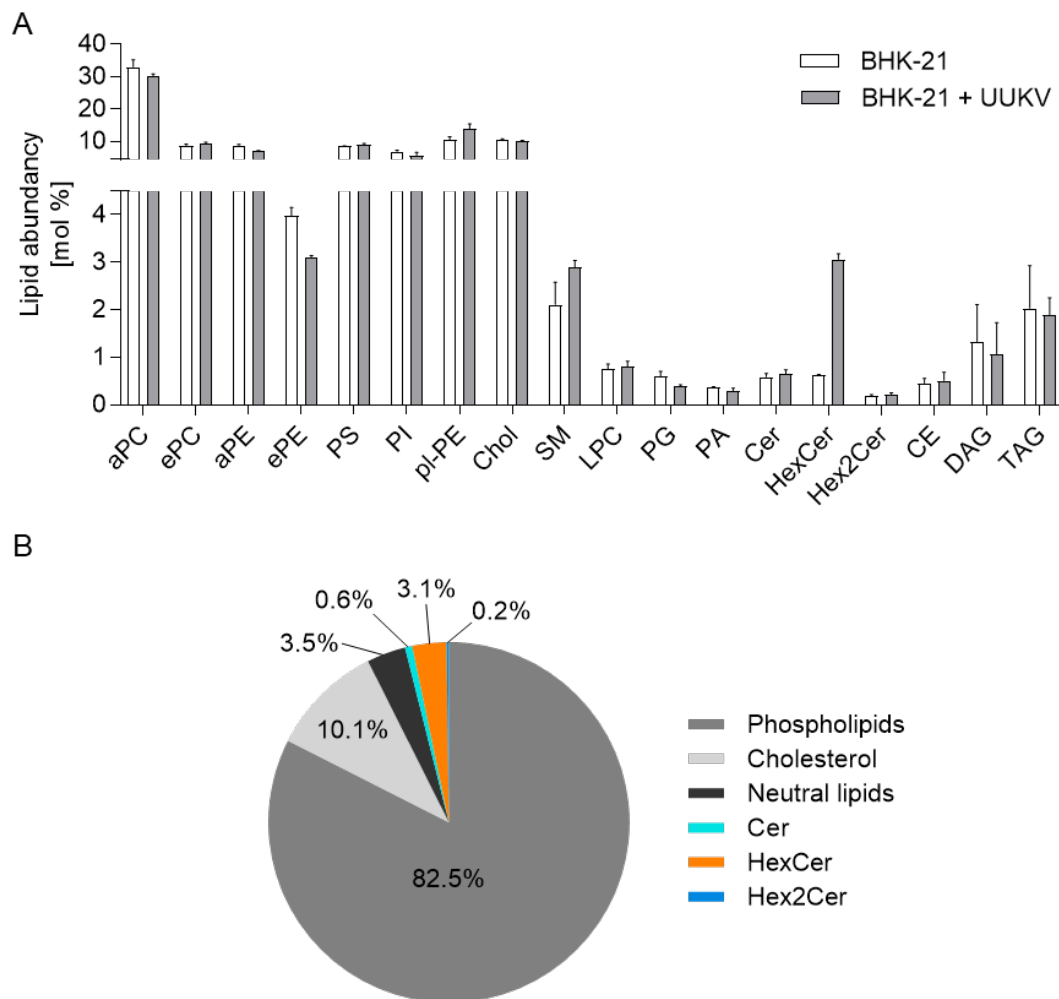


Figure 22. Lipidome analysis of UUKV-infected BHK-21 cells reveals enriched HexCer levels.

Lipid MS was performed by Magalie Mazelier in collaboration with Britta Brügger (BZH Heidelberg). (A) In a lipidomic screening approach, uninfected BHK-21 cells were compared to UUKV infected BHK-21 cells. (B) Lipid distributions in infected BHK-21 cells from A were depicted in a pie chart. Phospholipids include PC, PE, PS, PI, PG, PA, LPC, and additionally SM, while neutral lipids contain CE, DAG, and TAG.

aPC, diacyl phosphatidylcholine; ePC, ether phosphatidylcholine; aPE, diacyl phosphatidylethanolamine; ePE, ether phosphatidylethanolamine; PS, phosphatidylserine; PI, phosphatidylinositol; plPE, plasmalogen phosphatidylethanolamine; Chol, cholesterol; SM, sphingomyelin; LPC, lysophosphatidylcholine; PG, phosphatidylglycerol; PA, phosphatidic acid; Cer, ceramide; HexCer, hexosylceramide; Hex2Cer, dihexosylceramide; CE, cholesteryl ester; DAG, diacylglycerol; TAG, triacylglycerol.

2.4.2. UUKV infection is reduced upon silencing or inhibition of UGCG

Given that HexCer was enriched in the UUKV-infected cells, I next explored the role of GlcCer during UUKV infection. GlcCer is a HexCer that serves as the primary precursor for membrane GSLs. GlcCer is synthesized and further metabolized at the Golgi apparatus, which involves UGCG, the enzyme synthesizing GlcCer. In the first approach, I aimed to silence UGCG to assess the effect of GlcCer depletion for UUKV infection. To this end, I designed two non-overlapping siRNAs and reversely transfected BHK-21 cells 72 h before infection. Silencing of UGCG was confirmed via western blot analysis of transfected cells stained with an antibody targeting UGCG (LS Bio) showing a reduction of UGCG expression by more than 60% (Figure 23 A, B). Consistent with the silencing of UGCG, dot blot analysis of GlcCer in the siRNA-treated cells using an antibody targeting the lipid (Antibody Research) confirmed a decrease of GlcCer expression by at least 60% (Figure 23 C, D).

After proving successful silencing of GlcCer, I infected the siRNA-treated BHK-21 cells three days post transfection at an MOI of 0.1. Infected cells were fixed 24 hpi and then stained with an antibody recognizing the UUKV N protein. Infection levels were evaluated by flow cytometry revealing that UUKV infection of UGCG silenced cells decreased by roughly 60% compared to the control transfected cells (Figure 23 E). To summarize, these results indicate a role for UGCG and/or the lipid GlcCer during UUKV infection.

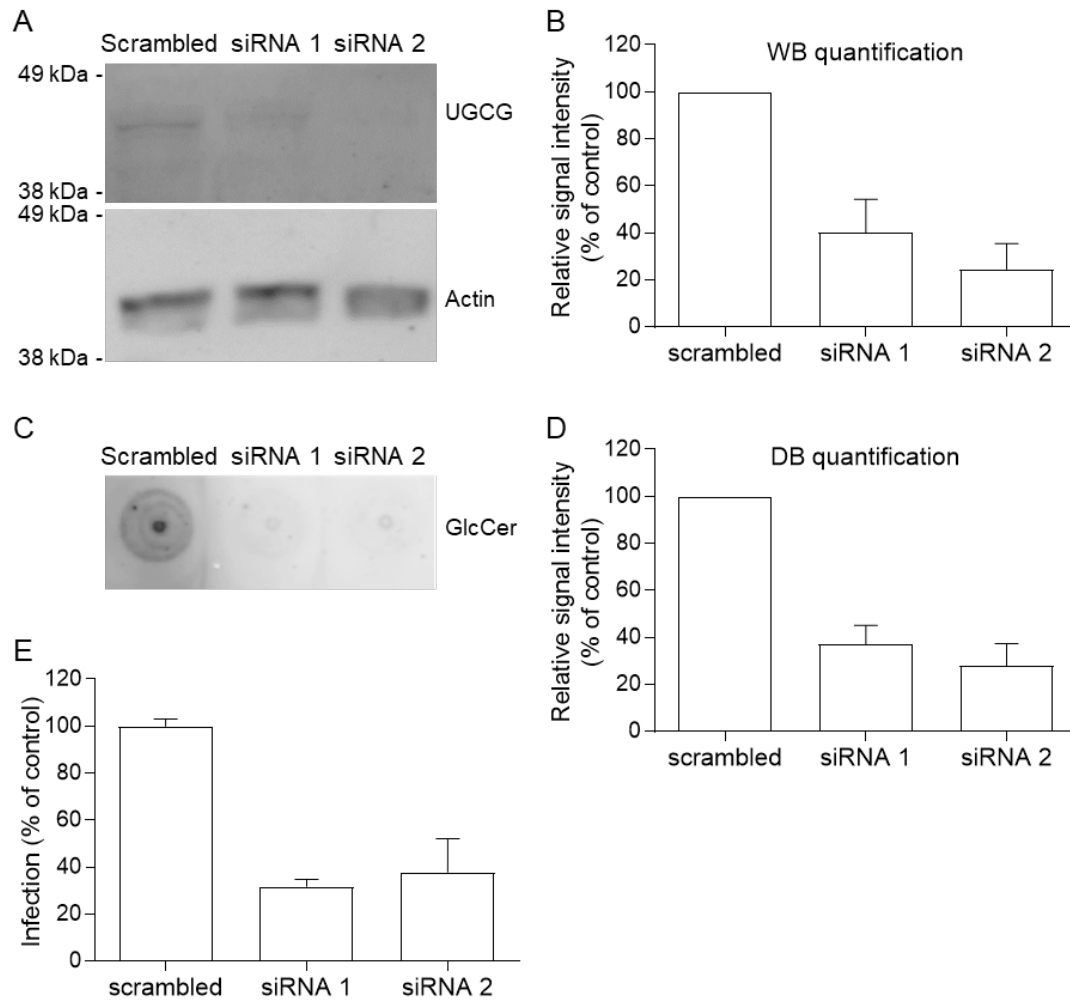


Figure 23. Silencing of glucosylceramide synthase (UGCG) reduced UUKV infection in BHK-21 cells.

BHK-21 cells were reversely transfected with two non-overlapping siRNAs targeting UGCG and a non-targeting siRNA (scrambled) served as a control. (A, B) siRNA silencing of UGCG was confirmed by western blotting (WB) and semi-quantified using the Image Studio Lite software (LiCOR). (C, D) Dot blot (DB) analysis of GlcCer upon UGCG silencing in BHK-21 cells was performed and semi-quantified with the Image Studio Lite software (LiCOR). As in B and D the individual experiments were performed in technical triplicates, no SEM could be depicted for the scrambled siRNA after normalization. (E) 72 hours post transfection (hpt), BHK-21 cells were infected with UUKV at an MOI of 0.1. UUKV infection levels were assessed 24 hpi by flow cytometry in UGCG-silenced BHK-21 cells.

To further document the importance of UGCG and GlcCer for UUKV infection, I used a complementary approach where pharmacological inhibition of UGCG was followed by UUKV infection. DL-*threo*-1-Phenyl-2-palmitoylamino-3-morpholino-1-propanol (PPMP) is a Cer analogue that specifically inhibits UGCG activity (164–166). First, I determined the maximal concentration of PPMP for which the drug does not induce cytotoxicity in target cells. For this purpose, I measured the release of lactate dehydrogenase (LDH) upon PPMP treatment. LDH is released into the supernatant of dying cells and can be quantified in a colorimetric assay (CytoTox 96® Non-Radioactive Cytotoxicity Assay, Promega). Up to 5 μ M PPMP did not induce cytotoxicity in BHK-21 or A549 cells, while 50 μ M PPMP induced LDH release, serving as a positive control in this assay (Figure 24 A). Therefore, in all following experiments, I limited the concentration of PPMP to a maximum of 5 μ M.

I then aimed to determine whether the non-cytotoxic concentrations were sufficient to block UGCG activity. To this end, cells were subjected to 2.5 μ M and 5 μ M PPMP for 16 h and subsequently exposed to UUKV at an MOI of 0.1 in the continuous presence of the drug. The infected cells were again assessed by lipid MS analysis 24 hpi. PC, PE, PS, PI, PA, LPC, cholesterol, and SM levels remained unaltered upon PPMP treatment, demonstrating that PPMP treatment did not unspecifically alter the host cell lipidome (Figure 24 B). Moreover, I could confirm the downregulation of HexCer levels in infected BHK-21 cells already after 2.5 μ M PPMP treatment (Figure 24 C). Additionally, GlcCer expression was detected with the anti-GlcCer antibody in dot blot analysis after PPMP treatment, verifying decreased GlcCer levels upon UGCG inhibition (Figure 24 D, E). Together, these results indicate that the HexCer enrichment upon UUKV infection (Figure 22), can be counteracted by the GlcCer-specific inhibitor UGCG. This observation further indicated an enrichment of GlcCer upon UUKV infection.

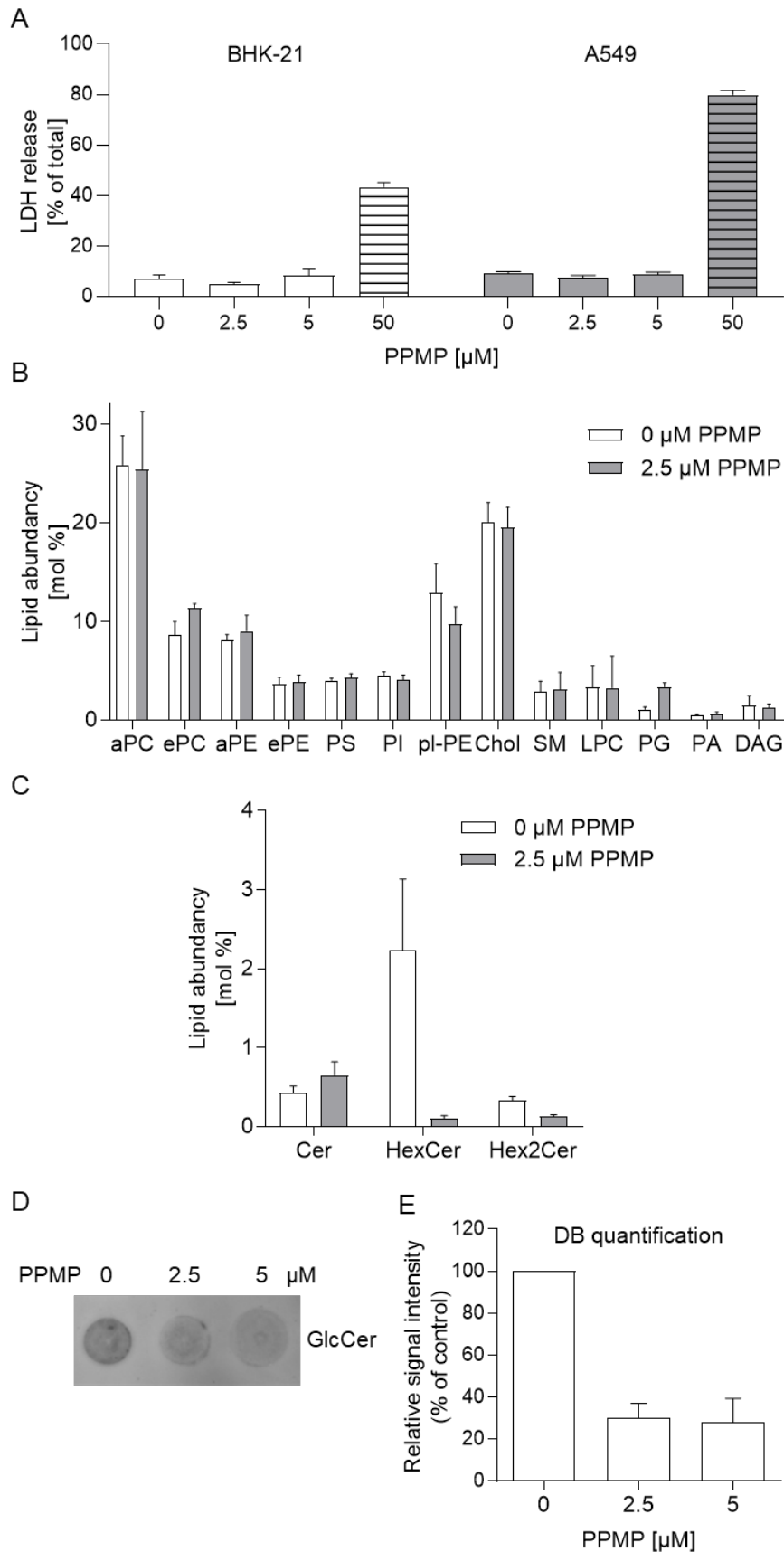


Figure 24. Blocking GlcCer metabolism by inhibiting UGCG decreases HexCer levels after UUKV infection.

(A) The lactate dehydrogenase (LDH) release was measured in BHK-21 and A549 cells after treatment with up to 5 μ M PPMP. The lined bars represent positive controls with a

high concentration of PPMP, which induces LDH release and was not used for follow-up assays. The experiments were performed in two replicates. (B, C) Lipid MS analysis of UUKV-infected cells after 2.5 μ M PPMP treatment. Lipid MS results were obtained by Britta Brügger and Christian Luchtenborg (BZH Heidelberg). (D, E) Dot blot analysis of GlcCer was performed in PPMP-treated and UUKV-infected BHK-21 cells. As in E the individual experiments were performed in technical monoplicates, no SEM could be depicted for the control treatment after normalization.

After validating reduced GlcCer levels in UUKV-infected BHK-21 cells after PPMP treatment, the next step was to assess whether UGCG inhibition alters UUKV infection. PPMP-treated BHK-21 cells were infected with UUKV at an MOI of 0.1 for up to 24 h before flow cytometric analysis of infection levels (Figure 25 A). UUKV infection was decreased by PPMP treatment in a dose-dependent manner. Similar results were obtained in A549 cells, suggesting that the dependence of UUKV on GlcCer for infection was not limited to BHK-21 cells (Figure 25 B). Furthermore, I tested the effect of N-[2-hydroxy-1-(4-morpholinylmethyl)-2-phenylethyl]-decanamide (PDMP), another Cer analogue hampering UGCG activity, on UUKV infection (Figure 25 C). Consistent with the results obtained using PPMP, UUKV infection in BHK-21 cells was reduced with increasing concentrations of PDMP.

To complete the previous approach, I assessed the effect of the UGCG inhibitors N-Butyldeoxynojirimycin (NB-DNJ) and N-Butyldeoxygalactonojirimycin (NB-DGJ) on UUKV infection. In contrast to the ceramide analogues PPMP and PDMP, NB-DNJ and NB-DGJ are two glycan analogues that inhibit UGCG activity (167–169). When BHK-21 cells were pretreated with NB-DNJ or NB-DGJ for 24 h prior to the exposure to UUKV for 24 h, both glycan analogues inhibited UUKV infection in a dose-dependent manner (Figure 25 D).

From the four different inhibitors of UGCG tested here, all of them reduced UUKV infection to a similar extent. For this reason, PPMP was used for follow-up experiments targeting to explore the role of GlcCer on the viral envelope. Although it cannot be completely excluded that GalCer might contribute to UUKV infection, my data supports the view that the major effects of HexCer enrichment upon UUKV infection can be attributed to GlcCer.

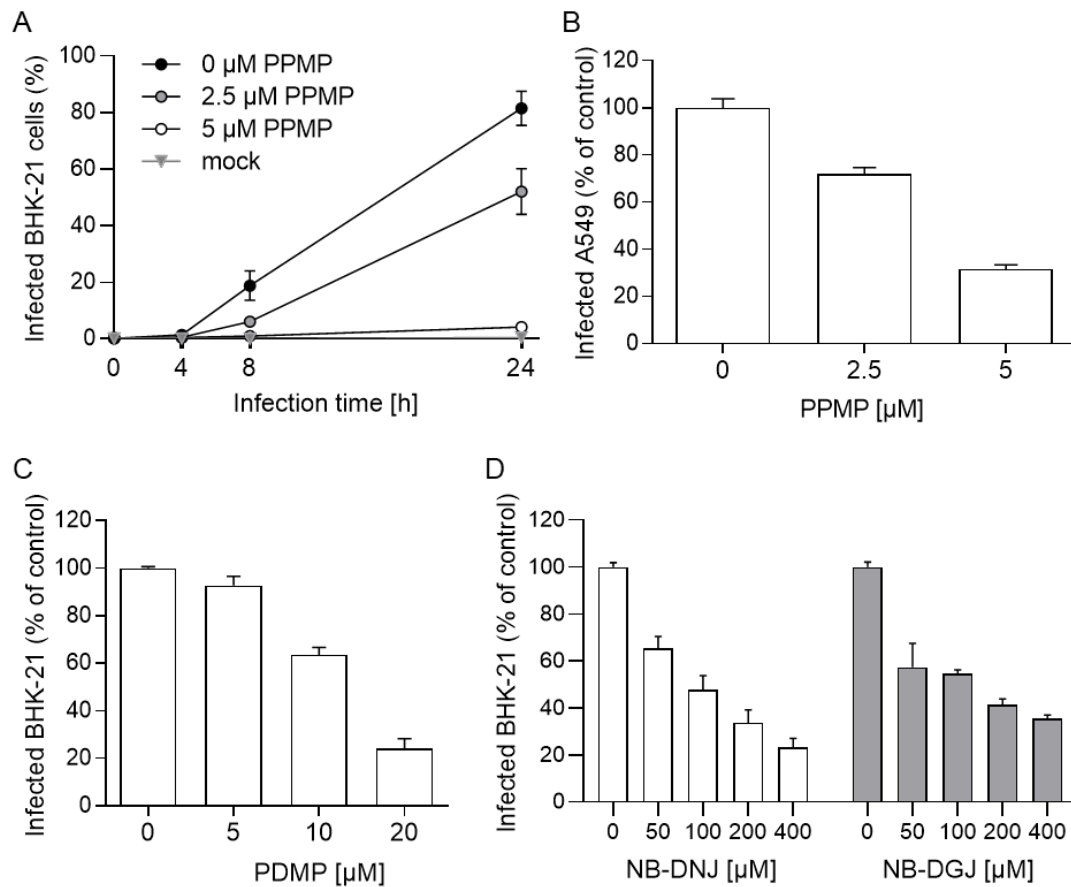


Figure 25. Inhibition of UGCG reduces UUKV infection levels in BHK-21 and A549 cells.

(A) BHK-21 cells were pretreated with the UGCG inhibitor PPMP for 16 h at the indicated concentrations and then infected with UUKV for up to 24 h in presence of the drug. Infection levels were monitored by flow cytometry after immunofluorescent staining of the viral N protein. (B) UUKV infection levels 8 hpi were assessed in A549 cells that were previously treated with the indicated concentrations of PPMP for 16 h. (C) PDMP pretreatment of BHK-21 cells for 16 h was followed by UUKV infection for 24 h. (D) BHK-21 cells were pretreated with NB-DNJ and NB-DGJ for 24 h and subsequently infected with UUKV for 24 h in presence of the inhibitors. UUKV infection levels were measured by flow cytometry.

2.4.3. The release of infectious UUKV virions is decreased by PPMP treatment

My results suggest that GlcCer is involved in UUKV infection. To pursue this possibility, I next sought to determine the step of the viral life cycle that requires GlcCer. Therefore, I aimed to characterize viral progeny produced in the absence of GlcCer. Supernatants from UUKV-infected cells in the presence of PPMP were harvested 24 hpi and used to infect freshly plated BHK-21 cells, *i.e.*, not previously exposed to the virus or the inhibitor, for 8 h. In BHK-21 cells, no more than one round of infection is performed by UUKV within 8 h (64), meaning that only the input viral particles account for the observed infection levels in this assay. Infectious supernatants obtained from cells treated with PPMP led to a significantly lower infection of freshly plated BHK-21 cells than the mock-treated supernatant (Figure 26 A). To further assess the titer of UUKV particles produced in the presence of 2.5 μ M PPMP, I titrated the cell supernatant using a standard ffu titration assay. The infectious supernatant released from PPMP-treated cells was about 90% less infectious than the one from untreated cells (Figure 26 B).

These results raised the questions whether PPMP treatment influences the total number of UUKV particles that are produced, or if it reduces the infectivity of individual virions. To address these questions experimentally, I evaluated the quantity of the viral proteins G_N, G_C, and N associated with the supernatant of UUKV-infected BHK-21 cells by western blot analysis. The total amount of these structural viral proteins correlates with the total number of released viral particles in the supernatant of infected cells, *i.e.*, the sum of infectious and defective particles. When producer cells were exposed to 2.5 μ M PPMP during UUKV infection and production, I observed a reduction of ~50 % of UUKV proteins in the supernatant (Figure 26 C, D). However, the decrease was significantly lower than the massive decrease of the titer determined in Figure 26 B (~ 90%). Therefore, the decline in infectivity could not only be explained by the reduction in the total number of virions. Indeed, the ratio of infectious virions to total released UUKV virions was lowered by ~ 80% when produced in the presence of PPMP, illustrating that virus particles were largely defective when produced in cells lacking physiological levels of GlcCer (Figure 26 E). Taken together, this analysis demonstrated that the infectivity of produced UUKV particles strongly depends on GlcCer.

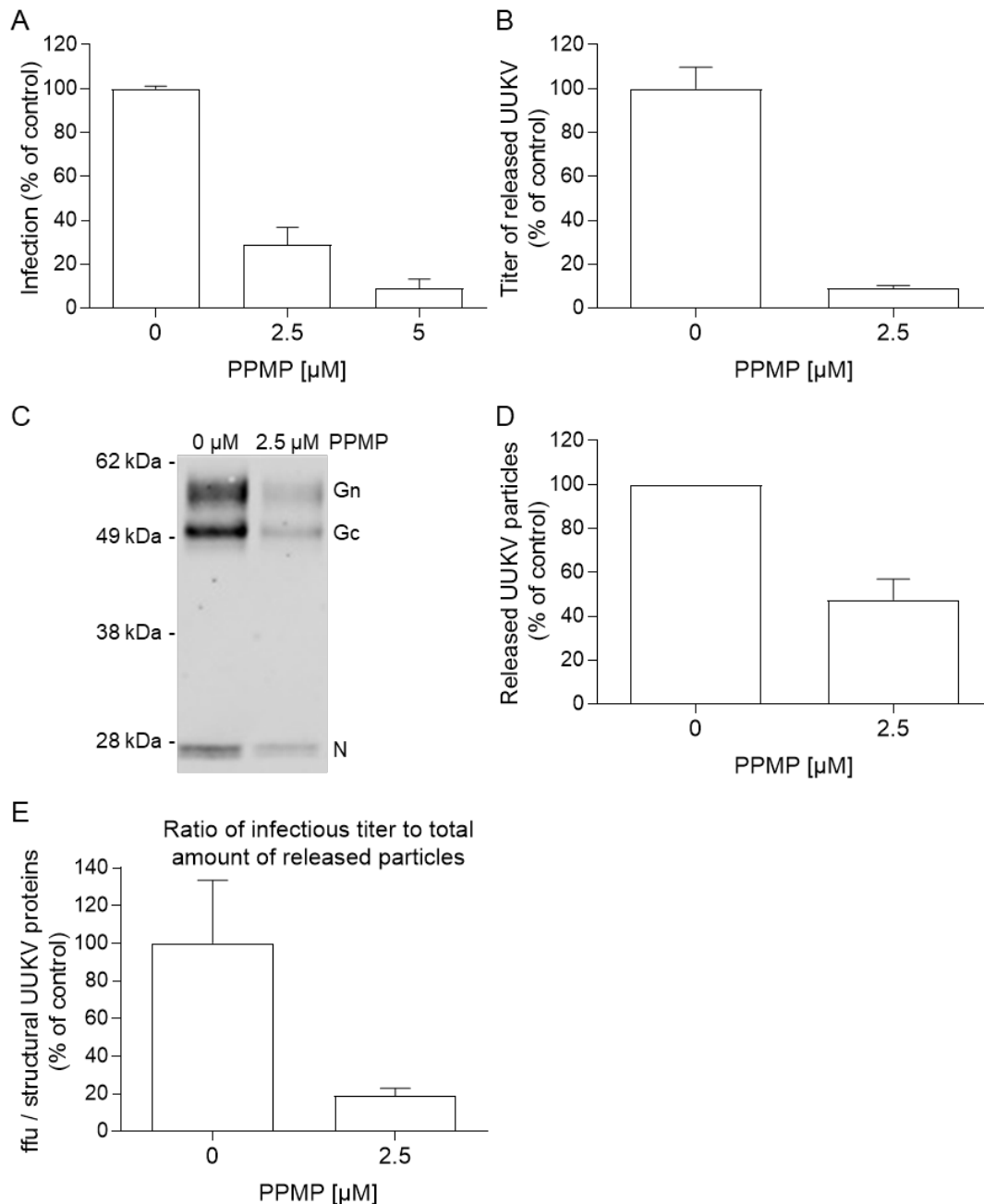


Figure 26. A lack of GlcCer in the producer cells leads to decreased infectivity of offspring UUKV particles.

(A) BHK-21 cells were infected with the infectious supernatant harvested from PPMP-treated and UUKV-infected BHK-21 cells 24 hpi. (B) Infectious titers of produced UUKV stocks produced in the presence or absence of the UGCG inhibitor PPMP was determined by a ffu titration assay. (C, D) Immunoblotting of the viral supernatant was performed to assess the total amount of produced and released UUKV particles in the presence or absence of 2.5 μM PPMP. The bars in D represent the relative intensities of Gn, Gc, and N summed together from the supernatants blotted in C. As in D the individual experiments were performed in technical triplicates, no SEM could be shown for the control treatment after normalization. (E) The ratio of infectious virions (ffu) per total viral structural protein amount revealed that UUKV particles released from cells lacking GlcCer were less infectious.

2.4.4. GlcCer is incorporated into the UUKV particles

As GlcCer seems to play a role for infectivity of UUKV particles, I sought to explore whether GlcCer is present in the virions. Therefore, the lipidome of UUKV particles was analyzed by lipid MS in a single experiment. The supernatant of not infected BHK-21 cells was concentrated and purified in parallel to the viral particles and acquired as a control (Figure 27). Overall, the lipid concentrations especially in the purified control supernatant were very low and the experiment needs to be optimized and repeated. The level of plasmalogen PE (pPE) was too low to be detected in the analysis of viral particles. Preliminary analysis of a single virus stock showed a ~ 2.5-fold enrichment of HexCer in virions compared to the purified control supernatant (mock). Phospholipids were generally enriched in the viral particles compared to the purified control supernatant (Figure 27 A).

Comparing the lipidome of UUKV-infected BHK-21 cells with the lipidome of the virions (Figure 22 B and 27 B), it became obvious that less phospholipids than present in the cells (~ 83%), were incorporated into the particles (~ 48%). As mentioned previously, the expression of SM was not enriched in UUKV infected cells, but it was present at a higher fraction in the viral particles (~ 10%) than in the producer cells (~ 3%) (Figures 22 A and 27 A). Moreover, an enrichment of HexCer was detected in UUKV particles, making up ~ 6% of the virion's lipidome, while Cer and Hex2Cer remained below 1% (Figure 27 B). The incorporation of HexCer into the UUKV particles together with the decreased infectivity of virions produced in cells lacking GlcCer, suggests that GlcCer in the viral envelope is involved in the infection process of UUKV.

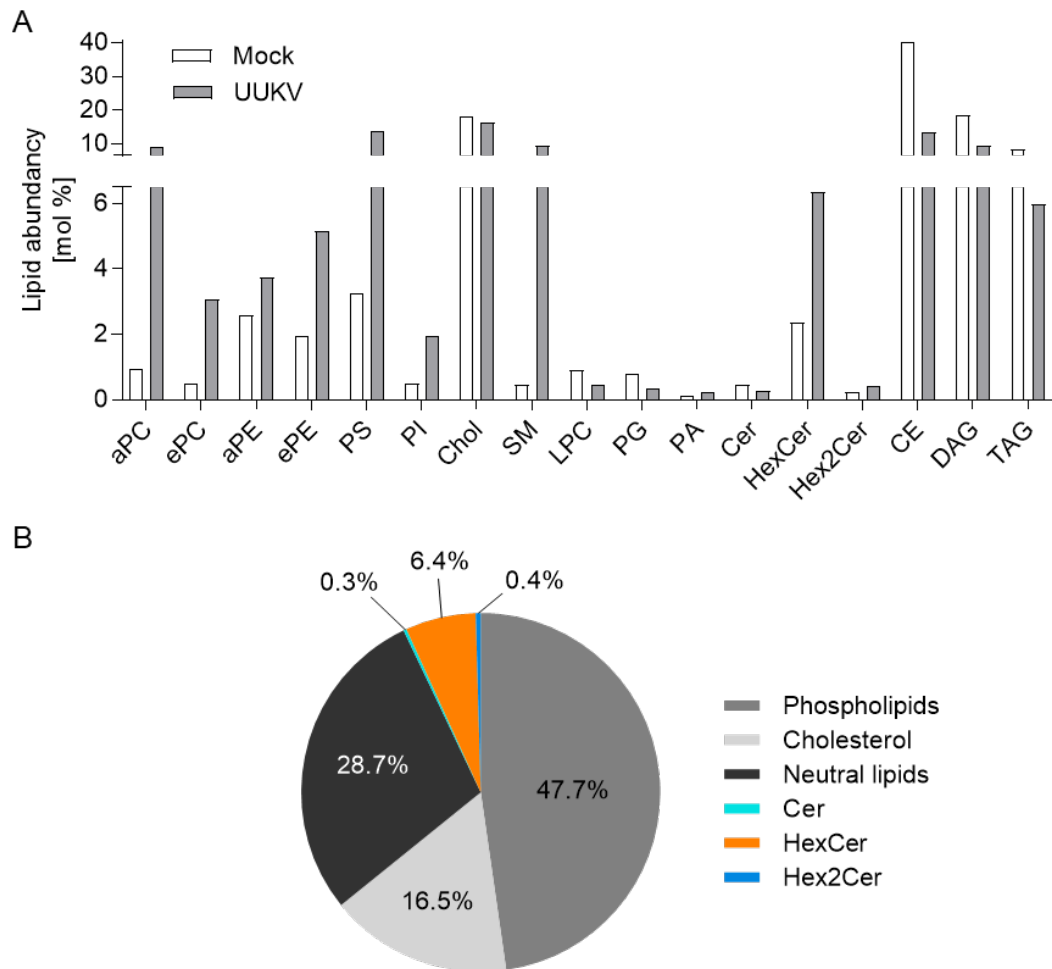


Figure 27. Lipidome analysis of UUKV particles reveals enriched HexCer levels.

Lipid MS was performed by Magalie Mazelier in collaboration with Britta Brügger (BZH Heidelberg). (A) In a lipidomic MS screening approach, the lipid distributions in UUKV particles were compared to the purified control supernatant of not infected cells treated in the same way as the virions (mock). (B) The lipidome of virions from A were depicted in a pie chart. Phospholipids include PC, PE, PS, PI, PG, PA, LPC, and additionally SM, while neutral lipids contain CE, DAG, and TAG. The virus particle lipidome analysis was determined in a single experiment and will be repeated in the future.

2.4.5. UUKV binding is supported by GlcCer present in viral particles

Previously, I demonstrated that GlcCer is essential for the infectivity of produced virions and proposed that GlcCer is present in the viral envelope. This suggests that GlcCer could facilitate the early steps of infection, most likely viral entry into target cells. Therefore, I first examined the possibility that GlcCer promotes virus attachment to target cells. To this end, UUKV produced in the presence or absence of 2.5 μ M PPMP was bound to BHK-21 cells on ice. To ensure the same numbers of total viral particles, *i.e.*, sum of infectious and defective virions, the input of viral particles in this assay was not normalized by MOI, but instead based on the UUKV N protein. Virus binding was evaluated by SDS-PAGE and subsequent western blotting after several washing steps. The amount of UUKV N protein bound to target cells was measured and revealed that the number of cell-bound viral particles was reduced by ~ 60-70% when lacking GlcCer in their envelope (Figure 28 A, B).

To exclude that the block in virus binding was due to a default of incorporation of the glycoproteins G_N and G_C in viral particles when UUKV is produced in the presence of PPMP, I determined the ratios of glycoproteins to N protein in the virions by western blot analysis (Figure 28 C). This ratio should not change if the structural organization of virions is preserved, and the presence of GlcCer had no statistically significant impact on the glycoprotein to N protein ratio in viral particles. The UUKV glycoproteins G_N and G_C have four *N*-glycans each. These oligosaccharides were previously demonstrated to be involved in interactions with viral receptors, namely DC-SIGN (52, 53). Hence, I tested the hypothesis that GlcCer depletion in virions has no impact on *N*-glycosylation of the viral glycoproteins and cannot account for the block in virus attachment to target cells. To do so, G_N and G_C were subjected to treatment with endoglycosidase H (Endo H) and peptide *N*-glycosidase F (PNGase F). While Endo H cuts chitobiose cores of mannose glycans, PNGase F cleaves asparagine residues. Viral glycoproteins were then analyzed by western blot using specific antibodies against G_N and G_C (Figure 28 D). No differences in the *N*-glycan residues of the glycoproteins could be detected. These results showed that the lack of GlcCer does not impact the *N*-glycosylation of the viral glycoproteins, and therefore, that the decrease in binding of UUKV lacking GlcCer is not due to the *N*-glycans exhibited on G_N and G_C .

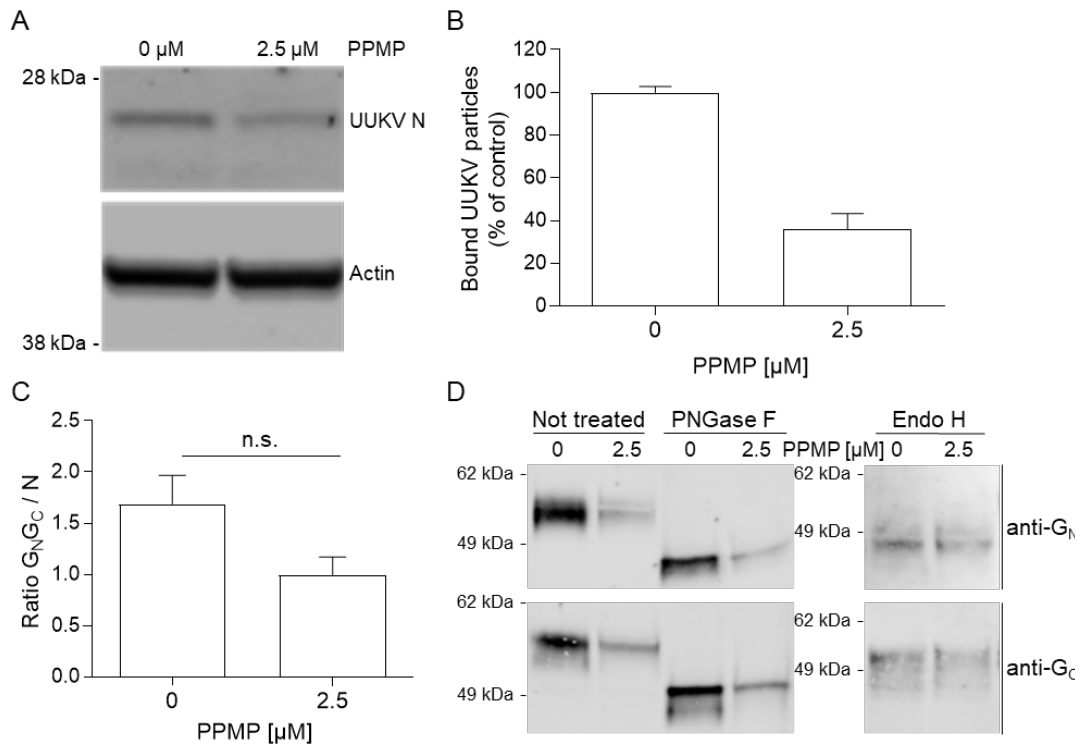


Figure 28. Virus binding of UUKV particles lacking GlcCer is hampered.

UUKV particles were produced in BHK-21 cells treated with PPMP. (A, B) Target cells were exposed to virions for 2 h on ice and virus binding was evaluated by western blot analysis (A) and semi-quantified using Image Studio Lite software (LiCOR) (B). Input virus was normalized to the N protein. (C) The ratio of glycoprotein to N protein in viral particles released from PPMP-treated BHK-21 cells was monitored by western blotting. (D) The *N*-glycans of UUKV G_N/G_C proteins were digested by endoglycosidase H (Endo H) and peptide *N*-glycosidase F (PNGase F) treatment, and the *N*-glycosylation patterns were assessed by western blotting using antibodies raised against the viral glycoproteins. A representative western blot is shown.

To validate the dependence of UUKV on GlcCer for virus binding, I used a complementary approach and performed a binding competition between a soluble short-chain version of GlcCer (C6-GlcCer) and UUKV-Atto488. Fluorescently labeled UUKV particles were allowed to bind to BHK-21 cells pretreated with C6-GlcCer (Figure 29 A). Binding of UUKV-Atto488 to BHK-21 cells was monitored by flow cytometry (Figure 29 B). Consistent with the previous data, competition of UUKV-Atto488 with C6-GlcCer led to a decrease in virus binding to both, BHK-21 and A549 cells in a concentration-dependent manner (Figure 29 C). Previously it was described that DC-SIGN, a human CLR, functions as an endocytic receptor for UUKV (52, 53). DC-SIGN binds to the *N*-glycans carried by G_N and G_C . Cells expressing DC-SIGN should thus be competent to bind UUKV regardless of the presence of GlcCer in the viral envelope. This represents an interesting model to test the specific dependence of UUKV binding on GlcCer in cells lacking DC-SIGN expression. Therefore, I stably expressed DC-SIGN in BHK-21 cells (Figure 29 D) and assessed the influence of DC-SIGN expression in a binding competition assay involving UUKV particles and C6-GlcCer. I found that pre-binding of C6-GlcCer to BHK-21 cells stably expressing DC-SIGN did not impair UUKV-Atto488 binding, starkly contrasting with the BHK-21 cells that do not express DC-SIGN (Figure 29 C). Interestingly, UUKV-Atto488 binding to parental HeLa cells, an epithelial cell line that does not express DC-SIGN or L-SIGN, was not impaired by C6-GlcCer pre-binding (Figure 29 C). This means, in contrast to A549 and BHK-21 cells, soluble C6-GlcCer does not compete with UUKV binding in HeLa cells.

In a similar approach I bound C6-GlcCer to cells on ice and subsequently added UUKV at an MOI of 0.5. After the cells were exposed to UUKV for 1 h on ice, media was exchanged to remove unbound virus particles. Infection was allowed to proceed for 8 h at 37°C and infection levels were analyzed by flow cytometry using an antibody staining of the N protein in infected cells as readout. Similar to the binding competition assays, UUKV infection was reduced when the cells were saturated by C6-GlcCer binding (Figure 29 E). Altogether, these findings support the hypothesis that GlcCer in the UUKV envelope serves as a host-derived viral lipid attachment factor important for UUKV binding.

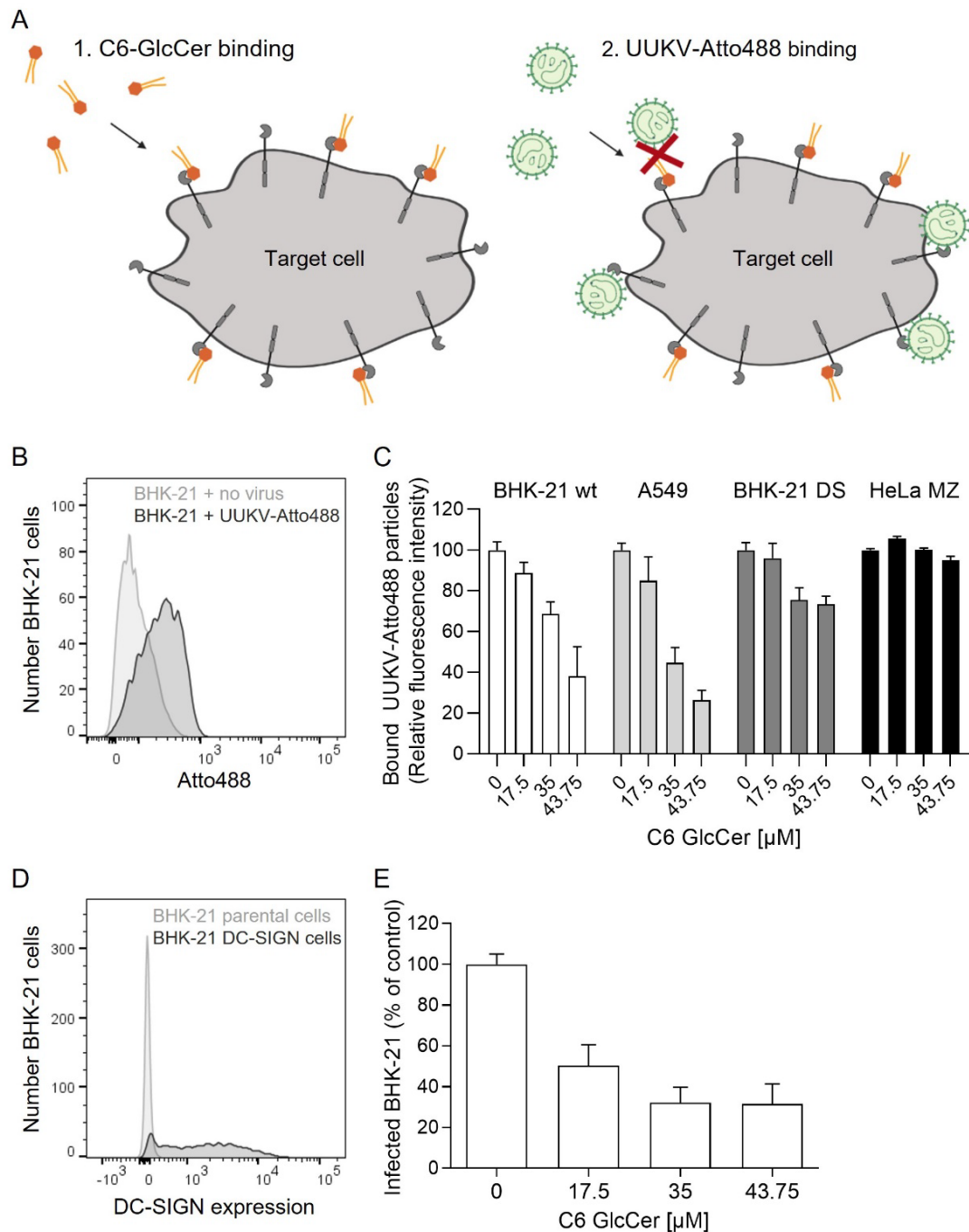


Figure 29. C6-GlcCer competes with UUKV-Atto488 for binding to BHK-21 and A549 cells.

(A) The binding competition workflow was as follows: C6-GlcCer was prebound to cells and then UUKV-Atto488 was added. UUKV-Atto488 binding was detected by flow cytometry. The scheme was generated in BioRender. (B) Binding of UUKV-Atto488 to untreated BHK-21 cells on ice for 1 h resulted in an increase of the mean fluorescence signal intensity as visualized in the histogram. (C) Indicated concentrations of C6-GlcCer were bound to BHK-21 cells, A549 cells, BHK-21 cells stably expressing DC-SIGN, and HeLa MZ cells on ice for 2 h. Subsequently, UUKV-Atto488 was added for 1 h on ice and virus binding was assessed by flow cytometry after washing away unbound virions. (D) Expression of DC-SIGN in BHK-21 cells was confirmed with immunostaining with an antibody raised against DC-SIGN prior to by flow cytometry analysis. (E) BHK-21 cells

were treated with the indicated concentrations of C6-GlcCer on ice followed by UUKV binding for 1 h. Not attached C6-GlcCer and unbound viral particles were washed away, and infection was allowed for 8 h at 37°C. UUKV infection was detected by flow cytometry.

2.4.6. Receptors that recognize UUKV through GlcCer remain to be identified

CLRs interact with carbohydrate groups and as such, appear as interesting potential receptors for GlcCer through the glucose residue carried by this lipid. To investigate this possibility, I tested 14 murine CLRs for their capacity to bind UUKV particles in an enzyme-linked immunosorbent assay (ELISA)-based experiment (Figure 30 A). The plates were coated with UUKV particles, the soluble CLRs were added, and antibody staining assessed CLR binding. The human CLRs DC-SIGN and L-SIGN, which act as an entry receptor and attachment factor for UUKV, respectively, served as positive controls (52, 53). The relative absorption values for virus binding obtained from the ELISA assay, were normalized to UUKV binding to DC-SIGN. In addition, Dectin-1, Dectin-2, specific intercellular adhesion molecule-3-grabbing nonintegrin-related 1 (Sign-R1), Sign-R3, DC immunostimulating receptor (DCAR), Langerin (C-type Lectin Domain Family 4 Member K, Clec4K), MICAL (C-type lectin domain family 12 member A, Clec12A), C-Type Lectin Domain Family 12 Member B (Clec12B), macrophage galactose-type lectin (MGL-1), and macrophage inducible C-type lectin (Mincle) showed greatly increased binding to UUKV particles compared to binding to the mock-control in this assay (Figure 30 A). Interestingly, the CLR Mincle was previously described to interact with GlcCer, rendering Mincle an interesting hit for follow-up studies on receptors of GlcCer in the UUKV envelope (170). Mincle is a Ca^{2+} -dependent receptor that is present on monocytes, macrophages, and DCs (Matsumoto et al., 1999).

To confirm the involvement of Mincle in viral particles binding processes, a new virus-cell binding assay was established. Murine bone marrow cells (mBMCs) kindly provided by Bernd Lepenies were differentiated into bone marrow-derived dendritic cells (mBMDCs), which express cluster of differentiation (CD)11c (Figure 30 B). Binding of UUKV-Atto488 to mBMDCs resulted in similar binding efficiency of UUKV to wt and Mincle KO cells suggesting that either Mincle does not play a role in UUKV binding or that other CLRs can take over a potential Mincle-specific function (Figure 30 C). The identity of UUKV receptors that can recognize GlcCer in the UUKV envelope thus remain to be investigated.

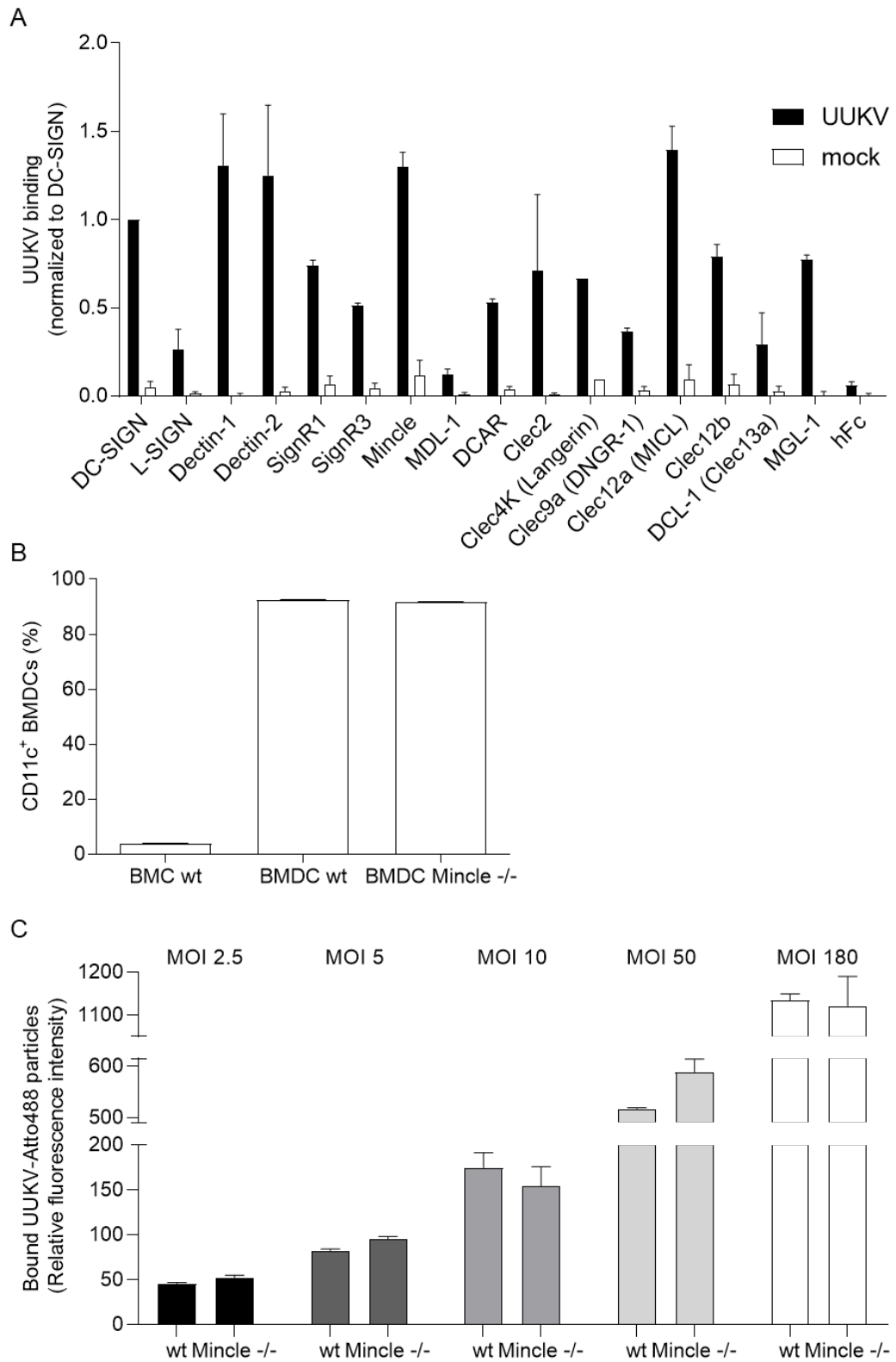


Figure 30. An ELISA-based screen suggests UUKV binding to Mincle.

(A) In collaboration with Kathleen Schön (Lepenies group, University of Veterinary Medicine Hannover), a CLR fusion protein library was screened for UUKV interactions. UUKV particles were immobilized in wells and incubated with CLR-Fc fusion proteins. Binding was detected by measuring absorption at 495 nm. Background was subtracted using the buffer control and the signal was normalized to UUKV binding to DC-SIGN. The

experiment was performed twice with each three technical triplicates. (B) Differentiation of BMCs into BMDCs was validated by cluster of differentiation (CD)11c staining in flow cytometry. BMCs were kindly provided by Bernd Lepenies (University of Veterinary Medicine Hannover). (C) UUKV-Atto488 was bound to BMDC wt and Mincle KO cells on ice for 2 h and binding was analyzed by flow cytometry. Indicated MOIs correspond to titers determined by ffu titration assays on BHK-21 cells. In B and C data from a single experiment is depicted.

2.4.7. TOSV infectivity depends on GlcCer

Given that virus binding was decreased by a lack of GlcCer in the UUKV particles, I next aimed to assess whether the dependency on GlcCer for infectivity is shared among other viruses. TOSV, another phenuivirus that buds from ER, ERGIC, and Golgi compartments, and SFV, a togavirus budding from the plasma membrane (117), were allowed to infect BHK-21 cells in order to compare HexCer levels between uninfected and infected cells (Figure 31 A, B). In TOSV-infected BHK-21 cells ~ 1.5-fold higher levels of HexCer were observed compared to uninfected cells, while SFV infection of BHK-21 cells did not lead to an enrichment of HexCer. TOSV and SFV infection levels were evaluated after PPMP treatment resulting in a dose-dependent decrease of TOSV infection 24 hpi, while SFV infection was not affected by PPMP treatment (Figure 31 C). One infection cycle takes roughly 3 h for SFV in BHK-21 cells (171). When cells were infected for 24 h, nearly 100% of cells were infected, regardless of the used MOI. The reason for this is that multiple cycles of infection took place during this period of time. Hence, I additionally evaluated SFV infection of PPMP-treated BHK-21 cells after 5 h, which also remained unaltered (Figure 31 D).

Next, I examined the effect of GlcCer depletion on the production of TOSV and SFV progeny. For this purpose, 24 hpi the number of infectious TOSV and SFV particles present in the supernatant of infected cells in the presence of PPMP were assessed with a standard pfu titration assay (Figure 31 E). Compared to SFV, I observed that TOSV lost infectivity when produced in GlcCer-depleted cells, *i.e.*, titers dropped by ~ 80% when the supernatant originated from infected cells treated with PPMP.

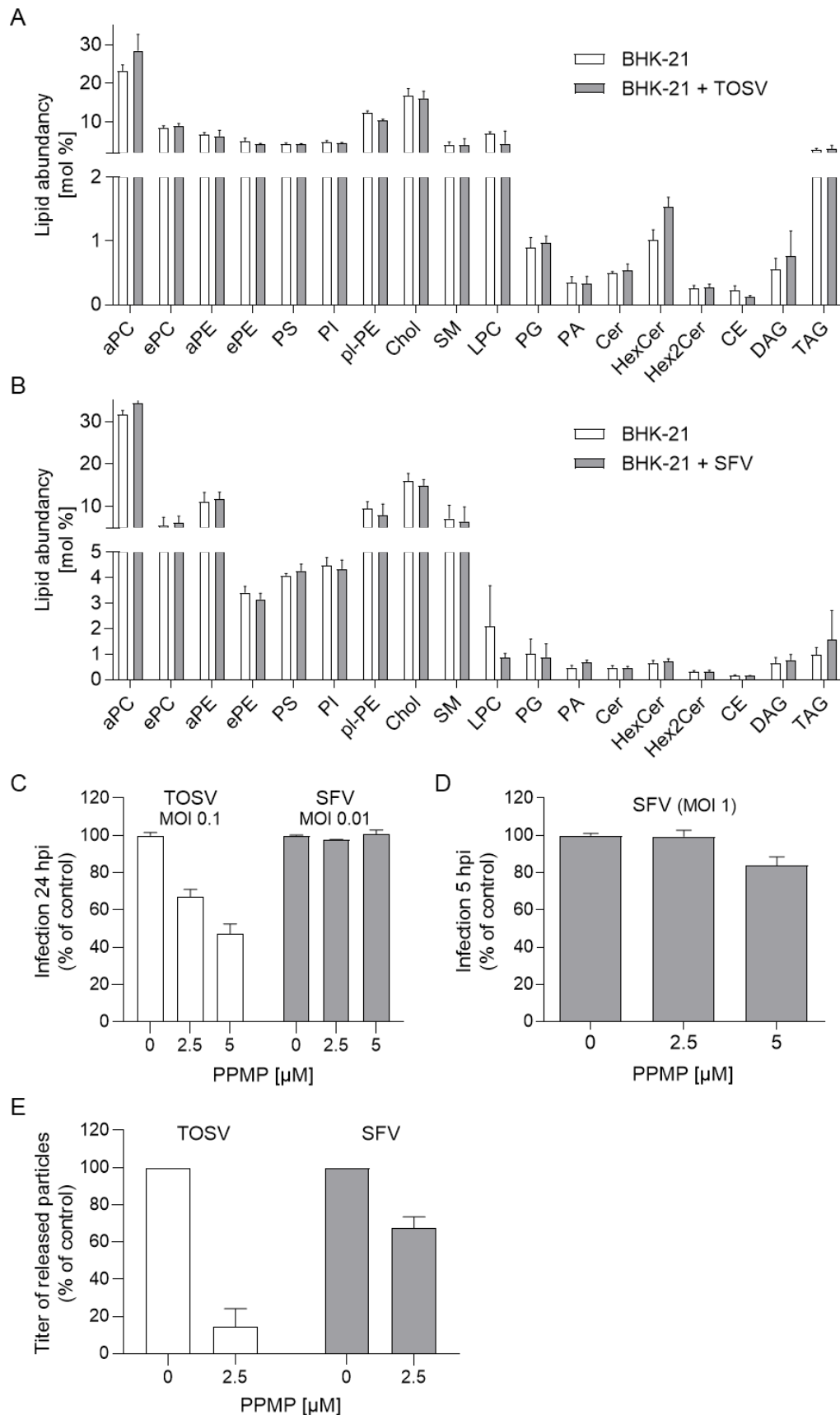


Figure 31. GlcCer plays a role for TOSV infectivity while it can be omitted for SFV infection.

(A, B) HexCer levels of TOSV- and SFV-infected BHK-21 cells were compared to uninfected cells. Lipid MS was performed by Britta Brügger and Christian Luchtenborg

(BZH Heidelberg). (C) BHK-21 cells were pretreated with PPMP for 16 h and then infected with TOSV (MOI of 0.1) and SFV (MOI of 0.01) in continuous presence of the drug. Infections levels 24 hpi were assessed by flow cytometry after antibody staining against TOSV structural proteins and SFV envelope protein 2 (E2), respectively. (D) Due to the fast life cycle of SFV in BHK-21 cells, after 24 h (C) infection was always saturated. Hence, the experiment was repeated with an infection time of 5 h and an MOI of 1. (E) The infectious titers of TOSV and SFV stocks 24 hpi prepared in the presence of PPMP were determined by a standard pfu titration assay.

2.4.8. GlcCer is involved in TOSV binding

My results indicated that GlcCer is important in the envelope of UUKV particles to mediate virus binding to host cells. To test if TOSV also relies on GlcCer in its envelope for binding to host cells, I performed a binding competition assay with C6-GlcCer as described for UUKV in Figure 29. In these experiments, I also sought to test a virus whose lipidome shows no enrichment of GlcCer, which could be used as a negative control to further assess the specific contribution of GlcCer in UUKV and TOSV binding. To reach this objective, together with my collaborators Sophie Winter (Chlanda group, Bioquant Heidelberg) and Britta Brügger (BZH Heidelberg), I determined the lipidome of Ebola VLPs with the lipidomic MS approaches. EBOV is a zoonotic virus causing frequent endemic outbreaks on the African continent. It buds from the plasma membrane, and therefore HexCers which are predominantly located in ER, ERGIC, and Golgi compartments should not be incorporated in Ebola VLPs. As anticipated, Ebola VLPs contained $0.5 \pm 0.01\%$ Cer, $1.7 \pm 0.05\%$ HexCer, and $0.4 \pm 0.25\%$ Hex2Cer out of total lipids, which can be considered neglectable (Figure 32 A). For comparison, UUKV particles contained 6.4% of HexCer (Figure 27 B), *i.e.*, nearly four times more than Ebola VLPs.

Next, I used Ebola VLPs that express GFP (Ebola-GFP VLPs) to assess their binding capacity to BHK-21 cells preincubated with soluble C6-GlcCer on ice. Consistent with my hypothesis, it became apparent that soluble GlcCer did not interfere with Ebola VLP binding (Figure 32 B). Similarly, the binding of a VSV-G pseudotyped, GFP-expressing, and transcription-incompetent derivative of HIV-1 (VSV-HIVLP-GFP), which also buds from the plasma membrane, was tested. As expected, C6-GlcCer did not compete with VSV-HIVLP-GFP for binding to BHK-21 cells (Figure 32 B).

In addition, BHK-21 cells were saturated with C6-GlcCer and then exposed to TOSV fluorescently labeled with Atto488 NHS ester (TOSV-Atto488). TOSV binding

was clearly prevented by C6-GlcCer in a concentration-dependent manner (Figure 32 B). In this series of assays, I also included GERV, a related bunyavirus to UUKV and TOSV but from a different viral family. C6-GlcCer was also competing with GERV-Atto488 binding, which reduced GERV binding to C6-GlcCer-treated BHK-21 cells in a dose-dependent manner (Figure 32 B). In sum, not only UUKV appeared to use GlcCer to attach cells, but also other bunyaviruses such as TOSV and GERV, which share the properties to assemble and bud from ER, ERGIC, and Golgi compartments with UUKV. In contrast, EBOV and VSV, two viruses egressing the cells from the plasma membrane, did not rely on HexCer for binding to target cells.

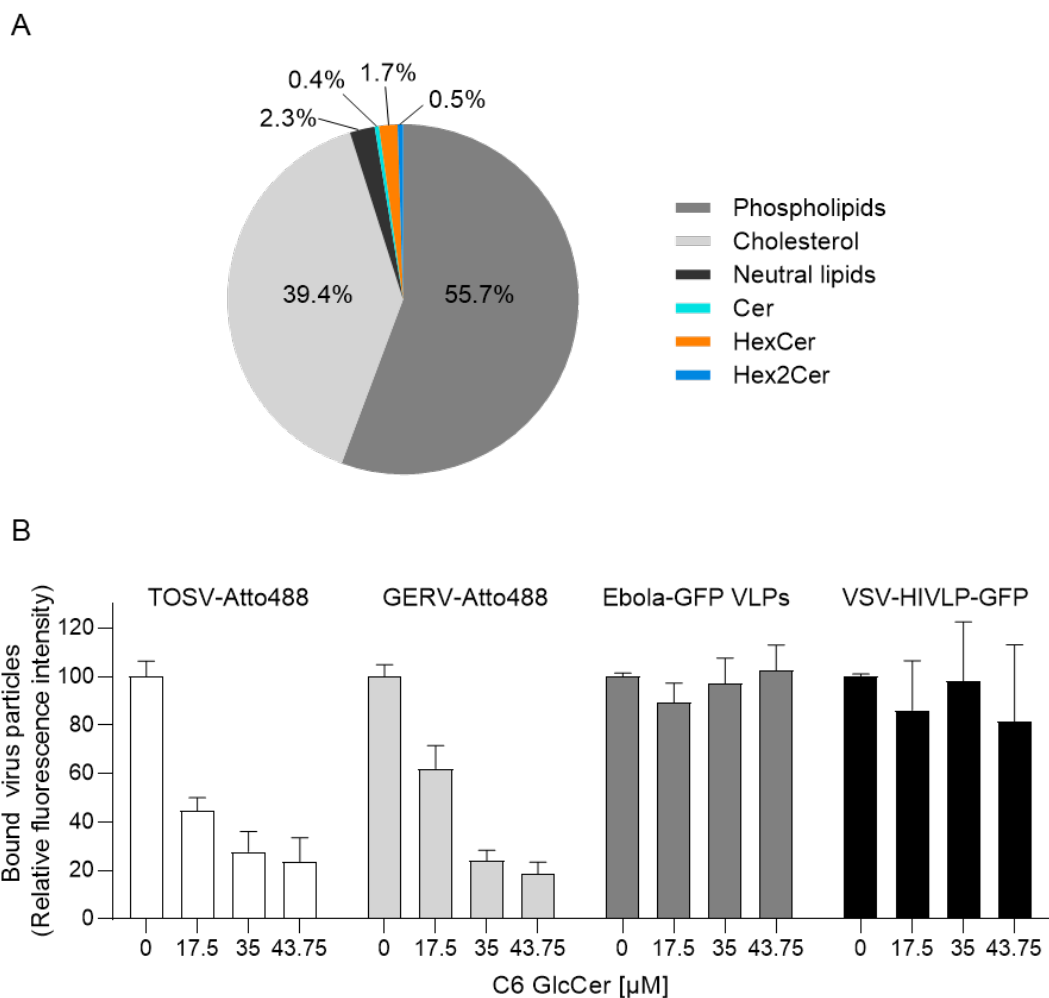


Figure 32. GlcCer plays a role for TOSV and GERV binding to target cells.

(A) Ebola VLP lipidome analysis was performed by lipid MS conducted by Britta Brügger (BZH Heidelberg) using VLPs provided by Sophie Winter (Chlanda group, Bioquant Heidelberg). Phospholipids include PC, PE, PS, PI, PG, PA, LPC, and additionally SM, while neutral lipids contain CE, DAG, and TAG. (B) In the binding competition assays described before, soluble C6-GlcCer was bound to BHK-21 cells on ice for 2 h. Then binding of TOSV-Atto488, GERV-Atto488, Ebola-GFP VLPs, and VSV-G pseudotyped

and GFP-expressing HIV-1 VLPs (VSV-HIVLP-GFP) was allowed for 1 h. Virus binding was measured by flow cytometry and analyzed using FlowJo software. Ebola-GFP VLPs and VSV-HIVLP-GFP were kindly provided by Sophie Winter and Thorsten Müller (Kräusslich group, CIID Heidelberg), respectively.

2.4.9. GlcCer and RVFV infection

RVFV is another highly pathogenic phenuivirus that is closely related to UUKV. In this last section, I intended to determine whether GlcCer also contributes to RVFV binding to host cells. To this end, I tested RVFV wt and RVFV Δ NSs GFP, a RVFV strain genetically engineered to express GFP instead of the non-structural protein NSs, the major factor of RVFV virulence. PPMP-treated cells were infected and fixed in 4% paraformaldehyde (PFA) 8 hpi or 24 hpi, before infection levels were determined by flow cytometry (Figure 33 A-D). Surprisingly, RVFV wt infection in BHK-21 cells was not influenced by the lack of GlcCer, whereas RVFV Δ NSs GFP infection was reduced in a dose-dependent manner (Figure 33 A, C). In contrast, when A549 cells were exposed to RVFV Δ NSs GFP in the presence of PPMP, infection was not affected 8 hpi (Figure 33 B). Moreover, PPMP treatment of A549 cells did not influence RVFV wt infection levels (Figure 33 B, D).

Next, I determined the titer of RVFV stocks prepared in the presence of PPMP. I found that RVFV wt and RVFV Δ NSs GFP infectivity was reduced by ~ 60-70% when produced from BHK-21 cells in the absence of GlcCer (Figure 33 E, F). Collectively, RVFV might, at least in some cell types, depend on both GlcCer and the expression of NSs. These intriguing results warrant further investigations to understand the link between GlcCer and NSs in the case of RVFV.

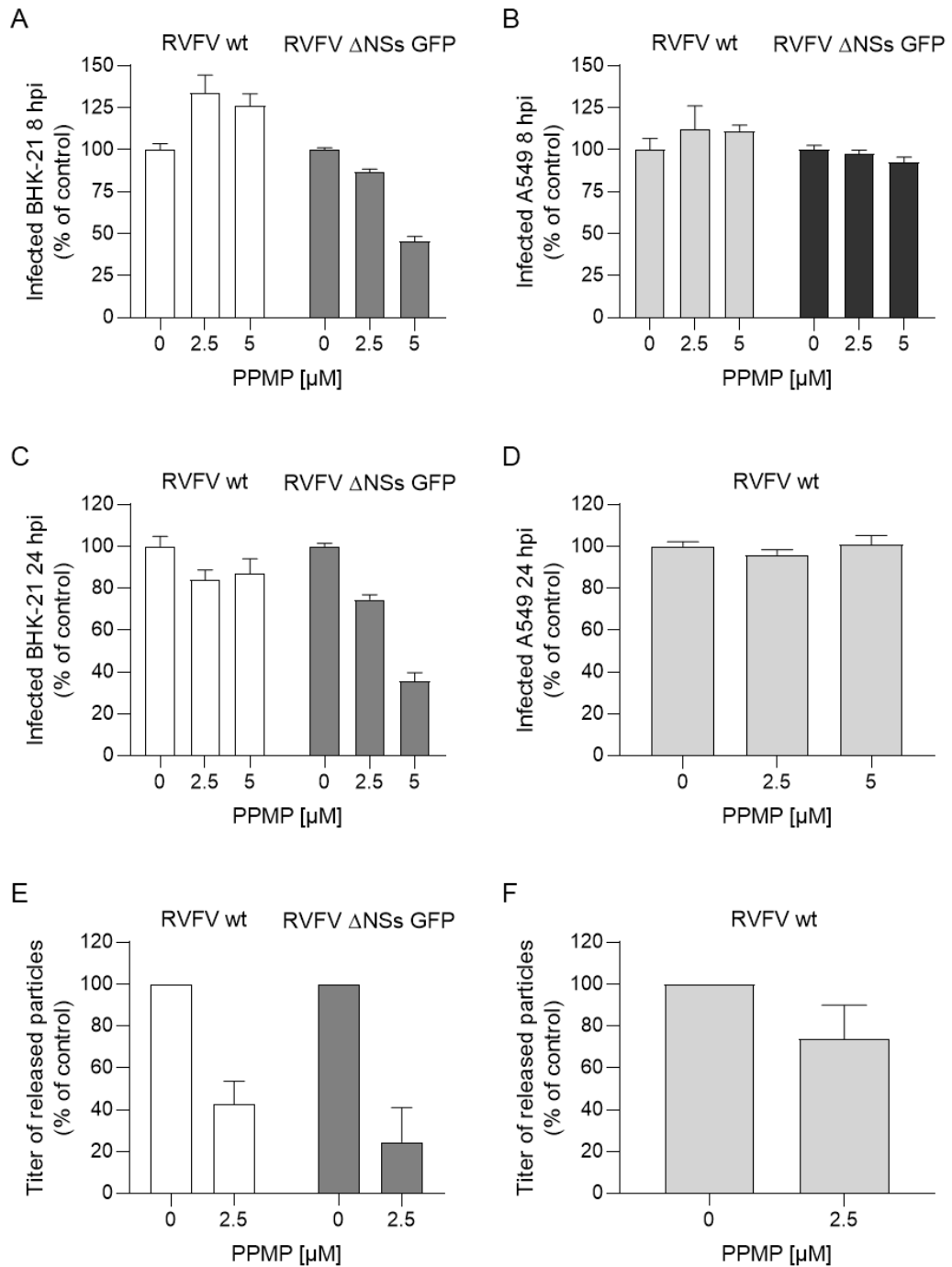


Figure 33. The role of GlcCer during RVFV infection remains elusive.

(A-D) RVFV wt (white, light grey) and RVFV Δ NSs GFP (dark grey, black) infection of BHK-21 (left panel: white, dark grey) and A549 cells (right panel: light grey, black) in the presence of indicated concentrations of PPMP was assessed by flow cytometry. (A, B) Infection was terminated after 8 h. (C, D) Cells were harvested 24 hpi. (E, F) Titers of released RVFV wt and RVFV Δ NSs GFP by PPMP-treated producer cells were determined by pfu or ffu titration assay, respectively. Infectious supernatant was harvested 24 hpi. All experiments with RVFV Δ NSs GFP were performed in the BSL-2 laboratory together with the rotation student Paulina Schad.

3. Discussion

My in-depth work combined molecular and cellular tools to shed light on novel facets of arbovirus-host cell interactions. First, the morphology of UUKV particles produced from mammalian cells was compared to virions derived from tick cells by cryo-EM. It became obvious that the size of tick cell-derived virions is more heterogeneous and on average smaller than the viral particles produced in mammalian cells. These results, together with those obtained by Mazelier and colleagues (150), emphasize how essential it is to understand the structural and cellular biology of arboviral particles produced in both, their respective arthropod vector cells and their respective mammalian host cells.

Furthermore, this thesis investigated host factors involved in infection of mammalian cell-derived UUKV particles by proteomic and lipidomic MS approaches. A label-free protein MS approach revealed several interaction partners of the UUKV glycoproteins in host cells, of which the Golgi apparatus resident GEF GBF1 was identified and validated as a proviral host factor for UUKV infection. GBF1 was shown to play a role for UUKV replication and particle release. This infection-promoting host factor additionally plays a role for other arboviruses such as TOSV, RVFV Δ NSs, and SFV, suggesting that also more viruses that replicate in the cytoplasm could rely on GBF1. Altogether, my results brought new insights into UUKV infection mechanisms and characterized a novel protein host factor for UUKV infection. Still, many of the host cellular interactants identified in this first approach remain to be confirmed and explored for potential biological functions.

Finally, I performed a lipidomic MS analysis of both, infected cells and UUKV particles, and shed light on the lipids incorporated into the viral envelope. This work indicated that the glycolipid GlcCer was enriched in UUKV-infected cells. I explored the functions of the lipid GlcCer during UUKV infection, suggesting that GlcCer, as a glycolipid in the viral envelope, is important for virus binding to target cells. This study suggests a possibly novel type of attachment of virions to target cells, *i.e.*, via viral glycolipids, and opens new avenues for virus-lipid research. Importantly, host cell partners of GlcCer that participate in attachment of UUKV and other phenuiviruses still remain to be identified. Moreover, I observed that the RVFV non-structural protein NSs alters the need of GlcCer for infection, which raises new questions regarding the involvement of NSs in lipid metabolism disruption during infection. It would also be interesting to explore the lipidome of other viruses that

bud from ER, ERGIC, and Golgi compartments to find out if the utilization of GlcCer is conserved among the viruses that rely on these networks for egressing cells.

3.1. Tick and mammalian cell-derived UUKV particles differ in size

Even though arboviruses that infect the mammalian host are usually transmitted by an arthropod bite, and are thus produced by arthropod vectors, most studies trying to investigate arbovirus infections usually produce the viruses of interest from mammalian cells. Using UUKV as a surrogate for more pathogenic tick-borne bunyaviruses, Mazelier et al. demonstrated that UUKV acquires different molecular characteristics when produced from tick cells compared to the standard production in the mammalian cell line BHK-21 (150).

Another study revealed that the RVFV genome was more efficiently packaged when produced in mosquito cells compared to mammalian cells (172). Bunyaviruses possess a trisegmented RNA genome which complicates assembly of progeny virus regarding packaging of a full set of RNA segments. Studies suggested that this process is non-selective for bunyaviruses and lacking specific mechanisms to incorporate all three segments (173, 174). Bermúdez-Méndez and colleagues propose that the balance of S, M, and L vRNP content in a single cell influences genome packaging efficiency (172). However, the reasons for more efficient genome packaging in mosquito cells remain elusive, but could be another hint towards an arthropod origin of arboviruses from the *Bunyavirales* order (8, 172).

My laboratory described that arboviruses produced in arthropod vector cells are more efficient to infect mammalian cells. For example, UUKV (tick cells) and GERV (mosquito cells) were demonstrated to possess higher infectivity when produced in their respective vector cells (150) and (unpublished data by Colin Xin in the Lozach group), respectively. It is tempting to hypothesize that mammalian cell-derived particles could have an advantage to infect arthropod cells. This would mean that arboviruses have optimally adapted to their dual life cycle. On the other hand, it is also possible that arboviral particles produced in mammalian cell do not show increased infection efficiency in arthropod cells. This, together with the proposed co-evolution of arboviruses with their arthropods, would further suggest a bigger importance of the vector compared to the vertebrate host for virus propagation.

Moreover, my group demonstrated that UUKV Δ NSs was less efficient to replicate in IRE/CTVM-19 tick cells, while no differences were observed for IDE-8

tick cells or mammalian BHK-21 cells (unpublished data acquired by Magalie Mazelier). Interestingly, IRE/CTVM-19 cells derive from the species of ticks transmitting UUKV, which raises the question whether NSs could be important for the host switch between vector and vertebrate host. My group also revealed that RVFV wt and Δ NSs were both capable to infect and replicate in mammalian or mosquito cell culture. However, RVFV Δ NSs was not efficiently produced from some cell lines, such as HeLa cells, while RVFV wt was produced to high titers (unpublished data acquired by Pysylvia Léger). In contrast to UUKV NSs, the NSs protein of RVFV was previously associated to play a role for counteracting IFN responses *in vivo* (60–62).

Together, the findings comparing arthropod and mammalian cell-derived arboviruses highlight the importance of studying arboviruses derived from both, their host and their vector cells. These studies open up many more questions towards functional differences between virions produced in arthropod cells versus mammalian cells.

3.1.1. Tick derived UUKV particles are smaller than mammalian derived virions

Considering previous findings, I aimed to further explore the morphological specificities of UUKV particles depending on the producer cells. By Coomassie blue staining of the UUKV stocks, I observed larger quantities of the viral glycoproteins compared to the nucleoprotein when particles were produced in IDE-8 cells, consistent with results previously published by my group (150). Notably, the cryo-EM analysis performed in collaboration with Martin Obr (Schur group, IST Austria) revealed that particles produced in IDE-8 tick cells were smaller and in general more heterogenous in size than virions originating from BHK-21 cells. In agreement with the increased glycoprotein to nucleoprotein ratio, IDE-8 cell-derived virions additionally appeared to be more decorated with G_N and G_C .

Mazelier et al. also previously reported that UUKV particles produced from tick cells are more infectious towards mammalian cells in comparison to virus particles amplified in mammalian cells (150). Thus, the ratio of infectious to defective virions may be higher when UUKV was produced in IDE-8 cells possibly because of more efficient genome packaging of UUKV particles produced in tick cells as demonstrated for RVFV in mosquito cells (172). However, results from this thesis provide another possible explanation for the observed difference. The increased

infectivity may also be explained by the possibly denser decoration of IDE-8-derived particles with the glycoproteins. This gives rise to the question if the structural arrangement and the functionality of glycoproteins differ between mammalian and tick cell-produced UUKV particles. To further analyze the infectivity of individual viral particles, future studies will require careful determination of the specific infectivity based on the total amount of viral particles present in the sample. To assess this experimentally, one could use a flow virometry assay. Flow virometry is a flow cytometry-based method which has been established recently and proven to allow detection, quantification, and characterization of individual virus particles. This innovative method rapidly advanced over the past years (175–180).

Furthermore, UUKV particles produced from IDE-8 cells were more diverse in size. This leads to the question whether there are differences in virus assembly and budding of UUKV in mammalian versus tick cells. Moreover, it is not clear whether this constitutes an actual advantage for infection, or whether this is simply a byproduct of a distinct egress mechanism in tick cells. While phenuivirus budding is partially described in mammalian cells (80, 81, 83), little is known about the egress in arthropod cells. After protein synthesis of UUKV, the virions assemble and bud through ER, ERGIC, and Golgi compartments in mammalian cells. Virus particles are then transported to the plasma membrane in vesicles, being released from the cell (82, 84). However, as of yet UUKV budding was not studied by state-of-the-art microscopic analysis such as cryo-EM. For UUKV and RVFV it was shown that the glycoproteins are crucial for packaging of N protein and RdRp as well as for virus release (83, 181). However, factors influencing assembly, budding, and egress remain largely elusive.

Preliminary results of subtomogram averaging of a single UUKV particle produced from IDE-8 cells revealed a highly organized lattice structure of the surface glycoproteins. Analyzing a larger set of imaged particles is necessary to reach higher resolution and allow comparisons at the angstrom level between UUKV produced in tick and mammalian cells which is the only way to shed light into the ultrastructural details of viral particles. This is currently a work in progress, enabled by the purification protocols I established to obtain large volumes of high purity viral particles from both tick and mammalian cells.

3.1.2. Virus stocks derived from tick cells contain small 25 nm particles

Another difference between the virus stocks prepared in IDE-8 and BHK-21 cells and analyzed by cryo-EM, was the presence of small, enveloped structures, here referred to as mini-particles with a diameter of around 25 nm (membrane-membrane distance) in the samples produced from IDE-8 cells. These mini-particles were largely absent in the viral stocks produced from BHK-21 cells. The presence of internal electron densities and visible glycoprotein spikes indicated that they could constitute UUKV particles. If so, these UUKV mini-particles might only harbor two RNA segments or less, which could further explain the higher glycoprotein content in tick cell-derived samples. However, this would indicate big differences within the supergroup of arboviruses as for example increased genome packaging efficiency for RVFV was described in mosquito cells compared to mammalian cells (172).

For example for Hepatitis B virus (HBV), it was shown that during infection a large quantity of noninfectious, so called subviral particles (SVPs) are produced (182, 183). These SVPs outnumber the infectious viral particles (Dane particles) by a factor of at least 1000 and were associated with immune evasion of HBV by inhibiting innate and adaptive immune responses (184). For instance, they interfere with cytokine signaling and Toll-like receptor (TLR) function, inhibit HBV-specific B cell functions, reduce the efficacy of HBV-specific antibodies, and lead to HBV-specific T-cell exhaustion (185–189). It would be interesting to investigate whether the mini-particles found in the UUKV production could also contribute to immune evasion. However, in case of UUKV, much lower fractions of mini-particles were found. Moreover, these mini-particles were mostly present in the virus productions obtained from tick cells, meaning that they would not be present inside the mammalian host. Thus, it could be possible that the observed mini-particles possess biological functions for UUKV infection in ticks, potentially they could be involved in immune evasion mechanisms.

The tick immune system remains largely uncharacterized (190–192). Ticks produce lysozymes and antimicrobial peptides such as defensins (193, 194). Furthermore, phagocytosis, lectins, and reactive oxygen species were shown to constitute potential barriers (195, 196). Similar as for mosquitoes, RNA interference (RNAi) was demonstrated to be an important antiviral mechanism in ticks (197–199). Possibly, the mini-particles found in UUKV productions derived from IDE-8 cells could be involved in establishing a persistent infection in the arthropod vector.

An alternative hypothesis is that the tick cells were intrinsically infected with another, possibly endogenous, virus. Production of this virus could be triggered by additional UUKV infection. An example of a described endogenous virus in ticks is the nonenveloped orbivirus St Croix River virus (SCRV), which was previously detected in various tick cell lines (200, 201). EM-studies of the SCRIV described the virions to have a size of around ~ 60 nm spike-spike distance (202) and thereby, they are bigger than the mini-particles detected in the UUKV stocks. Sequencing of the isolated mini-particles from tick cells could give more answers to the previous questions, as could simpler approaches such as a western blot using antibodies raised against the UUKV proteins N, G_N, and G_C.

The differences in size distribution of UUKV particles derived from BHK-21 versus IDE-8 cells, together with the differences in infectivity and glycoprotein to nucleoprotein ratio, raise many interesting questions. It would be of particular interest to visualize UUKV assembly, budding, and egress in both mammalian and tick cells using high resolution light microscopy or EM methods. Additionally, since the dual life cycle of arboviruses remains largely uncharacterized, the tick-to-human transmission of phenuiviruses should be investigated. It would be compelling to employ proteomic and lipidomic approaches to compare virions derived from tick and mammalian cells. Moreover, the proteome and lipidome of infected tick cells should be explored. Following incoming virus particles during infection of skin organoid models, mice, or potentially also ticks via multiphoton microscopy could furthermore elucidate the differences of mammalian and arthropod cell-derived viral particles during entry (203–205). Taken together, UUKV particles produced from mammalian and tick cells possess distinct morphological and molecular features and their potential implications in biological functions remain to be determined.

In the following section of this discussion, I will focus on the applied OMICS approaches to UUKV particles which were produced in mammalian cells. This will lay the groundwork for follow up studies with virions produced from tick cells and allow comparison between UUKV originating from arthropod and mammalian producer cells.

3.2. GBF1 is a host protein involved in UUKV infection

3.2.1. A protein MS approach identifies GBF1 as an UUKV interaction partner

Rapid technological advances of recent years led to the development and increasing accessibility of screening methods which enable the investigation of new pro- and antiviral host factors (86, 206). Here, a co-immunoprecipitation with the UUKV glycoproteins followed by label-free protein MS identified 39 proteins as potential host factors interacting with UUKV. GOCC analysis was applied to cluster the hits according to their location relative to cellular structures revealing that most potential host factors were membrane annotated. Molecular network enrichment analysis using the Ingenuity Pathway Analysis software package (Qiagen) showed that “Cellular Assembly and Organization” was the most abundant network. Based on these analyses, nine membrane annotated hits from that network, and the three potential host factors with the highest significance in this network were selected for further analysis. The role of these twelve proteins for UUKV infection was further evaluated by siRNA silencing and subsequent infection of A549 cells. These experiments revealed that GBF1 as an infection-promoting host factor necessary for UUKV infection. GBF1 is a GEF resident at the Golgi apparatus, the ERGIC system, and in lipid droplets. It is involved in direct or indirect functions for COPI dependent Golgi-ER transport, lipid droplet metabolism, and clathrin-independent endocytosis (91).

Silencing of the other eleven proteins did not impair UUKV infection. However, it is noteworthy that silencing was only confirmed for GBF1 and not for the other proteins. Hence, the proteins ERLEC1, GOLPH3, GOLPH3L, HEATR3, MARS, SAAL1, SEL1L, SURF4, TNOP3, TRAPPC2L, and VDAC2 could possess biological functions during UUKV infection and should not be completely excluded from future studies.

3.2.2. Various RNA viruses depend on GBF1 for infection

The importance of GBF1 for UUKV infection was confirmed by genetic silencing and pharmacological inhibition of GBF1. After that, I applied the same approach to other viruses, to investigate whether GBF1 only possesses a specific role for UUKV or maybe a more general function involved also for other viruses. The closely related viruses TOSV and RVFV Δ NSs, as well as the alphavirus SFV from the family *Togaviridae* also depended on GBF1 expression for infection. As

mentioned in the introduction, GBF1 was previously also described to be involved in the replication of the RNA viruses DENV, HCV, hCoV 229E, VSV, YFV, CVB, HEV, and poliovirus (88–90, 92–95). In a collaborative work, it was confirmed that GBF1 played a role for VSV, HCV, and hCoV 299E infection (data not shown, (163)). In addition, my collaborators demonstrated that GBF1 is also involved during infection with the alphavirus CHIKV, the tick-borne flaviviruses Langkat virus (LGTV) and TBEV, and the mosquito-borne flavivirus Japanese encephalitis virus (JEV) (data not shown, (163)). While GBF1 seems to be important for many RNA viruses, the DNA virus HAdV-5 did not require GBF1 for efficient infection. Similarly, the retrovirus HIV-1 did not rely on GBF1. As trafficking between and interactions of ER and Golgi are necessary for HIV-1 infection, it suggests that these pathways were fully functional when GBF1 was silenced or inhibited. Thus, my results indicate that GBF1 is a proviral factor rather specific to RNA viruses that replicate in the cytosol.

The structural and genomic organization of the numerous viruses that depend on GBF1 for infection is diverse. There are non-enveloped (e.g., HEV, poliovirus, CVB) and enveloped viruses, positive stranded (e.g., SFV, CHIKV, VSV, HCV, JEV, etc.) and negative stranded (UUKV, RVFV, TOSV) viruses. Although they have such distinct characteristics, the viruses mentioned above all share the property of having an RNA genome that replicates exclusively in the cytosol (58, 207, 208). Therefore, it seems likely that GBF1 could be involved in a general mechanism shared by all these viruses.

However, taking into consideration that GBF1 is present at various cellular locations and possesses multiple cellular functions, it opens the possibility that GBF1 might play different roles for different viruses. Interestingly, GBF1 was also demonstrated to be involved in productive IAV infection. IAV belongs to the family *Orthomyxoviridae*, which constitutes RNA viruses, which unlike most RNA viruses, replicate in the nucleus. The findings suggested that GBF1 is important for the IAV assembly process (209–211). On the other hand, for DENV, HCV, hCoV 229E, VSV, YFV, CVB, and HEV, GBF1 was linked with efficient replication (88–90, 92, 93). Some viruses were shown to employ GBF1 for the formation of replication complexes, for others the role of GBF1 during replication remains uncharacterized. Counterintuitively, using different truncation versions of GBF1, poliovirus replication was described not to rely on GBF1 activity but rather on the expression of the N-terminal region of GBF1. This region was shown to directly interact with viral

proteins, however, the mechanism of how this interaction is beneficial for poliovirus replication remains elusive (95, 212, 213).

3.2.3. GBF1 plays a role during UUKV replication and egress

To further delineate a concrete step of UUKV infection in which GBF1 is involved, assays targeting single steps of infection were employed. Inhibition of GBF1 activity using GCA impaired UUKV egress, but also had an adverse effect on replication (Figure 34), consistent with experiments performed using other viruses (88–90, 93). As mentioned above, UUKV relies on ER, ERGIC, and Golgi compartments for assembly and release. Considering that co-immunoprecipitations revealed an interaction between GBF1 and the glycoproteins, this interaction could play a crucial role during UUKV budding and release. However, the effect of GBF1 on replication cannot be simply explained from the current standpoint. Potentially, other viruses depending on GBF1 for replication could additionally employ GBF1 for virus budding and release, and it would be an interesting venture to explore the intricacies of these mechanisms for viruses other than UUKV. To this end, the UUKV VLP release assay, which was established in this thesis to uncouple other infection steps from the virus release process, could be adapted for other viruses. In the absence of such a system, assessing ratio of virus particles trapped inside the producer cells versus released particles can also be explored using virus isolates.

UUKV seems to reshape cellular organelles during infection in what is proposed to be a viral factory. The link between viral replication, assembly, and release with as many functions described for GBF1 could reflect that ER, ERGIC, and Golgi compartments may be reorganized during UUKV infection. Potentially, it could be spatially advantageous for the virus to reorganize organelles to enable replication, assembly, and budding at the same localization within the cells. Possibly, GBF1 could play a role in these structures which could explain the usage of GBF1 by many distinct viruses. It would be interesting to image GBF1 in parallel with cell organelles such as ER, ERGIC, and Golgi apparatus during virus infection to characterize the location and functions of GBF1 in more detail.

I demonstrated here that GBF1 acts as a proviral factor for many pathogenic RNA viruses from numerous virus families including *Flaviviridae*, *Phenuiviridae*, and *Togaviridae*. This renders GBF1 an attractive druggable target for developing new antiviral strategies against, not only UUKV, but all the viruses that require GBF1 for

their amplification and spread. Indeed, 2.5-10 μM GCA can reversely inhibit GBF1 activity and GCA was shown here to possess broad antiviral activity against several viruses from different families. In the absence of alternative, more specific antiviral agents, GCA itself or a derivative could serve as starting structure for development of a therapeutic antiviral compound to inhibit GBF1 transiently.

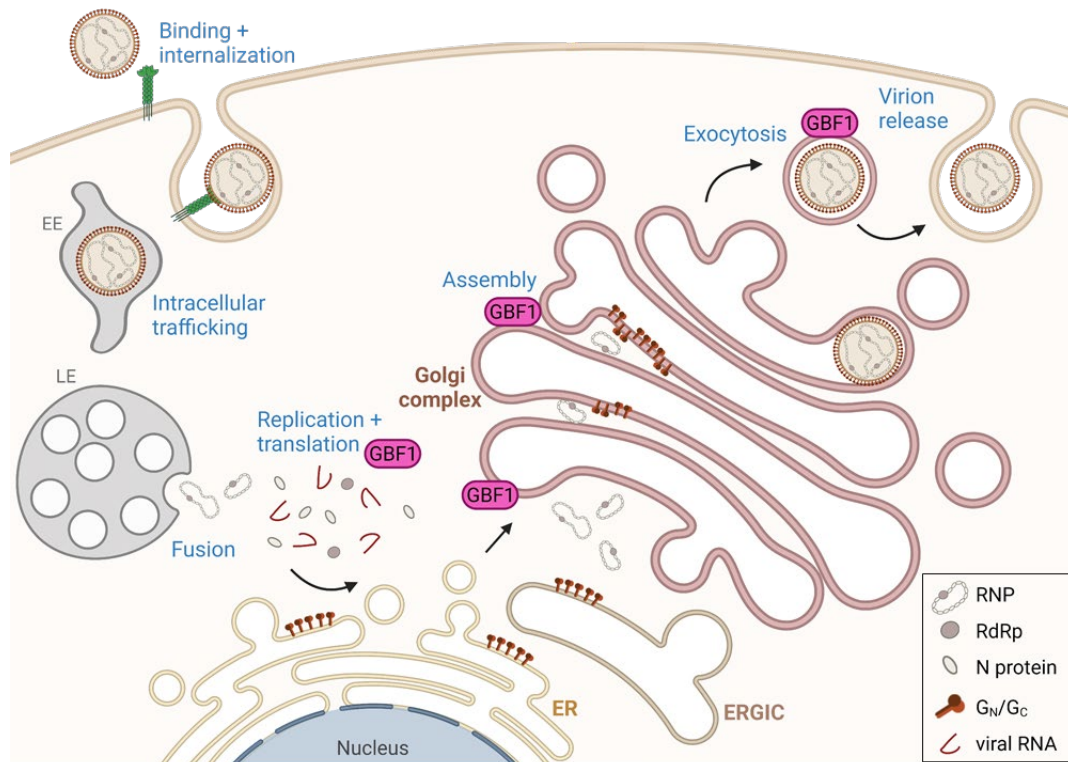


Figure 34. GBF1 involvement in UUKV infection.

UUKV binds to the target cell via receptors as for example via DC-SIGN or L-SIGN. It is internalized and traffics in endosomal compartments until reaching a low pH in late endosomes. The low pH induces fusion of the viral membrane with the endosomal membrane. Virus entry is completed by the release of the viral genome into the cytosol. The complete process of UUKV entry occurs regardless of GBF1. In this thesis, I found that GBF1 is important for UUKV replication and translation in the cytosol, as well as for viral progeny assembly and release at ER, ERGIC, and Golgi compartments. The figure was prepared using BioRender.

3.3. Host-derived GlcCer on the viral envelope promotes UUKV infection

3.3.1. Lipid MS indicates enriched HexCer in UUKV particles and infected cells

Lipid MS is a powerful method to screen for lipids involved in different stages of virus infections. Recently, increasing numbers of studies described lipid-virus interactions that are pivotal for infection and thus present important perspectives for the development of new antiviral agents (214–216). As mentioned above, phenuiviruses are enveloped viruses known to bud from ER, ERGIC, and Golgi structures (217, 218). However, which lipids are specifically required for entry, replication, and egress, and how the lipid composition of host cells affects virus infection remains unknown. Despite the recent advances in lipid MS, as of yet only few viral lipidomes were explored, likely because preparing suitable samples is technically difficult and often limited by the quantity of pure viral material. First, the respective viral particle stocks need to be produced to high quantities and sufficiently purified to be free of lipid contaminants. Secondly, the fixation method needs to be compatible with the MS protocol, but at the same time needs to ensure inactivation of the viral stock for the according BSL-level. In this thesis, I have established and optimized a workflow to produce, purify, characterize, and inactivate the phenuivirus UUKV for both, protein and lipid MS analysis.

Subsequently, lipidome analysis of UUKV particles and infected cells revealed an enrichment of the Golgi-resident glycolipid GlcCer in UUKV-infected BHK-21 cells and viral particles. Silencing and pharmacological inhibition of UGCG, the enzyme catalyzing the synthesis of GlcCer, impacted UUKV infection and particle production in BHK-21 cells. Interestingly, I found that the GlcCer in the UUKV envelope promotes virus binding to target cells and hence represents a plausible binding co-factor on the viral surface thereby mediating attachment and viral infection.

The preliminary lipid MS analysis of the UUKV particles that pointed towards an enrichment of GlcCer in virions was only performed once and the concentration of viral particles must be improved. The lipid concentration of the purified supernatant of uninfected cells, which served as a control in this assay, was close to baseline. Therefore, it might be helpful to employ another virus that does not incorporate GlcCer, such as SFV, as a negative control. The production and purification methods I established, will be applied to UUKV particles and further lipidome analyses will be performed in the near future. Additionally, GlcCer levels

could be assessed in UUKV particles, SFV particles, and the purified supernatant of non-infected cells using a dot blot with the antibody raised against GlcCer.

SFV particles acquire the lipid envelope during the budding process at the plasma membrane (116, 117). The lipidome of SFV particles was shown to be generally similar to the lipid composition of the plasma membrane of producer cells (118). Compared to the plasma membrane, the sphingolipid SM and the glycerophospholipid PS were enriched in the virions, while the glycerophospholipids PG and PI, as well as monosialodihexosylganglioside (GM3) were present in lower quantities. No enrichment of HexCer was found in SFV particles (118). Consistently, I could demonstrate that SFV infection of BHK-21 cells did not lead to enhanced GlcCer levels in infected cells, and infection and production of infectious particles was not impaired by PPMP treatment inhibiting GlcCer synthesis in producer cells. In this thesis, I suggest that TOSV particles could also incorporate GlcCer into their viral membrane, but the lipidome of the virions still remains to be defined. In future studies, it will be interesting to investigate whether GlcCer enrichment is a general feature of viruses which bud through ERGIC and Golgi compartments.

GlcCer is an intermediate in the metabolism to complex GSLs and is usually not present in high amounts in cells (219, 220). Taking into consideration that the lack of physiological GlcCer levels in producer cells impairs UUKV infectivity, this suggests a specific upregulation by UUKV during infection. As I did not characterize the mechanisms of GlcCer enrichment in UUKV-infected cells during my study, the different possible reasons for this enrichment are open to discussion. One explanation could be that GlcCer is not further metabolized to Hex2Cer and more complex GSLs. UUKV budding from ER, ERGIC, and Golgi compartments might hamper cellular functions of these networks including GSL synthesis. Another possibility could be that viral proteins directly or indirectly regulate host factors, thereby interfering with the GSL metabolic pathway. Inhibition of GBA or upregulation of UGCG could for instance lead to enriched GlcCer levels.

Some diseases such as diabetes, cancer, or cardiovascular diseases are known to alter GlcCer levels in tissues and cells. In general, GlcCer enrichment was associated with increased cell proliferation (221). Caused by mutations in GBA, Gaucher disease leads to prolonged elevated levels of GlcCer, displaying many problematics of GlcCer imbalances as patients suffer from fatigue, anemia, and enlargement of the liver and spleen (222). It would be of interest to explore, whether

patients infected with pathogenic viruses related to UUKV suffer from similar symptoms associated with elevated GlcCer levels.

3.3.2. GlcCer is required for infectivity of progeny UUKV particles

In this thesis, I found that UUKV upregulated GlcCer levels drastically during infection suggesting that GlcCer possesses a not yet described function during UUKV infection. Strikingly, UUKV particles produced in cells depleted from GlcCer exhibit greatly reduced infectivity (~ 80%). Previously, UGCG, the enzyme essential for GlcCer metabolism, was shown to be important for DABV infection (143). DABV infection in humans was associated with diarrhea, fever, multiple organ failure, and thrombocytopenia (27, 28). Like UUKV, DABV is a tick-borne phenuivirus. Drake and colleagues observed that silencing and inhibiting UGCG leads to reduced DABV infection levels. However, they did not analyze GlcCer levels in viral particles or assessed the effect on virus production. Due to the similarities between DABV and UUKV, it is possible that DABV also contains high GlcCer levels in the viral envelope and might also use GlcCer for binding to target cells. This hypothesis should be tested in future studies by analyzing the DABV lipidome and by producing DABV in the presence of UGCG inhibitors followed by characterizing the infectivity of produced DABV particles.

While for UUKV an enrichment of GlcCer in producer cells seems to be beneficial in order to incorporate GlcCer into the viral envelope, for IAV it was suggested that homeostatic and highly regulated amounts of GlcCer are optimal for infection (139–141). GBA, which degrades GlcCer into Cer and glucose, and UGCG were both knocked out in different cell lines, and then IAV infection was monitored. IAV infection was reduced in UGCG KO and GBA KO cells lines. Thereby, GBA and UGCG were both related to IAV entry, more precisely intracellular trafficking of virions and viral escape from endosomes (135, 136). It was shown that the IAV envelope was only marginally enriched in HexCer and more enriched in Hex2Cer (121). Possibly, IAV does not incorporate GlcCer in the viral envelope, but rather employs GlcCer during entry, more specifically during fusion from endosomes. While UUKV buds through ER, ERGIC, and Golgi network, IAV acquires its envelope by budding through the plasma membrane (223). This could be an explanation why IAV does not incorporate GlcCer, as this GSL is not present in the plasma membrane to a significant extent. The utilization of GBA and UGCG during IAV entry is of particular

interest, as IAV, like UUKV, is a late-penetrating virus, *i.e.*, these viruses rely on late endosomes for fusion and entry (224). Therefore, additionally to the role of GlcCer on the UUKV envelope described in this thesis, GBA and UGCG could also be involved in UUKV intracellular trafficking and/or fusion, as demonstrated for IAV. It would be interesting to test this hypothesis by monitoring UUKV entry in GBA and UGCG KO cells. Nevertheless, the utilization of GlcCer seems to be very different to UUKV, for which high GlcCer levels in infected cells as well as in virions seem advantageous.

3.3.3. GlcCer seems to play an ambiguous role for RVFV infection

I next expanded the investigation of GlcCer to a highly pathogenic phenuivirus, namely RVFV. RVFV is a mosquito-borne phlebovirus responsible for frequent outbreaks in cattle, sheep, and goats in sub-Saharan Africa (35–37). Interestingly, I observed different phenotypes of RVFV infection levels upon UGCG inhibition, which essentially depended on the expression of its non-structural protein NSs. While RVFV infection was not hampered by PPMP treatment of BHK-21 cells when the virus expressed NSs, RVFV Δ NSs infection levels in BHK-21 cells decreased upon GlcCer synthesis inhibition. In contrast, neither RVFV wt nor RVFV Δ NSs infection in A549 cells relied on GlcCer. It is very intriguing that the involvement of GlcCer during RVFV infection seems to depend on the expression of the non-structural protein NSs, as well as on the infected cell line, as it suggests different infection mechanisms including the employment of distinct infection-promoting factors.

The first main observation was that NSs expression influenced the dependence of RVFV on GlcCer for infection. NSs is the major virulence factor for RVFV but is not essential for viral infection and replication in cell lines. The RVFV NSs protein was described to antagonize innate immune responses and is present as *punctae* in cytoplasm and filaments in nuclei of infected cells (59–61). A plausible explanation as to why RVFV did not rely on GlcCer for infection in BHK-21 cells, while the mutant lacking NSs did, could be that NSs expression enables RVFV to infect cells so efficiently that GlcCer as a proviral host factor becomes insignificant. Taking the broad functions and the high expression of NSs in RVFV-infected cells into consideration, NSs could influence lipid or protein expression of infected cells. Possibly, NSs modulates expression pathways of a different lipid, which could replace GlcCer efficiently rendering it redundant. Of note, RVFV wt was not purified

before infecting new cells, but instead the infectious supernatant harvested from producer cells was employed, which possibly also affects the early infection steps.

Secondly, the dependence of RVFV Δ NSs on GlcCer was influenced by the cell line in which the virus was produced. The inhibition of GlcCer synthesis decreased RVFV Δ NSs infection in BHK-21 cells, while infection of A549 cells remained the same. It is tempting to speculate, that A549 cells express another yet elusive protein or lipid that facilitates virus infection, rendering GlcCer redundant for RVFV Δ NSs infection in this cellular system. In contrast, I showed earlier that UUKV depends on GlcCer expression also in A549 cells.

However, in the absence of GlcCer, the production of infectious RVFV wt and RVFV Δ NSs particles from BHK-21 cells was reduced by ~ 60-70%. In summary, it would be of interest to characterize and compare the lipidomes of RVFV wt- and RVFV Δ NSs-infected cells, to exclude that NSs somehow prevents the accumulation of GlcCer caused by other viral proteins. Additionally, comparing the lipidome of RVFV-infected BHK-21 and A549 cells might help to understand the differences observed between the cell lines. It would also be of great interest to explore the viral lipidome and assess whether GlcCer is enriched in the RVFV envelope. Further experiments investigating binding of RVFV could help to estimate whether GlcCer possesses a role for RVFV infectivity. In conclusion, follow-up research will be required to decipher the complex link between GlcCer, RVFV, and NSs.

3.3.4. GlcCer in the UUKV envelope promotes binding to target cells

A role for GlcCer during UUKV binding was observed via two complementary approaches. First, virus produced in the absence of GlcCer was less efficient in binding to BHK-21 cells. In the second approach, prebound soluble C6-GlcCer competed with UUKV binding to BHK-21 and A549 cells. Pre-binding of C6-GlcCer also decreased TOSV and GERV binding to BHK-21 cells. While UUKV and GERV do not represent an evident threat to public health, TOSV is a neglected human pathogen endemic in Southern Europe where it represents the main cause of seasonal meningitis and encephalitis during the summer (41, 46, 225, 226). GERV is mosquito-borne bunyavirus belonging the family of *Peribunyaviridae* closely related to LACV, the causative agent of pediatric encephalitis (21, 22). Together, these results suggest, that GlcCer on the viral envelope could act as a binding factor

enhancing infection for UUKV, TOSV, and GERV. Thus, GlcCer in the viral envelope possesses biological importance for infection.

Ebola-VLP binding, on the other hand, was not affected by soluble GlcCer, consistent with the absence of GlcCer within the Ebola-VLP envelope revealed by the lipidomic analysis. As UUKV and TOSV, GERV is believed to bud through ER, ERGIC, and Golgi compartments which leads to the question whether GlcCer incorporation into the viral envelope and involvement for attachment could be a common feature of viruses that bud through these networks. On the contrary, the glycolipid is generally not enriched in viruses budding from the plasma membrane as here demonstrated for EBOV and as previously described for IAV, HIV-1, VSV, and SFV (118, 121, 122).

To the best of my knowledge, the only lipid that has been suggested to be incorporated into the viral envelope and thereby facilitate binding to target cells, is the glycerophospholipid PS. Many enveloped viruses, such as CHIKV, DENV, VACV, EBOV, and HIV-1 possess PS associated to the viral envelope functioning as an attachment factor during viral infection (111–115). PS-dependent uptake is mediated by specific receptors as for example Tyro3/Axl/Mer (TAM) receptors or T-cell immunoglobulin and mucin domain (TIM) receptors that usually sense apoptotic cells (227–229). The exact localization of PS within the lipid bilayer serves as a viability signal: in normal conditions it is present at the inner leaflet of the plasma membrane, whereas upon oxidative stress, apoptosis, or the activation of other stress signaling pathways, the lipid is displayed on the outer leaflet leading to rapid phagocytosis (230). However, PS is a negatively charged glycerophospholipid which is an important building block of the plasma membrane and hence, present in high quantities (126, 231). On the contrary, GlcCer is a Golgi-resident GSL intermediate, that is usually present in the cells at low levels, suggesting that UUKV and TOSV exert different and specific mechanisms to enrich and incorporate GlcCer in the viral envelope.

The orientation of GlcCer incorporation into the viral envelope remains unknown also rendering the mode of binding to the host cell speculative. A hypothesis could be that interactions between GlcCer on the viral particle and clusters of lipids on the plasma membrane lead to UUKV attachment and thereby might bring UUKV in proximity to receptors needed for virus entry. Similar mechanisms were previously demonstrated where for example cholesterol-rich lipid microdomains on the target cell can facilitate virus entry as for instance shown for

IAV, HIV, EBOV, and SARS-CoV-2 (103–105, 107, 232). However, taking into consideration how densely the viral glycoproteins G_N and G_C cover the envelope of UUKV particles, it is difficult to imagine that GlcCer forms clusters on the viral envelope, rendering this hypothesis possible but unlikely.

Alternatively, it is possible that GlcCer on the virion could directly interact with the viral glycoproteins and thereby might play a role for their incorporation during budding, their multimerization, or their stability. By influencing the lipid content of the viral envelope, GlcCer could also influence the fluidity of the membrane which could in turn influence UUKV glycoprotein organization. However, these hypotheses are not supported by the competition of binding between soluble C6-GlcCer and UUKV particles. Nevertheless, it would be interesting to explore the UUKV particles which were produced in the absence of GlcCer for their overall morphology and more specifically concerning their glycoprotein organization by cryo-EM. For this, a workflow to produce higher amounts of virions from PPMP-treated cells and purify the UUKV particles needs to be established and optimized.

The most likely mode of action to explain how GlcCer in the viral envelope interacts with a target cell seems that cellular receptors recognize and bind either the lipid or glycan part of GlcCer. In the Golgi apparatus GlcCer is present in either direction, as it is faced to the cytoplasm when glucose is added by UGCG to form GlcCer. Then, a flippase translocates newly synthesized GlcCer into the Golgi lumen where more sugar molecules are added to form complex GSLs (138). Hence, theoretically UUKV particles could incorporate GlcCer in either direction. However, due to the hydrophilic nature of glucose and potential steric hindrance inside the particle, it is tempting to speculate that the glycan is facing outwards, while the lipid backbone is incorporated into the viral particle envelope. The possibilities of GlcCer-target cell interactions are summarized in Figure 35.

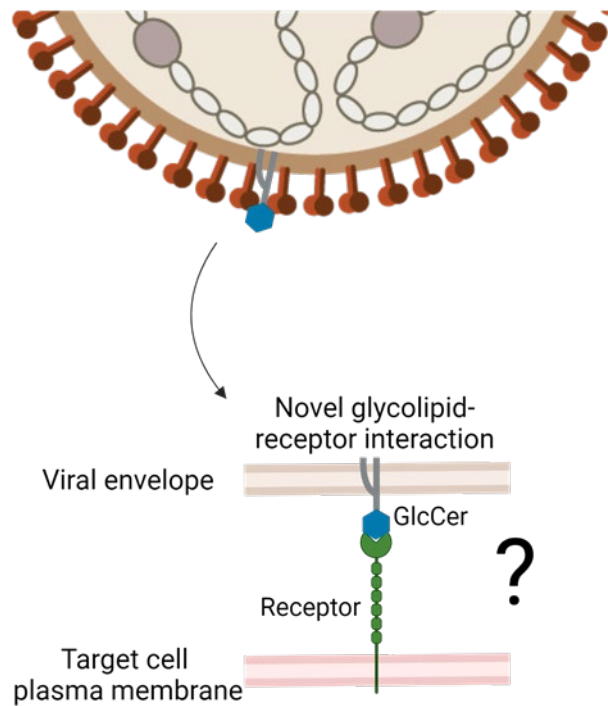


Figure 35. Potential GlcCer-receptor cell interaction during virus binding.

UUKV incorporates GlcCer while budding between ER and Golgi apparatus. The orientation of GlcCer on the viral envelope remains unknown. If the hydrophobic fatty acid-sphingosine is presented to the outside, lipid-lipid interactions could bring UUKV into proximity of entry receptors or could specifically bound by a receptor. Due to steric hindrance and hydrophilicity of the glycan, it seems likely that glucose is facing outwards. GlcCer could interact with the viral glycoproteins to stabilize them or modulate viral envelope fluidity in favor of virus binding. Alternatively, GlcCer could be recognized by a receptor that interacts with carbohydrates such as the CLR Mincle. The figure was prepared using BioRender.

To identify possible host cell receptors of GlcCer on the viral envelope, I collaborated with the team of Bernd Lepenies (University of Veterinary Medicine Hannover) to perform an ELISA-based screen of CLRs. In general, CLRs detect carbohydrate structures of exogenous pathogen associated molecular patterns (PAMPs) and endogenous damage associated molecular patterns (DAMPs) (233), meaning they could in theory interact with the glucose of GlcCer. Several viruses exploit CLRs as binding factors or entry receptors, for instance DC-SIGN and L-SIGN act as entry receptor and co-receptor for many different phenuiviruses as well as for HCV (52, 53, 234). In the ELISA-based CLR binding study, in addition to the positive controls DC-SIGN and L-SIGN, also Dectin-1, Dectin-2, Sign-R1, Sign-R3, MGL-1, DCAR, Clec4K, Clec12A, Clec12B, and Mincle showed increased binding to UUKV.

Mincle is a CLR that detects and binds to glucose residues, and was recently demonstrated to interact with GlcCer (170). This CLR is present on myeloid cells as for example DCs, macrophages, and monocytes which are among the first cells to encounter incoming arboviral particles in the skin of mammalian hosts (235). Moreover, Mincle was recently associated with the entry pathway of the bunyavirus LACV (236). As previously mentioned, LACV is closely related to GERV which was used for binding competition studies with C6-GlcCer in this thesis (21). Furthermore, the phlebovirus RVFV was recently described to bind to Mincle in an ELISA-based CLR binding assay (237).

Therefore, I aimed to study UUKV binding to Mincle in a cellular context. For this purpose, I tested UUKV binding to parental and Mincle KO BMDCs differentiated from murine BMCs obtained via my collaboration with Bernd Lepenies (University of Veterinary Medicine Hannover). My results did not indicate an involvement of Mincle in UUKV binding in a cellular context. However, I cannot rule out that other receptors, such as murine homologs of the human DC-SIGN and L-SIGN, which are expressed in mBMDCs (238–243), could render a Mincle-specific interaction with GlcCer on the virion redundant for UUKV binding to these cells. These homologs could display a similar effect as observed in the binding competition assay of C6-GlcCer and UUKV on BHK-21 cells expressing DC-SIGN. Further experiments are required to clarify a possible role of Mincle in UUKV attachment. For instance, it would be interesting to bind the Mincle fusion protein used in the ELISA-assay to UUKV particles before infecting BHK-21 or A549 cells. Thereby, the saturation of potential Mincle-binding sites on the viral envelope (*i.e.*, presumably GlcCer) could result in decreased virus binding and infection.

Collectively, in the presented study I suggest a novel type of interaction between virions and target cells, specifically a host cell-derived glycolipid in the viral particle that may facilitate virus binding to target cells. The glycolipid GlcCer was shown to be a critical compound of the UUKV envelope that is involved in virus attachment to target cells. The interaction partner of GlcCer on the host cell surface remains to be identified and the exact strategies allowing the virus to enrich GlcCer levels upon infection opens room for follow-up studies. Virus receptor interactions are in general an important target for experimental investigations. Indeed, receptors represent an obvious target to disrupt virus attachment and in turn infection early on. Nevertheless, the identity of many virus receptors remains obscure. In order to find virus receptors, laboratories routinely screen the capacity of viral glycoproteins for

interactions with receptors on the host cell (96). However, up to date lipidome analyses were only rarely performed on viral particles and virus-infected cells. To my knowledge PS is the only lipid present in viral envelopes described to facilitate attachment to target cells (111–115) and with GlcCer, this thesis expanded the list.

Here, I suggest that glycolipids which are incorporated into the viral envelope should also be taken into consideration for future work on the characterization of viral receptors. Lipid analyses might lead to identifying novel virus-receptor interactions.

4. Conclusion

The goal of my PhD project was to provide a better understanding of phenuivirus infection in mammalian cells. My work provides the basis for future studies aiming to compare virions derived from mammalian and arthropod cells. In addition, I contributed to studying the unique dual life cycle of arboviruses by comparing morphological characteristics of virions produced in mammalian and tick cells. My thesis highlights the necessity to study arboviral infections in the context of their biological cycle including infection of and transmission between vertebrates and arthropods. Thereby, these investigations will provide a better characterization of the complex molecular and cellular mechanisms behind the arboviral host switch.

My work has resulted in the establishment of robust production and purification methods for UUKV particles from tick and mammalian cells. These techniques could also be applied to other arboviruses and unrelated viruses to allow, for among others, cryo-EM and OMICS MS analyses. Using these methods and large stocks of highly purified UUKV particles, lipidomic and proteomic MS approaches were optimized and used to analyze UUKV particles and the infected cells from which they derived. The proviral host factor GBF1 was identified in a protein MS analysis, and subsequent in-depth molecular and cellular characterization revealed a function of GBF1 related to UUKV replication and egress. Testing several different viruses, it became apparent, that GBF1 is highly likely a general infection-promoting factor for viruses that replicate in the cytoplasm and/or bud through ER/ERGIC/Golgi networks. With a lipid MS approach, I also identified a GSL, GlcCer, which is enriched in the UUKV envelope and involved in virus binding to target cells. As no

glycolipid was yet described to play such a role, this finding has the potential to represent a novel type of virus-receptor interactions. Altogether, the results I obtained during my PhD study have strong implications for potential pharmacological intervention strategies and characterization of future virus-host cell interactions.

Some arboviruses, such as CHIKV, CCHFV, RVFV, and YFV are zoonotic pathogens and regarded as a potential pandemic threat (1–4). The COVID19 pandemic caused by the emerging coronavirus SARS-CoV-2 is a recent example indicating how destructive a zoonotic virus can be for a previously naïve population. Jana Koch and I also conducted a project on SARS-CoV-2 that provided an overview of the molecular and cellular processes used by SARS-CoV-2 to enter host cells (154). In the context of a global pandemic, knowledge of receptor interactions is essential as they could be used as obvious druggable targets. With this PhD thesis, my work lays the basis for future investigations into virus-receptor interactions and subsequent early viral infection steps.

5. Materials and Methods

5.1. Materials

Table 3. Small interfering RNAs (siRNAs)

siRNA	siRNA sense sequence	Information
siRNA_ERLEC1_1	CCUACAGAAUUGAGUCUUA	(163)
siRNA_ERLEC1_2	GGACUUACGAAGUAUGUCA	(163)
siRNA_GBF1_1	CAACCACAAUGUUCGUAAA	(163)
siRNA_GBF1_2	GCAUAGUUUCGGUCAUCUA	(163)
siRNA_GBF1_3	GAGCACUACUUGUACAUGA	(163)
siRNA_GOLPH3_1	GUACGGGAACGAUUAGCUA	(163)
siRNA_GOLPH3_2	CUAUUAACAAGAAAGGUAA	(163)
siRNA_GOLPH3L_1	CCGCCUUACUCUUAUGGAA	(163)
siRNA_GOLPH3L_2	GAGAAACAGCGACUAGUGA	(163)
siRNA_HEATR3_1	GUCUUUCAGUGCUACAGCA	(163)
siRNA_HEATR3_2	GUGACGCAUUUAUGGAGAA	(163)
siRNA_MARS_1	GGAGCUGAGGAUAACUAUA	(163)
siRNA_MARS_2	CAGAGCAAGUGGACCUGUA	(163)
siRNA_SAAL1_1	CAUCCAGCUAUUUUAUGAUA	(163)
siRNA_SAAL1_2	GCAAGAGUAUCUAAAGAUA	(163)
siRNA_SEL1L_1	GGCUUAUGACUGCCUAUAA	(163)
siRNA_SEL1L_2	GCACCGAUGUAGAUUAUGA	(163)
siRNA_Control_A549	AllStars Negative	Qiagen
siRNA_Control_BHK-21	Scrambled	Sigma
siRNA_SURF4_1	UCAUAGCUCUGCAGACGAU	(163)
siRNA_SURF4_2	AGUUCCUCCGUGUCACAAA	(163)
siRNA_TNPO3_1	GGGACUCAUUGCUAACCCA	(163)
siRNA_TNPO3_2	CCUUACGAAUUGGAGCUAA	(163)
siRNA_TRAPPC2L_1	AGCCCUUCGAGACAACGAA	(163)
siRNA_TRAPPC2L_2	AGGUGAAGUUUGUCAUGGU	(163)
siRNA_UGCG_1	GUAAGAAACUGCUUGGGAA	(163)
siRNA_UGCG_2	GGUUACACCUCAACAAGAA	(163)
siRNA_VDAC2_1	AUCAAGUCUUCUACAAGA	(163)
siRNA_VDAC2_2	GGAGGAUCAUUUAUCAGA	(163)

Table 4. List of cell lines and primary cells.

Cells	Culture medium	Information
A549	DMEM (10% FBS, 1x NEAA)	(244)
BHK-21	GMEM (10% TPB, 5% FBS)	(245)
BHK-21 DC-SIGN	GMEM (10% TPB, 5% FBS)	This thesis.
BMC Mincle KO	IMDM (10% FBS, 2 mM L-glutamine)	(236)
BMC wt	IMDM (10% FBS, 2 mM L-glutamine)	(246)
BMDC Mincle KO	IMDM (10% FBS, 10% X63/GM-CSF supernatant)	(236)
BMDC wt	IMDM (10% FBS, 10% X63/GM-CSF supernatant)	(236, 246)
HEK 293T	DMEM (10% FBS)	(247)
HeLa MZ	DMEM (10% FBS)	(248)
HeLa TZM-bl	DMEM (10% FBS)	(249)
IDE-8	L-15 (10% TPB, 5% FBS, 0.1 % bovine lipoprotein, 1x GlutaMAX)	(250)
IRE/CTVM-19	L-15 (20% FBS, 10% TPB, 1x GlutaMAX)	(147)
Vero E6	DMEM (10% FBS)	(251)

Table 5. List of plasmids.

Plasmid	Notes	Information
pCMV Δ R.91 (HIV gag/pol/rev/tat)	Lentiviral packaging plasmid	Addgene
pMD2-G (VSV-G)	Expression of VSV-G	Addgene
pUUK-G _N /G _C	Expression of UUKV glycoproteins	(83)
pUUK-L	Expression of UUKV RdRp	(83)
pUUK-N	Expression of UUKV nucleoprotein N	(83)
pRF108-L	Anti-genomic full length UUKV L segment	(150)
pRF108-M	Anti-genomic full length UUKV M segment	(150)
pRF108-S	Anti-genomic full length UUKV S segment	(150)
pRF108-S. Δ NSsGFP	Anti-genomic UUKV S segment lacking NSs but expressing GFP	(163)
pTRIP-DC-SIGN wt	Lentiviral vector expressing DC-SIGN	(252)

Table 6. List of antibodies.

Antibody	Dilution	Information
Donkey anti-mouse IRDye 680RD	1:10,000 WB	LiCOR, 926-68072
Donkey anti-mouse 800CW	1:10,000 WB	LiCOR, 926-32212
Donkey anti-rabbit IRDye 680RD	1:10,000 WB	LiCOR, 926-68073
Donkey anti-rabbit 800CW	1:10,000 WB	LiCOR, 926-32213
eFluor 450 anti-murine CD11c	1:500 flow cytometry	Thermo Fisher Scientific, 48-0114-80
Goat anti-mouse AF488	1:500 flow cytometry	Thermo Fisher Scientific, A-11001
Goat anti-rabbit AF488	1:500 flow cytometry	Thermo Fisher Scientific, A-11034
Goat anti-rabbit HRP	1:500 ffu titration	Vector Laboratories, PI-1000
Mouse anti-actin	1:5,000 WB	Sigma-Aldrich, A2228
Mouse anti-GBF1	1:500 WB	Santa Cruz, sc-136240
Mouse anti-human DC-SIGN+DC-SIGNR AF405	1:200 flow cytometry	R&D Systems, FAB16211V
Mouse anti-human DC-SIGN+DC-SIGNR PE	1:200 flow cytometry	R&D Systems, FAB1621P
Mouse anti-RVFV N (ID8)	1:5000 flow cytometry	(253)
Mouse anti-SFV E2 (E2-1)	1:400 flow cytometry	(254)
Mouse anti-TOSV	1:4000 flow cytometry	(53)
Mouse anti-UUKV N (8B11A3)	1:800 flow cytometry, 1:1000 WB	(255)
PE anti-murine CD11c	1:200 flow cytometry	Thermo Fisher Scientific, 12-0114-81
Rabbit anti-Gc (K5)	1:100 WB	(256)
Rabbit anti-GlcCer	1:250 dot blot	Antibody Research Corporation, 111586
Rabbit anti-Gn (K1224)	1:100 WB	(256)
Rabbit anti-RVFV N (SE2323)	1:8000 flow cytometry 1:4000 ffu titration	(52)
Rabbit anti-UGCG	1:500 WB	LS Bio, LS-C107639
Rabbit anti-UUKV (U2)	1:4000 ffu titration, 1:2000 WB	(52)

Table 7. List of viruses.

Virus	Producer cells	Reference
GERV	BHK-21 cells	(20)
RVFV	BHK-21 cells, Vero E6 cells	(257)
RVFV Δ NSs GFP	BHK-21 cells, Vero E6 cells	(163, 258)
SFV	BHK-21 cells	(171)
TOSV	BHK-21 cells	(259)
UUKV	BHK-21 cells, IDE-8 cells, IRE/CTVM-19 cells	(150, 260)

Table 8. List of reagents and enzymes.

Reagent	Solvent (if applicable)	Company, Cat#
AF488 NHS ester	DMSO	Thermo Fisher Scientific, A20000
Atto488 NHS ester	DMSO	Atto-TEC, AD 488-31
C6-GlcCer	MeOH	Biomol, Cay24474-5
C6-GlcCer	MeOH	Biomol, MTY-1539
C6-GlcCer	MeOH	Biozol, LAR-56-1049-4
Endo H		New England Biolabs, P0702S
Golgicide A	MeOH	Sigma-Aldrich, G0923
NB-DGJ	MeOH, DMSO	Biomol, Cay19520-1
NB-DNJ	MeOH, DMSO	Biomol, Cay21065-1
PDMP	MeOH	Cayman Chemical, 10005276
PNGase F		New England Biolabs, P0704S
PPMP	MeOH	Cayman Chemical, 17236

Table 9. List of buffers.

Buffer	Composition
Agarose overlay (pfu titration)	2.5% FBS, 1% agarose, 0.4% Sodium bicarbonate in GMEM
CMC overlay (ffu titration)	16 g/l CMC, 4.25 g/l NaCl, 5% TPB, 2.5% FBS in GMEM
Crystal violet solution	3 g/l crystal violet, 4% PFA, 10% EtOH in H ₂ O
Fixing solution (gels)	40% methanol, 10% acetic acid in H ₂ O
FACS permeabilization buffer (FPB)	2% FBS, 50 mM ethylenediaminetetraacetic acid (EDTA), 0.2% NaN ₃ , 1 g/l saponin in PBS
HNE buffer	10 mM HEPES, 150 mM NaCl, 1 mM EDTA in H ₂ O (pH 7.3)
Lysis buffer 1	20 mM Tris-HCl, 50 mM NaCl, 2 mM EDTA 0.1% Triton X-100, 1x complete protease inhibitor in H ₂ O
Lysis buffer 2	50 mM HEPES, 150 mM NaCl, 10% glycerol, 1% NP-40, 1 mM CaCl ₂ in H ₂ O

Table 10. List of chemicals, media, and kits.

Chemical	Company
Agarose (ultrapure)	Thermo Fisher Scientific
Bovine lipoprotein	MP Biomedicals
Bovine serum albumin (BSA)	Roth
β -mercaptoethanol	Sigma
Carboxymethyl cellulose sodium (CMC)	Sigma
Complete EDTA-free protease inhibitor cocktail	Roche
CytoTox96 Non-Radioactive Cytotoxicity colorimetric assay (kit)	Promega
DAB + Ni Substrate (kit)	Biozol
D-glucose	Sigma
Dimethyl sulfoxide (DMSO)	Merck
Dithiothreitol (DTT)	Biomol
Dulbecco's modified Eagle's medium (DMEM)	Thermo Fisher Scientific
DNA ladder 1kb	NEB
DNA loading buffer 6X	NEB
DNA Restriction enzymes	NEB
Ethylenediaminetetraacetic acid (EDTA)	Thermo Fisher Scientific
Fetal bovine serum (FBS)	Thermo Fisher Scientific
GlutaMAX	Thermo Fisher Scientific
Glasgow's minimal essential medium (GMEM)	Thermo Fisher Scientific
4-(2-hydroxyethyl)-1-piperazineethanesulfonic acid (Hepes) 1M	Thermo Fisher Scientific
Hoechst 33258	Thermo Fisher Scientific
Iscove's modified Dulbecco's medium (IMDM)	Pan Biotech
Imperial Protein Stain	Thermo Fisher Scientific
Intercept blocking buffer	LiCOR
Leibovitz (L)-15	Thermo Fisher Scientific
Lipofectamine2000	Thermo Fisher Scientific
Lipofectamine RNAiMAX	Thermo Fisher Scientific
MeOH	Sigma
Ammonium Chloride (NH ₄ Cl)	Sigma
NP-40	Merck
NuPAGE™ MOPS SDS Running Buffer	Thermo Fisher Scientific
PFA	Merck
Penicillin	Capricorn
Phosphate Buffer Saline (PBS) (w/o Ca ²⁺ or Mg ²⁺)	Merck
Precast gel 4-12% bis tris	Thermo Fisher Scientific
Precast gel 10% bis tris	Thermo Fisher Scientific
Prestained protein marker	Thermo Fisher Scientific
Protease inhibitor cocktail	Roche

Saponin	Sigma
Streptomycin	Capricorn
Sucrose	MP biomedical
See Blue Plus strand	Thermo Fisher Scientific
Triton X-100	Sigma
Trypsin	Pan Biotech
Tryptose phosphate broth (TPB)	Sigma
Tween20	Roth

Table 11. Lipid MS internal standard master mix ingredients.

Lipid	Information
50 pmol PC (13:0/13:0, 14:0/14:0, 20:0/20:0; 21:0/21:0)	Avanti Polar Lipids
50 pmol SM (d18:1 with N-acylated 13:0, 17:0, 25:0)	Semi-synthesized (261)
100 pmol deuterated cholesterol (D7-cholesterol)	Cambridge Isotope Laboratory
27 pmol PI (17:0/ 20:4)	Avanti Polar Lipids
25 pmol PE (14:1/14:1, 20:1/20:1, 22:1/22:1)	Semi-synthesized (261)
25 pmol PS (14:1/14:1, 20:1/20:1, 22:1/22:1)	Semi-synthesized (261)
25 pmol DAG (17:0/17:0)	Larodan
25 pmol CE (9:0, 19:0, 24:1)	Sigma
24 pmol TAG (LM-6000/D5-17:0,17:1,17:1)	Avanti Polar Lipids
5 pmol Cer (d18:1 with N-acylated 14:0, 17:0, 25:0) or Cer (d18:1/18:0-D3)	Semi-synthesized (261) or Matreya
5 pmol GlcCer (d18:1 with N-acylated 14:0, 19:0, 27:0) or GlcCer (d18:1/17:0)	Semi-synthesized (261) or Avanti Polar Lipids
5 pmol Hex2Cer (d18:1 with N-acylated C17 fatty acid)	Semi-synthesized (261)
10 pmol PA (17:0/20:4)	Avanti Polar Lipids
10 pmol PG (14:1/14:1, 20:1/20:1, 22:1/22:1)	Semi-synthesized (261)
10 pmol LPC (17:1)	Avanti Polar Lipids
22 pmol pPE-mix 1 (16:0p/15:0, 16:0p/19:0, 16:0p/25:0)	Semi-synthesized (262)
31 pmol pPE-mix 2 (18:0p/15:0, 18:0p/19:0, 18:0p/25:0)	Semi-synthesized (262)
43 pmol pPE-mix 3 (18:1p/15:0, 18:1p/19:0, 18:1p/25:0)	Semi-synthesized (262)

Table 12. List of machines.

Machine	Company
Casting system compact gel electrophoresis	Biometra
Centrifuge 5430 R	Eppendorf
Consort EV231 power supplies	Merck
Eclipse Ts2 microscope	Nikon
FiveEasy pH meter	Mettler Toledo
Flow cytometer Canto	BD
Flow cytometer Celesta	BD
Flow cytometer Verse	BD
Heraeus Fresco 21 Centrifuge	Thermo Fisher Scientific
Heraeus Megafuge 40R Centrifuge	Thermo Fisher Scientific
iBlot gel transfer device	Thermo Fisher Scientific
Infinite M200Pro plate reader	Tecan
L8-60M Ultracentrifuge	Beckman Coulter
Leica SP8 microscope	Leica
LI-COR Odyssey CLx scanner	LiCOR
Minifold®-1 Dot-Blot System	Whatman
Optima L-90K Ultracentrifuge	Beckman Coulter

Table 13. List of software.

Software	Notes	Company/Reference
Adobe Illustrator	Figure design	Adobe Inc
BD FACS Diva	Acquisition, analysis	BD
BD FACS Suite	Acquisition	BD
BioRender	Figure design	BioRender.com
ChemSketch	Figure design	ACD/Labs, www.acdlabs.com , 2022
Fiji	Analysis	(263)
FlowJo v10.8.1	Analysis	Treestar
GraphPad Prism v9.1.1	Analysis, figure design	GraphPad Software
ImageJ	Analysis	(264)
Image Studio Lite	Acquisition, analysis	LiCOR

5.2. Methods

5.2.1. Cells

Cell culture. Mammalian cell lines and primary cells were kept in an atmosphere of 5% CO₂ at 37°C, while arthropod cells were grown at 28°C. Cell culture products were purchased from Thermo Fisher Scientific or Merck. BHK-21 cells were cultured in Glasgow's minimal essential medium (GMEM) supplemented with 10% tryptose phosphate broth (TPB) and 5% FBS. A549, HEK 293T, HeLa, and Vero E6 cells were grown in Dulbecco's Modified Eagle's Medium (DMEM) supplemented with 10% FBS. For A549 cells, DMEM was additionally supplemented with 1x non-essential amino acids (NEAA). Bone marrow cells from C57BL/6 mice were kindly provided by Bernd Lepenies (University of Veterinary Medicine Hannover) and the isolation was described elsewhere (246). To differentiate BMCs into BMDCs, 5% of granulocyte macrophage colony-stimulating factor (GM-CSF) supernatant derived from X63 cells was used in Iscove's Modified Dulbecco's Media (IMDM) supplemented with 10% FBS (265). After 48 h, fresh differentiation medium was added on top and on day four, the medium was exchanged. Nine days after the start of the differentiation, cells were tested for CD11c surface expression using the antibody PE anti-murine CD11c to confirm differentiation into BMDCs by flow cytometry acquisition and FlowJo analysis. Experiments with these cells were performed on days nine and ten. IDE-8 (*Ixodes scapularis*) tick cells were cultured in Leibovitz (L)-15 medium supplemented with 10% TPB, 5% FBS, 0.1% bovine lipoprotein, and 1x GlutaMAX, while IRE/CTVM-19 (*Ixodes Ricinus*) tick cells were grown in L-15 medium supplemented with 20% FBS, 10% TPB, and 1x GlutaMAX. For a complete list of used cells refer to table 4.

Lentivirus production. Lentiviruses to transduce BHK-21 cells to achieve a stable expression of DC-SIGN were produced in HEK 293T cells. Approximately 5x10⁶ cells in 10 cm-dishes were co-transfected with the plasmids pCMV ΔR.91 (HIV gag/pol/rev/tat), pMD2-G (VSV-G) (both Addgene) and pTRIP-DC-SIGN wt (252) using Lipofectamine 2000. For a complete plasmid list refer to table 5. The medium was exchanged 16 hpt, and the lentiviral supernatant was harvested 24 h later. After eliminating cell debris via centrifugation (1500 x g, 20 min, 4°C), the supernatant was directly used to transduce BHK-21 cells or stored at -80°C.

Lentiviral transduction to create stable cell lines. To create BHK-21 cell stably expressing DC-SIGN, roughly 3x10⁵ cells per well in a 6-well-plate were

transduced using the lentivirus-containing supernatant in different concentrations. 12 h later the medium was exchanged and 48 h post transduction, cells were sub-cultured and tested for DC-SIGN expression using the antibody mouse anti-human DC-SIGN+DC-SIGNR AF405/PE detecting DC-SIGN on the cell surface. Subsequently, expression levels were determined by flow cytometry acquisition and FlowJo analysis.

siRNA-mediated silencing. Cells were reversely transfected using Lipofectamine RNAiMAX reagents as described previously and then seeded (163). Briefly, 20 nM final concentration of each siRNA (table 5) was used to transfect approximately 2.5×10^4 cells three days before infection or analysis to confirm silencing. Non-targeting siRNAs were used as controls in every experiment. At least two non-overlapping siRNAs were tested for each gene of interest, for a complete list refer to table 3.

Drug treatments of cells. GCA, NB-DGJ, NB-DNJ, PDMP, and PPMP were all dissolved in MeOH. To pharmacologically inhibit GBF1, cells were pretreated with the indicated GCA concentrations for 1 h before infection. For UGCG inhibition experiments, cells were pretreated with the indicated drug concentrations for 16 h in case of PPMP or PDMP, or for 24 h with NB-DNJ or NB-DGJ (24 h).

5.2.2. Viruses

Virus particle production. All viruses were amplified from susceptible cell lines according to standard protocols. UUKV, GERV, RVFV wt, RVFV Δ NSs GFP, SFV, and TOSV could all be produced from BHK-21 cells and were previously described (table 7) and (20, 150, 163, 171, 257–260). For efficient production, roughly 70-80% confluent BHK-21 cells were infected with a low MOI (e.g., MOI 0.05 for UUKV) in the absence of FBS. After 1 h the medium was exchanged to remove unbound input virus. The infectious supernatant was harvested when cytopathogenic effects became observable (UUKV ~48 h, TOSV ~48 h, RVFV wt ~36 h, RVFV Δ NSs GFP ~60 h, GERV ~36 h, SFV ~24 h) and cell debris were cleared by centrifugation (1500 x g, 20 min, 4°C). UUKV was additionally produced in IDE-8 tick cells, where FBS was applied during production. Cells were infected at an MOI of ~ 0.001 and after 12 h half of the input was discarded, and fresh medium was added. An aliquot of the infectious supernatant was taken starting from three days post infection for at least 12 weeks and half of the supernatant was harvested

and replaced whenever the viral titer in the supernatant was higher than 5×10^7 ffu/ml. Ebola VLPs were kindly provided by Sophie Winter (Chlanda group, Bioquant Heidelberg) and the production was published elsewhere (266). Production of VSV-G pseudotyped and GFP-expressing HIV-1 VLPs (VSV-HIVLP-GFP) was previously described and VLPs were kindly provided by Thorsten Müller (Kräusslich group, CIID Heidelberg) (267).

Semi-purification of virus particles. The infectious supernatant was semi-purified through a 25% sucrose cushion (in HNE buffer) by ultracentrifugation ($96,000 \times g$, 2 h, 4°C). Viral pellets were resuspended in HNE buffer and characterized by titration and protein semi-quantification. As in the CIID BSL-3 facilities RVFV wt is not allowed to be ultracentrifuged, here I used the cleared infectious supernatant for titration and further experiments.

Titration of viral preparations. Virus titers were determined on BHK-21 cells by either pfu titration (GERV, TOSV, RVFV wt, SFV) or ffu titration (UUKV, RVFV Δ NSs GFP) and the MOI for every experiment is given based on this titer determined on BHK-21 cells. Titration assays via pfu were performed in 6-well-plates. Approximately 80-90% confluent BHK-21 cells were infected with a serial dilution of the viral stock in 500 μl and after 1 h an agarose solution was added so that viral spread through the supernatant was not possible. After three (SFV), four (GERV, RVFV wt), or five (TOSV) days, the agarose was fixed in 4% PFA and subsequently removed. Then, the cell layer was fixed in 4% PFA and stained with a crystal violet solution. After washing, plaques were counted, and the viral infectious titer was determined as $\text{pfu/ml} = \text{number of plaques} \times 2 \times \text{dilution factor}$. Titration of UUKV and RVFV Δ NSs GFP was determined via ffu assay. Here, about 1.6×10^5 BHK-21 cells were infected in a 24-well-plate by serial dilutions of the respective virus in 200 μl . A CMC solution was added after 1 h to prevent viral spread through the medium and 30 (RVFV Δ NSs GFP) or 72 (UUKV) hpi the medium was removed, and the wells were fixed in 4% PFA. Foci were visualized by an antibody staining using rabbit anti-RVFV N (SE2323) or rabbit anti-UUKV (U2) antibodies and a secondary antibody goat anti-rabbit horseradish peroxidase (HRP). DAB/nickel substrate was applied for a dark grey reaction product visualizing infected foci. The viral infectious titer was determined as $\text{ffu/ml} = \text{number of foci} \times 5 \times \text{dilution factor}$. For a list of antibodies and buffers refer to table 6 and table 9, respectively.

Semi-quantification of viral proteins via Coomassie blue staining. In order to determine the nucleoprotein to glycoprotein ratio, to semi-quantify the

glycoproteins for labeling, and to ensure viral preparation are free of contaminants, I separated the viral proteins by SDS-PAGE. Three different volumes of the viral stock (e.g., 2.5 μ l, 5 μ l, 10 μ l) were applied and a BSA standard serial dilution (62.5, 125, 250, 500, 1000 ng) on the same gel was used for semi-quantification. After separation, the gel was fixed for 1 h in 50% MeOH and 10% acetic acid in H₂O and then it was stained using imperial protein stain (Thermo Fisher Scientific). Washing was performed in H₂O, gels were acquired using the LiCOR Odyssey imaging system, and analysis was performed employing Image Studio Lite or Image J. A standard curve was determined for the serial dilution of BSA (Figure 11 C), enabling the semi-quantification of the structural viral proteins G_N, G_C, and N.

Fluorescent labeling of virions. Viral glycoproteins were labeled using AF488 (results 2.3.) or Atto488 (results 2.4.) amine-reactive NHS esters as previously described (156). Roughly 100 μ g of glycoproteins were labeled in molecular glycoprotein to dye ratios of 1:2 (UUKV, RVFV Δ NSs GFP, and TOSV), 1:3 (GERV), or 1:30 (SFV). I optimized these ratios for the viruses labeled so that infectivity was not impacted, but at the same time the labeling appeared sufficiently bright.

Gradient-purification of viral particles. For OMICS approaches, cryo-EM, CLR binding studies, and after labeling, virus stocks were purified over a sucrose gradient ranging from 15% to 65% sucrose in HNE. After ultracentrifugation (96,000 x g, 4°C, 1.5 h, brakes off), a viral band became visible and was extracted. Optionally, the sucrose in the purified viral stock was washed away in HNE buffer using another ultracentrifugation step (96,000 x g, 4°C, 2 h). Viral preparations were characterized for infectivity, absence of contaminants, and nucleoprotein to glycoprotein ratios.

Reverse genetics system for UUKV. Plasmids to reversely transcribe UUKV have been described elsewhere (150). Briefly, 6x10⁵ BHK-21 cells were transfected with the plasmids pRF108-S, pRF108-M, and pRF108-L constituting the antigenomic full length UUKV S, M, and L RNA segments, respectively, as well as the expression plasmids pUUK-N and pUUK-L coding for the UUKV nucleoprotein and the RdRp under the control of a CMV promoter. Transfection was performed using Lipofectamine 2000, and 24 hpt medium was exchanged. When cytopathogenic effects were visible on day three, supernatant was harvested and viral particles were further passaged in BHK-21 cells by virus production protocols.

Minigenome system to investigate UUKV replication. To assess UUKV replication, the pRF108-M coding for the UUKV glycoproteins was omitted to ensure no progeny virus particles are released and the readout in this assay is only replication. To allow for easy quantification via flow cytometry, the plasmid pRF108-S. Δ NSsGFP was generated by synthesizing the cDNAs corresponding to the 5' noncoding region (NCR)-N sequence and GFP sequence-3' NCR by polymerase chain reaction (PCR) from plasmid DNA encoding the UUKV S segment and GFP. Then the cDNAs were amplified by the primers AATCGTCTCTAGGTACACAAAGACCTCCAACCTTAGCTATCG and AATCGTCTCTGGGCCGAAGCCCTTTAGAGTCC, and the primers AATCGTCTCTGCCCAAACCTAGAGTCCGGACTTGTACAGCTCG and AATCGTCTCTGGGACACAAAGACCCTCCAACATTAAGCATGGTGAGCAAGGGCGAGGAGC, respectively. After digestion, the PCR products were subcloned into the pRF108 plasmid vector (163).

UUKV VLP assay to explore virion release. For the UUKV VLP release experiment, the expression plasmids pUUK-G_N/G_C and pUUK-N coding for the viral glycoproteins and the nucleoprotein under a CMV promoter, were co-transfected. Cells and supernatant were harvested 48 hpt. Cells were lysed and VLPs were concentrated by ultracentrifugation. Subsequently, viral glycoproteins were assessed in cell lysates and UUKV VLPs by western blotting (163).

5.2.3. Flow cytometry-based assays

Flow-cytometry based virus infection experiments. Virus infections assays were performed as previously described (52). Briefly, cells were infected with the indicated MOIs of UUKV, TOSV, SFV, RVFV Δ NSs GFP, RVFV wt, or GERV. After 1 h, the viral input was discarded and replaced by fresh medium, incubated for the indicated infection times, and then fixed in 4% PFA. Infected cells were permeabilized by 0.1% saponin in the FACS permeabilization buffer (FPB) and viral antigens were stained by primary (1 h at room temperature or 16 h at 4°C) and secondary antibodies (45 min) listed in table 6. Only monitoring of RVFV Δ NSs GFP infection levels did not require an antibody staining as GFP expression served as a measure for viral replication. Infection levels were determined by flow cytometry and FlowJo analysis (Treestar).

Endosomal bypass assay. To delineate drug effects on virus intracellular trafficking, penetration, or replication, I forced UUKV fusion on the plasma membrane by adding a buffer with pH 5. Thereby endosomal trafficking and fusion from late endosomes was circumvented. Endosomal fusion was additionally inhibited in the samples where plasma membrane fusion was forced. This was achieved by applying the weak lysosomal base NH_4Cl (50 mM), which prevents the acidification of the endosomes during maturation.

Binding and internalization assay with fluorescently labeled virus particles. To assess virus binding to cells, AF488 or Atto488 fluorescently labeled viral particles were bound to target cells on ice. After washing steps in PBS to get rid of unbound virus particles, fluorescence was acquired by flow cytometry and analyzed via FlowJo (Treestar). For internalization assays, after binding, cells were washed in PBS and then rapidly warmed up to 37°C for 30 min to allow internalization of labeled virions. Afterwards trypan blue was employed to differentiate between viral particles that were bound to the cell surface and viral particles that were already taken up. Trypan blue has the capacity to quench AF488 or Atto488 fluorescence. However, as it is not cell permeable, fluorescent signal from already internalized viral particles cannot be quenched by trypan blue. Fluorescence signals were analyzed by flow cytometry and FlowJo (Treestar).

Binding competition assay. To determine, whether GlcCer can block binding sites of UUKV, soluble C6-GlcCer was bound to cells on ice for 2 h at the indicated concentrations and then fluorescently labeled virions were bound for 1 h. The experiment was schematically represented in Figure 29 A. Detection of virus binding was monitored by flow cytometry and analyzed with FlowJo (Treestar).

5.2.4. Cryo-EM imaging of UUKV particles

Cryo-EM sample preparation and data acquisition were performed by Martin Obr (Schur group, IST Austria).

Sample preparation and data acquisition. For cryo-EM imaging of virions, the produced viral particles were gradient-purified and washed as described earlier. Then, samples were fixed in 4% PFA for 20 min and then vitrified and imaged as previously published for GERV (20). Briefly, the fixed virion solution was applied to degassed and glow discharged Quantifoil R2/2 Cu grids and then vitrified using EM GP2 plunge freezer (Leica) in liquid ethane. Data acquisition was performed with the

SerialEM software on a Glacios 200 kV transmission electron microscope equipped with Falcon 3 Direct electron detector (Thermo Fisher Scientific). The nominal magnification of high-resolution images was 73,000x resulting in a pixel spacing of 2.019 Å.

Image analysis. To determine the diameter of virions, the membrane-to-membrane distance was measured in Fiji from 2D EM images. The diameters along the shortest and longest axes were measured for at least 120 virions per sample. The aspect ratio was calculated for 37 virus particles by dividing the minimal diameter through the maximal diameter.

5.2.5. Label-free protein MS

The co-immunoprecipitation and the subsequent protein MS screen in four biological replicates were performed by Gisa Gerold and Lars Kühn (TWINCORE Hannover) and methods were described in (163).

Co-immunoprecipitation of host proteins with UUKV glycoproteins. UUKV particles were bound to A549 cells at an MOI of 2 for 2 h at 4°C. After two washing steps the cells were frozen, thawed, and then lysed in 1% NP 40 before immunoprecipitation. A549 cells with bound UUKV particles (A549 + UUKV) were compared to A549 cell which were incubated with the semi-purified supernatant of not infected cells (A549 + mock). Glycoprotein-specific antibodies were covalently bound to the aminolink plus protein A/G resin (Pierce) and incubated with the cell lysates for 16 h (268). Elution of the UUKV glycoproteins and associated host factors was performed in glycine buffer as previously described (269). Eluates of the immunoprecipitation assay were explored by LC-MS/MS analysis.

Label-free protein MS sample preparation. Eluates were prepared for protein MS analysis by reduction with 10 mM dithiothreitol, alkylation with 55 mM iodoacetamide and digestion with 1 µg LysC (Wako Chemicals) and 1 µg trypsin (Sigma) (270). Before loading of the samples to reversed phase C18 StageTips (3MTM Empore™, IVA Analysentechnik), digestion was terminated by 0.6% (v/v) trifluoroacetic acid and 2% (v/v) acetonitrile. Peptides were desalted in 0.5% (v/v) acetic acid, eluted using 80% (v/v) acetonitrile in 0.5% (v/v) acetic acid, and concentrated and dried by SpeedVac (Thermo Fisher Scientific). For MS acquisition, peptide mixtures were resuspended in 2% (v/v) acetonitrile, 0.1% (v/v) trifluoroacetic acid, 0.5% (v/v) acetic acid.

Label-free protein MS acquisition. Separation of peptides was achieved by employing a nanoflow UHPLC instrument (EASY-nLC 1200, Thermo Scientific). Then separated peptides were analyzed in a single run using the Xcalibur software (Thermo Scientific) by a quadrupole-Orbitrap instrument (Q Exactive HF mass spectrometer, Thermo Scientific) with a nanoelectrospray ion source (Thermo Scientific) which was coupled to the liquid chromatography instrument (270).

Label-free protein MS analysis. Proteins were identified and quantified using the computational proteomics platform MaxQuant (software version 1.5.5.2) and MAXLFQ algorithms (162). The acquired data was analyzed employing the software platform R, R Studio, and Persus (271, 272) and is available at the ProteomeXchange Consortium via the PRIDE partner repository (<http://www.proteomexchange.org>) using the identifier PXD015194 (273, 274). Protein interactions have been uploaded to the IMEx consortium (<http://www.imexconsortium.org>) with the data identifier IM-27097 (275). Potential interaction partners of the UUKV glycoproteins were explored by using A549 + mock as a negative control and the statistical analysis was performed by applying a parametric two-tailed Welch's t-test. To determine whether potential UUKV host factors differed in abundance, a false discovery rate (FDR) of 1% and a S_0 parameter of 1 were employed (276, 277). 43 significantly enriched proteins were identified in G_N/G_C co-immunoprecipitations from A549 + UUKV compared to A549 + mock. The four structural UUKV proteins G_N , G_C , N, and L were ignored for further analysis and the 39 host factors were characterized by annotation enrichment analysis using annotations from the UniProtKB Keywords (278). Host proteins were classified as membrane associated if annotated as "membrane", "plasma membrane" or "intracellular membrane-bounded organelle" according to GOCC (279). Pathway analysis was performed by using molecular network enrichment analysis of the ingenuity pathway analysis software package (Qiagen).

5.2.6. Lipid MS

The lipid MS screen and data evaluation was performed in collaboration with Christian Luchtenborg and Britta Brügger (BZH Heidelberg).

Lipid MS sample preparation. To analyze the lipidome of UUKV-infected BHK-21 cells and UUKV particles, cells were infected for approximately 48 h until cytopathogenic effects appeared. Cells were washed once in ice cold PBS, once in

ice cold 155 mM ammonium bicarbonate buffer (pH <7.6) and then scraped off in MeOH. Virions from the infectious supernatant and the not infected supernatant were semi-purified and subsequently gradient-purified by ultracentrifugation. After an additional wash in HNE buffer, 20 µl sample were taken up in 500 µl MeOH. All samples were kept at -80°C until acquisition. UUKV-infected BHK-21 cells which were treated with PPMP were harvested 24 hpi and treated as described above. TOSV- and SFV-infected BHK-21 cells were harvested approximately 36 hpi and 13 hpi, respectively, when cytopathogenic effects became apparent.

Lipid MS analysis. Lipid extractions, MS analysis, and data evaluation were previously described in (280). Lipid extractions from cells were performed using an acidic liquid-liquid extraction method (281). Exceptionally, plasmalogens were extracted under neutral conditions. In order to adapt extraction volumes of different samples to similar total lipid amounts, a test extraction determining the concentration of PC was done. Subsequently, similar amounts of lipids for each sample were subjected to extraction, if possible, approximately 2000 pmol for cells or 250 pmol for virus particles. Internal lipid standards for each lipid class resembling the structure of the endogenous lipid species were added prior to extractions to allow quantification. Using the master mix specified in table 11, lipid species were calculated based on the internal lipid standard intensities. For lipid analysis of viral particles, 0.5x the volume of the master mix was used for the lipid extraction. pPEs could not be quantified for virions as the concentration in the sample was too low. To evaporate the final CHCl₃ phase, a gentle stream of nitrogen was applied at 37°C. After lipid extraction, samples were either directly subjected to MS analysis, or were stored at -20°C until analysis. For the MS analysis, extracted lipids were resuspended in 10 mM ammonium acetate in 60 µl MeOH. To analyze cholesterol, lipid extracts were again evaporated and the acetylated as described in (282). MS analysis was performed using a QTRAP 6500+ mass spectrometer (Sciex) with chip-based (HD-D ESI Chip, Advion Biosciences) electrospray infusion and ionization via a Triversa Nanomate (Advion Biosciences). LipidView (Sciex) and an in-house developed software (ShinyLipids) were employed for data evaluation.

5.2.7. CLR binding studies

An ELISA-based assay to screen for CLRs interacting with UUKV was performed in collaboration with Kathleen Schön (Lepenies group, University of

Veterinary Medicine Hannover) using the methods reported by Monteiro and colleagues (236, 237).

CLR-hFc fusion protein library. The production of the CLR-hFc fusion protein library was previously described (283, 284). Briefly, amplified cDNA fragments of the CLR extracellular domain were ligated into a pFUSE-hlgG1-Fc expression vector (InvivoGen) which was transfected into Chinese hamster ovary (CHO)-S cells. CLR-hFc fusion proteins were purified from the supernatant by using a HiTrap protein G column (GE Healthcare).

ELISA-based UUKV/CLR binding studies. To assess UUKV binding to the respective CLRs, gradient-purified and washed UUKV stocks or not infected supernatant which was treated the same way were applied to half-area microplates (Greiner Bio-one) to coat them overnight at 4°C. After three washing three times with 150 µl 0.05% Tween-20 in 1x PBS, the wells were blocked in 150 µl 1% BSA in 1x PBS for 2 h. The plate was again washed. Then 250 ng/well CLR-Fc fusion proteins were added in 50 µl lectin binding buffer (50 mM HEPES, 5 mM MgCl₂, 5 mM CaCl₂) for 1 h. After three washing steps, 50 µl of anti-human IgG-HRP antibody (Dianova) diluted 1:5,000 in 1X PBS, 1% BSA and 0.05% Tween-20 was applied for 1 h. The plate was again washed. Subsequently, 50 µl of the substrate solution O-phenylenediamine dihydrochloride substrate tablet (Thermo Fisher Scientific) in 24 mM citrate buffer, 50 mM phosphate buffer and 0.04% H₂O₂ was applied, the reaction stopped with 50 µl of 2.5 M sulfuric acid after 5 min and absorbance was acquired at 495 nm using a Multiskan GO microplate spectrophotometer (Thermo Fisher Scientific).

5.2.8. Protein and lipid expression analysis

Western blotting. For protein analysis, cells were lysed in 0.1% Triton X-100 or NEB denaturing buffer (for *N*-glycosylation analysis of glycoproteins) and proteins were separated by SDS-PAGE. After proteins were transferred to polyvinylidene difluoride membranes (Thermo Fisher Scientific) by using the iBlot gel transfer device (Thermo Fisher Scientific), they were blocked in intercept blocking buffer (LiCOR). Membranes were incubated with primary antibodies against UGCG, UUKV proteins, UUKV G_N, UUKV G_C, GBF1, or actin for 1 h at room temperature or for 16 h at 4°C. After washing, LiCOR secondary antibodies were applied for 45 min at room temperature. For a complete antibody list refer to table 6. Membranes were acquired

with a LI-COR Odyssey CLx scanner and analyzed with Image Studio Lite or ImageJ.

Infectivity assay. UUKV particles produced in the presence or absence of PPMP were characterized regarding titer (described above in 5.2.2. Viruses – Titration of viral preparations) and regarding their viral protein content to enable conclusions regarding the number of infectious particles per total virus particles. The ratio of ffu/viral protein amount was determined by calculating ratio between infectious titer of released virions (ffu/ml) and the relative signal of the total amount of released viral particles (per ml). For each experiment, the ratio of ffu/viral protein amount was normalized to the sample not containing PPMP.

Binding assay. To compare the binding efficiency of UUKV particles produced in the absence or presence of PPMP, same total viral amounts (normalized to N) were bound to BHK-21 cells on ice for 2 h. The normalization of input virus was calculated based on previously performed western blot analyses of the viral stocks. After three washing steps, bound virions were monitored by western blot analysis of viral proteins described above.

Dot blotting. In addition to lipid MS analysis, GlcCer expression of cells was quantified by dot blot assays. Cells were lysed in 0.1% Triton X-100 and cell debris were eliminated by centrifugation. Lysates were directly applied to nitrocellulose membranes (Whatman) using the Minifold®-1 Dot-Blot System (Whatman). GlcCer expression was monitored applying an anti-GlcCer antibody (1:250, Antibody Research) and LiCOR secondary antibodies. Membranes were analyzed with a LI-COR Odyssey CLx scanner Image Studio Lite or ImageJ software.

5.2.9. Statistical analysis

Prism v9.1.1 (GraphPad Software) was used for graph plotting of numerical values and statistics. Figures show the means (\pm SEM) from at least three individually performed experiments and data was normalized to levels of cells transfected with non-targeting control siRNAs or solvent controls for the respective drug if not stated otherwise. Figure legends indicate sample sizes, statistical methods, and p values when appropriate.

6. Acknowledgements

This work was conducted under the supervision of Dr. Pierre-Yves Lozach in the Virology department of the CIID at the University Hospital Heidelberg and supported by the DFG and the CellNetworks cluster of excellence.

First, I want to express my great gratitude to Pierre-Yves for giving me the opportunity to perform my PhD in his group and to work on such interesting and versatile projects. Your positive and curious attitude towards unexpected or contradicting results (“that is interesting!”) amazed me. I enjoyed the productive discussions and the amazing working atmosphere you created with your constantly open door and positive thinking. Even the distance between Lyon and Heidelberg did not impair your continuous support. Thank you!

My gratitude extends to Prof. Dr. Oliver T. Fackler for taking the time to accompany my project throughout my time as a PhD student and for agreeing to be the first examiner of this work. I also want to thank Prof. Dr. Britta Brügger and Dr. Petr Chlanda for the great support and the valuable input during my TAC meetings as well as Prof. Dr. Bernd Lepenies and Dr. Marco Binder for agreeing to examine my thesis. Additionally, I would like to acknowledge our institute leader Prof. Dr. Hans-Georg Kräusslich for providing a stimulating research environment with excellent facilities.

During my time in the Lozach lab, I had the opportunity to collaborate with many other groups and I want to express my gratitude towards all collaborators that were involved in joint projects. Especially Lesley Bell-Sakyi needs to be acknowledged for kindly providing the tick cells and helping us with any problems that we encountered while establishing protocols with these cells in our laboratory. Martin Obr and Florian Schur provided beautiful cryo-EM images of so many viruses that we sent to them. Thanks to Rebecca Möller and Gisa Gerold for the fantastic teamwork during the GBF1 project. In addition, I thank Britta Brügger and Christian Lüchtenborg for all their lipid MS analyses and I want to thank Bernd Lepenies and Kathleen Schön for the fruitful collaboration and the nice stay in Hannover. Thank you, Thorsten Müller, Sophie Winter, and Petr Chlanda for providing VLPs and time and again constructive feedback during lively discussions. A special thanks also goes to Megan Stanifer and Steeve Boulant, who made it possible for Jana and me to accomplish a project on SARS-CoV-2 entry and fusion.

Many thanks to my group, I felt warmly welcomed in the “Lolo lab” and would like to thank all the members for the friendly atmosphere, open and enthusiastic scientific discussions, and relaxing times after work. Thank you Magalie for working with me the beginning of my PhD and for sharing all your protocols. Anja and Psylvia, you were so important for me to catch a good start in Heidelberg. I want to thank you for always answering all my (surely sometimes headless) questions and for the wonderful times in- and outside the lab. Stefan, you constantly managed to cheer me up during stressful times with many deadlines. Thanks to Jana for the incredible cooperation during our SARS-CoV-2 project and for staying in Heidelberg with me, when the lab here got smaller and smaller.

And there is one thing that goes well with the Lozach lab: students! Thank you to Antonia, Christian, Claudia, Felix, Franzi, Martin, Nina, Paulina, Tim, and Yannik for your contributions to different projects during my PhD. Moreover, I would like to thank all current and former CIID colleagues for establishing a nice atmosphere with productive discussion, relaxing coffee breaks, and fun times after work. Ann-Kathrin, Marta, Nadine, Rebecka, Robin, Sandra, Sophie, Tamara, Thorsten & Maike and many more: without you my time at the CIID wouldn't have been the same.

In Heidelberg I also met some significant people outside the lab. Thank you, Lilian, Raya, Lulu, and Yael for the unwinding times after work. And thanks to the HCH team for the friendly welcome and good times on the pitch. Furthermore, I would like to thank some friends that were already there long before the PhD times. Berit, Eva, Franzi, and Laura, you were the best “study buddies” I could think of. Anna and Katja, I cannot even remember the times before I met you. To the “Freitagsrunde”: thank you for being there whenever I needed your support. Hannah, it was a blessing that you and me by chance ended up in Heidelberg at the exact same time after spending our whole hockey-youth together back home.

Djordje, I am so happy that we met during our PhDs at the CIID. Thank you for believing in me and for bravely enduring me and my now and then possibly special stress coping mechanisms during the writing process(es) which mainly took place in our tiny flat. You are amazing.

Finally, I want to thank my family for the unconditional support ever since. Lotte, I really enjoyed the possibility to spend so much time with you in Heidelberg, but I know we'll also manage with more distance. My parents were always able to bring me down to earth and at the same time encouraged me to do things in my own way. I would not be where I am without your endless trust. Thank you!

7. References

1. D. Musso, A. J. Rodriguez-Morales, J. E. Levi, V.-M. Cao-Lormeau, D. J. Gubler, Unexpected outbreaks of arbovirus infections: lessons learned from the Pacific and tropical America. *The Lancet Infectious Diseases*. **18**, e355-e361 (2018), doi:10.1016/S1473-3099(18)30269-X.
2. M. A. Robert, A. M. Stewart-Ibarra, E. L. Estallo, Climate change and viral emergence: evidence from Aedes-borne arboviruses. *Current opinion in virology*. **40**, 41–47 (2020), doi:10.1016/j.coviro.2020.05.001.
3. M. Girard, C. B. Nelson, V. Picot, D. J. Gubler, Arboviruses: A global public health threat. *Vaccine*. **38**, 3989–3994 (2020), doi:10.1016/j.vaccine.2020.04.011.
4. O. W. Lwande *et al.*, Globe-Trotting Aedes aegypti and Aedes albopictus: Risk Factors for Arbovirus Pandemics. *Vector borne and zoonotic diseases (Larchmont, N.Y.)*. **20**, 71–81 (2020), doi:10.1089/vbz.2019.2486.
5. A. T. Ciota, L. D. Kramer, Insights into arbovirus evolution and adaptation from experimental studies. *Viruses*. **2**, 2594–2617 (2010), doi:10.3390/v2122594.
6. M. J. Conway, T. M. Colpitts, E. Fikrig, Role of the Vector in Arbovirus Transmission. *Annual review of virology*. **1**, 71–88 (2014), doi:10.1146/annurev-virology-031413-085513.
7. G. Kuno, G.-J. J. Chang, Biological transmission of arboviruses: reexamination of and new insights into components, mechanisms, and unique traits as well as their evolutionary trends. *Clinical microbiology reviews*. **18**, 608–637 (2005), doi:10.1128/CMR.18.4.608-637.2005.
8. M. Marklewitz, F. Zirkel, A. Kurth, C. Drosten, S. Junglen, Evolutionary and phenotypic analysis of live virus isolates suggests arthropod origin of a pathogenic RNA virus family. *Proceedings of the National Academy of Sciences of the United States of America*. **112**, 7536–7541 (2015), doi:10.1073/pnas.1502036112.
9. P. Léger, P.-Y. Lozach, Bunyaviruses: from transmission by arthropods to virus entry into the mammalian host first-target cells. *Future Virology*. **10**, 859–881 (2015), doi:10.2217/fvl.15.52.
10. W. R. Heath, F. R. Carbone, The skin-resident and migratory immune system in steady state and memory: innate lymphocytes, dendritic cells and T cells. *Nature immunology*. **14**, 978–985 (2013), doi:10.1038/ni.2680.
11. L. R. Petersen, M. P. Busch, Transfusion-transmitted arboviruses. *Vox sanguinis*. **98**, 495–503 (2010), doi:10.1111/j.1423-0410.2009.01286.x.
12. K. E. Jones *et al.*, Global trends in emerging infectious diseases. *Nature*. **451**, 990–993 (2008), doi:10.1038/nature06536.

13. M. Pfeffer, G. Dobler, Emergence of zoonotic arboviruses by animal trade and migration. *Parasites & Vectors*. **35** (2010), doi:10.1186/1756-3305-3-35.
14. B. M. Althouse *et al.*, Impact of climate and mosquito vector abundance on sylvatic arbovirus circulation dynamics in Senegal. *The American journal of tropical medicine and hygiene*. **92**, 88–97 (2015), doi:10.4269/ajtmh.13-0617.
15. T. Pereira-Dos-Santos, D. Roiz, R. Lourenço-de-Oliveira, C. Paupy, A Systematic Review: Is *Aedes albopictus* an Efficient Bridge Vector for Zoonotic Arboviruses? *Pathogens (Basel, Switzerland)*. **9** (2020), doi:10.3390/pathogens9040266.
16. Y. Y. Go, U. B. R. Balasuriya, C.-K. Lee, Zoonotic encephalitides caused by arboviruses: transmission and epidemiology of alphaviruses and flaviviruses. *Clinical and experimental vaccine research*. **3**, 58–77 (2014), doi:10.7774/cevr.2014.3.1.58.
17. J. Whitehorn, S. Yacoub, Global warming and arboviral infections. *Clinical medicine (London, England)*. **19**, 149–152 (2019), doi:10.7861/clinmedicine.19-2-149.
18. S. C. Weaver, M. Lecuit, Chikungunya virus and the global spread of a mosquito-borne disease. *The New England journal of medicine*. **372**, 1231–1239 (2015), doi:10.1056/NEJMra1406035.
19. G. J. Atkins, B. J. Sheahan, P. Liljeström, The molecular pathogenesis of Semliki Forest virus: a model virus made useful? *The Journal of general virology*. **80**, 2287–2297 (1999), doi:10.1099/0022-1317-80-9-2287.
20. S. Windhaber *et al.*, The Orthobunyavirus Germiston Enters Host Cells from Late Endosomes. *Journal of virology*. **96** (2022), doi:10.1128/jvi.02146-21.
21. S. Windhaber, Q. Xin, P.-Y. Lozach, Orthobunyaviruses: From Virus Binding to Penetration into Mammalian Host Cells. *Viruses*. **13** (2021), doi:10.3390/v13050872.
22. J. E. McJunkin *et al.*, La Crosse Encephalitis in Children. *N Engl J Med*. **344**, 801–807 (2001), doi:10.1056/NEJM200103153441103.
23. C. A. Whitehouse, Crimean-Congo hemorrhagic fever. *Antiviral research*. **64**, 145–160 (2004), doi:10.1016/j.antiviral.2004.08.001.
24. J. P. Messina *et al.*, The global distribution of Crimean-Congo hemorrhagic fever. *Transactions of the Royal Society of Tropical Medicine and Hygiene*. **109**, 503–513 (2015), doi:10.1093/trstmh/trv050.
25. J. R. Spengler, É. Bergeron, P. E. Rollin, Seroepidemiological Studies of Crimean-Congo Hemorrhagic Fever Virus in Domestic and Wild Animals. *PLoS*

- neglected tropical diseases*. **10**, e0004210 (2016), doi:10.1371/journal.pntd.0004210.
26. H. Nasirian, New aspects about Crimean-Congo hemorrhagic fever (CCHF) cases and associated fatality trends: A global systematic review and meta-analysis. *Comparative immunology, microbiology and infectious diseases*. **69**, 101429 (2020), doi:10.1016/j.cimid.2020.101429.
27. S. Liu *et al.*, Systematic review of severe fever with thrombocytopenia syndrome: virology, epidemiology, and clinical characteristics. *Reviews in medical virology*. **24**, 90–102 (2014), doi:10.1002/rmv.1776.
28. X.-Y. Lei, M.-M. Liu, X.-J. Yu, Severe fever with thrombocytopenia syndrome and its pathogen SFTSV. *Microbes and infection*. **17**, 149–154 (2015), doi:10.1016/j.micinf.2014.12.002.
29. E. J. Lefkowitz *et al.*, Virus taxonomy: the database of the International Committee on Taxonomy of Viruses (ICTV). *Nucleic acids research*. **46**, D708–D717 (2018), doi:10.1093/nar/gkx932.
30. J. Koch, Q. Xin, N. D. Tischler, P.-Y. Lozach, Entry of Phenuiviruses into Mammalian Host Cells. *Viruses*. **13** (2021), doi:10.3390/v13020299.
31. J. H. Kuhn *et al.*, 2020 taxonomic update for phylum Negarnaviricota (Riboviria: Orthornavirae), including the large orders Bunyavirales and Mononegavirales. *Archives of virology*. **165**, 3023–3072 (2020), doi:10.1007/s00705-020-04731-2.
32. D. Baltimore, Expression of animal virus genomes. *Bacteriological Reviews*. **35** (1971).
33. D. J. Gubler, The Global Emergence/Resurgence of Arboviral Diseases As Public Health Problems. *Archives of Medical Research*. **33**, 330–342 (2002), doi:10.1016/S0188-4409(02)00378-8.
34. A. El-Sayed, M. Kamel, Climatic changes and their role in emergence and re-emergence of diseases. *Environmental science and pollution research international*. **27**, 22336–22352 (2020), doi:10.1007/s11356-020-08896-w.
35. M.-M. Olive, S. M. Goodman, J.-M. Reynes, The role of wild mammals in the maintenance of Rift Valley fever virus. *Journal of wildlife diseases*. **48**, 241–266 (2012), doi:10.7589/0090-3558-48.2.241.
36. K. J. Linthicum, S. C. Britch, A. Anyamba, Rift Valley Fever: An Emerging Mosquito-Borne Disease. *Annual review of entomology*. **61**, 395–415 (2016), doi:10.1146/annurev-ento-010715-023819.
37. E. N. Grossi-Soyster, A. D. LaBeaud, Rift Valley Fever: Important Considerations for Risk Mitigation and Future Outbreaks. *Tropical medicine and infectious disease*. **5** (2020), doi:10.3390/tropicalmed5020089.

38. T. Ikegami, S. Makino, The pathogenesis of Rift Valley fever. *Viruses*. **3**, 493–519 (2011), doi:10.3390/v3050493.
39. M. O. Nanyingi *et al.*, A systematic review of Rift Valley Fever epidemiology 1931-2014. *Infection ecology & epidemiology*. **5**, 28024 (2015), doi:10.3402/iee.v5.28024.
40. M. H. A. Clark, G. M. Warimwe, A. Di Nardo, N. A. Lyons, S. Gubbins, Systematic literature review of Rift Valley fever virus seroprevalence in livestock, wildlife and humans in Africa from 1968 to 2016. *PLoS neglected tropical diseases*. **12**, e0006627 (2018), doi:10.1371/journal.pntd.0006627.
41. C. Terrosi, R. Olivieri, C. Bianco, C. Cellesi, M. G. Cusi, Age-dependent seroprevalence of Toscana virus in central Italy and correlation with the clinical profile. *Clinical and vaccine immunology : CVI*. **16**, 1251–1252 (2009), doi:10.1128/CVI.00376-08.
42. O. Fezaa, O. Bahri, N. B. Alaya Bouafif, H. Triki, A. Bouattour, Seroprevalence of Toscana virus infection in Tunisia. *International journal of infectious diseases : IJID : official publication of the International Society for Infectious Diseases*. **17**, e1172-5 (2013), doi:10.1016/j.ijid.2013.08.008.
43. S. Marchi, C. M. Trombetta, O. Kistner, E. Montomoli, Seroprevalence study of Toscana virus and viruses belonging to the Sandfly fever Naples antigenic complex in central and southern Italy. *Journal of infection and public health*. **10**, 866–869 (2017), doi:10.1016/j.jiph.2017.02.001.
44. M. E. Remoli *et al.*, Seroprevalence survey of arboviruses in workers from Tuscany, Italy. *La Medicina del lavoro*. **109**, 125–131 (2018), doi:10.23749/mdl.v109i2.5024.
45. A. Braitto *et al.*, Phlebotomus-transmitted toscana virus infections of the central nervous system: a seven-year experience in Tuscany. *Scandinavian journal of infectious diseases*. **30**, 505–508 (1998), doi:10.1080/00365549850161539.
46. R. N. Charrel, L. Bichaud, X. de Lamballerie, Emergence of Toscana virus in the mediterranean area. *World journal of virology*. **1**, 135–141 (2012), doi:10.5501/wjv.v1.i5.135.
47. H. M. Kolman JM, Antibodies against the tick-borne encephalitis and the Uukuniemi viruses in small mammals in a mixed natural focus of diseases. *Folia Parasitol*. **19**, 61–66 (1972).
48. M. Gondard *et al.*, Prevalence of tick-borne viruses in Ixodes ricinus assessed by high-throughput real-time PCR. *Pathogens and disease*. **76** (2018), doi:10.1093/femspd/fty083.

49. A. Petersen *et al.*, Field samplings of *Ixodes ricinus* ticks from a tick-borne encephalitis virus micro-focus in Northern Zealand, Denmark. *Ticks and tick-borne diseases*. **10**, 1028–1032 (2019), doi:10.1016/j.ttbdis.2019.05.005.
50. Z. Hubálek, I. Rudolf, Tick-borne viruses in Europe. *Parasitology research*. **111**, 9–36 (2012), doi:10.1007/s00436-012-2910-1.
51. A. Papa, H. Zelená, E. Papadopoulou, J. Mrázek, Uukuniemi virus, Czech Republic. *Ticks and tick-borne diseases*. **9**, 1129–1132 (2018), doi:10.1016/j.ttbdis.2018.04.011.
52. P.-Y. Lozach *et al.*, DC-SIGN as a receptor for phleboviruses. *Cell host & microbe*. **10**, 75–88 (2011), doi:10.1016/j.chom.2011.06.007.
53. P. Léger *et al.*, Differential Use of the C-Type Lectins L-SIGN and DC-SIGN for Phlebovirus Endocytosis. *Traffic (Copenhagen, Denmark)*. **17**, 639–656 (2016), doi:10.1111/tra.12393.
54. P. Överby, Insights into bunyavirus architecture from electron cryotomography of Uukuniemi virus. *PNAS* (2008).
55. A. N. Freiberg, M. B. Sherman, M. C. Morais, M. R. Holbrook, S. J. Watowich, Three-dimensional organization of Rift Valley fever virus revealed by cryoelectron tomography. *Journal of virology*. **82**, 10341–10348 (2008), doi:10.1128/JVI.01191-08.
56. S. Won, T. Ikegami, C. J. Peters, S. Makino, NSm protein of Rift Valley fever virus suppresses virus-induced apoptosis. *Journal of virology*. **81**, 13335–13345 (2007), doi:10.1128/JVI.01238-07.
57. S. R. Gerrard, B. H. Bird, C. G. Albariño, S. T. Nichol, The NSm proteins of Rift Valley fever virus are dispensable for maturation, replication and infection. *Virology*. **359**, 459–465 (2007), doi:10.1016/j.virol.2006.09.035.
58. Y. Sun, J. Li, G. F. Gao, P. Tien, W. Liu, Bunyavirales ribonucleoproteins: the viral replication and transcription machinery. *Critical reviews in microbiology*. **44**, 522–540 (2018), doi:10.1080/1040841X.2018.1446901.
59. P. Léger *et al.*, NSs amyloid formation is associated with the virulence of Rift Valley fever virus in mice. *Nature communications*. **11**, 3281 (2020), doi:10.1038/s41467-020-17101-y.
60. H. J. Ly, T. Ikegami, Rift Valley fever virus NSs protein functions and the similarity to other bunyavirus NSs proteins. *Virology journal*. **13**, 118 (2016), doi:10.1186/s12985-016-0573-8.
61. J. D. Wuerth, F. Weber, Phleboviruses and the Type I Interferon Response. *Viruses*. **8** (2016), doi:10.3390/v8060174.

62. J. D. Wuerth, F. Weber, NSs of the mildly virulent sandfly fever Sicilian virus is unable to inhibit interferon signaling and upregulation of interferon-stimulated genes. *The Journal of general virology*. **102** (2021), doi:10.1099/jgv.0.001676.
63. Z. M. Uckeley, J. Koch, N. D. Tischler, P. Léger, P.-Y. Lozach, Cell biology of phlebovirus entry. *Virologie (Montrouge, France)*. **23**, 176–187 (2019), doi:10.1684/vir.2019.0780.
64. P.-Y. Lozach *et al.*, Entry of bunyaviruses into mammalian cells. *Cell host & microbe*. **7**, 488–499 (2010), doi:10.1016/j.chom.2010.05.007.
65. U.-S. Khoo, K. Y. K. Chan, V. S. F. Chan, C. L. S. Lin, DC-SIGN and L-SIGN: the SIGNs for infection. *Journal of molecular medicine (Berlin, Germany)*. **86**, 861–874 (2008), doi:10.1007/s00109-008-0350-2.
66. A. A. Bashirova *et al.*, A dendritic cell-specific intercellular adhesion molecule 3-grabbing nonintegrin (DC-SIGN)-related protein is highly expressed on human liver sinusoidal endothelial cells and promotes HIV-1 infection. *The Journal of experimental medicine*. **193**, 671–678 (2001), doi:10.1084/jem.193.6.671.
67. S. M. de Boer *et al.*, Heparan sulfate facilitates Rift Valley fever virus entry into the cell. *Journal of virology*. **86**, 13767–13771 (2012), doi:10.1128/JVI.01364-12.
68. A. M. Riblett *et al.*, A Haploid Genetic Screen Identifies Heparan Sulfate Proteoglycans Supporting Rift Valley Fever Virus Infection. *Journal of virology*. **90**, 1414–1423 (2016), doi:10.1128/JVI.02055-15.
69. A. Pietrantoni, C. Fortuna, M. E. Remoli, M. G. Ciufolini, F. Superti, Bovine lactoferrin inhibits Toscana virus infection by binding to heparan sulphate. *Viruses*. **7**, 480–495 (2015), doi:10.3390/v7020480.
70. S. S. Ganaie *et al.*, Lrp1 is a host entry factor for Rift Valley fever virus. *Cell*. **184**, 5163-5178.e24 (2021), doi:10.1016/j.cell.2021.09.001.
71. H. Hofmann *et al.*, Severe Fever with Thrombocytopenia Virus Glycoproteins Are Targeted by Neutralizing Antibodies and Can Use DC-SIGN as a Receptor for pH-Dependent Entry into Human and Animal Cell Lines. *Journal of virology*. **87** (2013), doi:10.1128/JVI.02628-12.
72. J. Liu *et al.*, Single-Particle Tracking Reveals the Sequential Entry Process of the Bunyavirus Severe Fever with Thrombocytopenia Syndrome Virus. *Small*. **15**, e1803788 (2019), doi:10.1002/sml.201803788.
73. B. Harmon *et al.*, Rift Valley fever virus strain MP-12 enters mammalian host cells via caveola-mediated endocytosis. *Journal of virology*. **86**, 12954–12970 (2012), doi:10.1128/JVI.02242-12.

74. C. M. Filone *et al.*, Rift valley fever virus infection of human cells and insect hosts is promoted by protein kinase C epsilon. *PLoS one*. **5**, e15483 (2010), doi:10.1371/journal.pone.0015483.
75. C. C. Scott, J. Gruenberg, Ion flux and the function of endosomes and lysosomes: pH is just the start: the flux of ions across endosomal membranes influences endosome function not only through regulation of the luminal pH. *BioEssays : news and reviews in molecular, cellular and developmental biology*. **33**, 103–110 (2011), doi:10.1002/bies.201000108.
76. J. M. White, G. R. Whittaker, Fusion of Enveloped Viruses in Endosomes. *Traffic (Copenhagen, Denmark)*. **17**, 593–614 (2016), doi:10.1111/tra.12389.
77. A. Albornoz, A. B. Hoffmann, P.-Y. Lozach, N. D. Tischler, Early Bunyavirus-Host Cell Interactions. *Viruses*. **8** (2016), doi:10.3390/v8050143.
78. S. M. de Boer *et al.*, Acid-activated structural reorganization of the Rift Valley fever virus Gc fusion protein. *Journal of virology*. **86**, 13642–13652 (2012), doi:10.1128/JVI.01973-12.
79. P. Guardado-Calvo, F. A. Rey, The Envelope Proteins of the Bunyavirales. *Advances in virus research*. **98**, 83–118 (2017), doi:10.1016/bs.aivir.2017.02.002.
80. H. Jin, R. M. Elliott, Non-viral sequences at the 5' ends of Dugbe nairovirus S mRNAs. *The Journal of general virology*. **74**, 2293–2297 (1993), doi:10.1099/0022-1317-74-10-2293.
81. C. Prehaud, N. Lopez, M. J. Blok, V. Obry, M. Bouloy, Analysis of the 3' terminal sequence recognized by the Rift Valley fever virus transcription complex in its ambisense S segment. *Virology*. **227**, 189–197 (1997), doi:10.1006/viro.1996.8324.
82. J. Jääntti *et al.*, Immunocytochemical analysis of Uukuniemi virus budding compartments: role of the intermediate compartment and the Golgi stack in virus maturation. *Journal of virology*. **71**, 1162–1172 (1997), doi:10.1128/JVI.71.2.1162-1172.1997.
83. A. K. Overby, V. Popov, E. P. A. Neve, R. F. Pettersson, Generation and analysis of infectious virus-like particles of uukuniemi virus (bunyaviridae): a useful system for studying bunyaviral packaging and budding. *Journal of virology*. **80**, 10428–10435 (2006), doi:10.1128/JVI.01362-06.
84. M. Spiegel, T. Plegge, S. Pöhlmann, The Role of Phlebovirus Glycoproteins in Viral Entry, Assembly and Release. *Viruses*. **8** (2016), doi:10.3390/v8070202.
85. J. Huotari, A. Helenius, Endosome maturation. *The EMBO journal*. **30**, 3481–3500 (2011), doi:10.1038/emboj.2011.286.

86. R. Meier *et al.*, Genome-wide small interfering RNA screens reveal VAMP3 as a novel host factor required for Uukuniemi virus late penetration. *Journal of virology*. **88**, 8565–8578 (2014), doi:10.1128/JVI.00388-14.
87. A. Hoffmann, PhD thesis, University Hospital Heidelberg (2020).
88. J. Ferlin *et al.*, Investigation of the role of GBF1 in the replication of positive-sense single-stranded RNA viruses. *The Journal of general virology*. **99**, 1086–1096 (2018), doi:10.1099/jgv.0.001099.
89. L. Goueslain *et al.*, Identification of GBF1 as a cellular factor required for hepatitis C virus RNA replication. *Journal of virology*. **84**, 773–787 (2010), doi:10.1128/JVI.01190-09.
90. N. G. Iglesias *et al.*, Dengue Virus Uses a Non-Canonical Function of the Host GBF1-Arf-COPI System for Capsid Protein Accumulation on Lipid Droplets. *Traffic (Copenhagen, Denmark)*. **16**, 962–977 (2015), doi:10.1111/tra.12305.
91. B. Kaczmarek, J.-M. Verbavatz, C. L. Jackson, GBF1 and Arf1 function in vesicular trafficking, lipid homeostasis and organelle dynamics. *Biology of the cell*. **109**, 391–399 (2017), doi:10.1111/boc.201700042.
92. K. H. W. Lanke *et al.*, GBF1, a guanine nucleotide exchange factor for Arf, is crucial for coxsackievirus B3 RNA replication. *Journal of virology*. **83**, 11940–11949 (2009), doi:10.1128/JVI.01244-09.
93. R. Farhat *et al.*, Identification of GBF1 as a cellular factor required for hepatitis E virus RNA replication. *Cellular Microbiology*. **20** (2018), doi:10.1111/cmi.12804.
94. G. A. Belov *et al.*, Hijacking components of the cellular secretory pathway for replication of poliovirus RNA. *Journal of virology*. **81**, 558–567 (2007), doi:10.1128/JVI.01820-06.
95. G. A. Belov, G. Kovtunovych, C. L. Jackson, E. Ehrenfeld, Poliovirus replication requires the N-terminus but not the catalytic Sec7 domain of ArfGEF GBF1. *Cellular Microbiology*. **12**, 1463–1479 (2010), doi:10.1111/j.1462-5822.2010.01482.x.
96. S. Boulant, M. Stanifer, P.-Y. Lozach, Dynamics of virus-receptor interactions in virus binding, signaling, and endocytosis. *Viruses*. **7**, 2794–2815 (2015), doi:10.3390/v7062747.
97. M. Schelhaas, Come in and take your coat off - how host cells provide endocytosis for virus entry. *Cellular Microbiology*. **12**, 1378–1388 (2010), doi:10.1111/j.1462-5822.2010.01510.x.
98. D. Walsh, I. Mohr, Viral subversion of the host protein synthesis machinery. *Nature reviews. Microbiology*. **9**, 860–875 (2011), doi:10.1038/nrmicro2655.

99. N. S. Heaton, G. Randall, Multifaceted roles for lipids in viral infection. *Trends in microbiology*. **19**, 368–375 (2011), doi:10.1016/j.tim.2011.03.007.
100. I. Fernández de Castro, R. Tenorio, C. Risco, Virus assembly factories in a lipid world. *Current opinion in virology*. **18**, 20–26 (2016), doi:10.1016/j.coviro.2016.02.009.
101. B. Tsai *et al.*, Gangliosides are receptors for murine polyoma virus and SV40. *The EMBO journal*. **22**, 4346–4355 (2003), doi:10.1093/emboj/cdg439.
102. J. A. Low, B. Magnuson, B. Tsai, M. J. Imperiale, Identification of gangliosides GD1b and GT1b as receptors for BK virus. *Journal of virology*. **80**, 1361–1366 (2006), doi:10.1128/JVI.80.3.1361-1366.2006.
103. P. Scheiffele, M. G. Roth, K. Simons, Interaction of influenza virus haemagglutinin with sphingolipid-cholesterol membrane domains via its transmembrane domain. *The EMBO journal*. **16**, 5501–5508 (1997), doi:10.1093/emboj/16.18.5501.
104. J. Lee *et al.*, Ebola virus glycoprotein interacts with cholesterol to enhance membrane fusion and cell entry. *Nature structural & molecular biology*. **28**, 181–189 (2021), doi:10.1038/s41594-020-00548-4.
105. X. Li *et al.*, Dependence of SARS-CoV-2 infection on cholesterol-rich lipid raft and endosomal acidification. *Computational and structural biotechnology journal*. **19**, 1933–1943 (2021), doi:10.1016/j.csbj.2021.04.001.
106. Z. Liao, D. R. Graham, J. E. K. Hildreth, Lipid rafts and HIV pathogenesis: virion-associated cholesterol is required for fusion and infection of susceptible cells. *AIDS research and human retroviruses*. **19**, 675–687 (2003), doi:10.1089/088922203322280900.
107. Z. Liao, L. M. Cimasky, R. Hampton, D. H. Nguyen, J. E. Hildreth, Lipid rafts and HIV pathogenesis: host membrane cholesterol is required for infection by HIV type 1. *AIDS research and human retroviruses*. **17**, 1009–1019 (2001), doi:10.1089/088922201300343690.
108. G. C. Carter *et al.*, HIV entry in macrophages is dependent on intact lipid rafts. *Virology*. **386**, 192–202 (2009), doi:10.1016/j.virol.2008.12.031.
109. P. Guardado-Calvo *et al.*, A glycerophospholipid-specific pocket in the RVFV class II fusion protein drives target membrane insertion. *Science (New York, N.Y.)*. **358**, 663–667 (2017), doi:10.1126/science.aal2712.
110. D. Bitto, S. Halldorsson, A. Caputo, J. T. Huiskonen, Low pH and Anionic Lipid-dependent Fusion of Uukuniemi Phlebovirus to Liposomes. *The Journal of biological chemistry*. **291**, 6412–6422 (2016), doi:10.1074/jbc.M115.691113.

111. M. K. Callahan *et al.*, Phosphatidylserine on HIV envelope is a cofactor for infection of monocytic cells. *Journal of immunology (Baltimore, Md. : 1950)*. **170**, 4840–4845 (2003), doi:10.4049/jimmunol.170.9.4840.
112. L. Meertens *et al.*, The TIM and TAM families of phosphatidylserine receptors mediate dengue virus entry. *Cell host & microbe*. **12**, 544–557 (2012), doi:10.1016/j.chom.2012.08.009.
113. S. Moller-Tank, A. S. Kondratowicz, R. A. Davey, P. D. Rennert, W. Maury, Role of the phosphatidylserine receptor TIM-1 in enveloped-virus entry. *Journal of virology*. **87**, 8327–8341 (2013), doi:10.1128/JVI.01025-13.
114. S. Jemielity *et al.*, TIM-family proteins promote infection of multiple enveloped viruses through virion-associated phosphatidylserine. *PLoS pathogens*. **9**, e1003232 (2013), doi:10.1371/journal.ppat.1003232.
115. J. Kirui *et al.*, The Phosphatidylserine Receptor TIM-1 Enhances Authentic Chikungunya Virus Cell Entry. *Cells*. **10** (2021), doi:10.3390/cells10071828.
116. E. J. Patzer, R. R. Wagner, E. J. Dubovi, Viral membranes: model systems for studying biological membranes. *CRC critical reviews in biochemistry*. **6**, 165–217 (1979), doi:10.3109/10409237909102563.
117. K. Simons, G. Warren, Semliki Forest Virus: A Probe for Membrane Traffic in the Animal Cell. *Advances in Protein Chemistry*. **36**, 79–132 (1984), doi:10.1016/S0065-3233(08)60296-X.
118. L. Kalvodova *et al.*, The lipidomes of vesicular stomatitis virus, semliki forest virus, and the host plasma membrane analyzed by quantitative shotgun mass spectrometry. *Journal of virology*. **83**, 7996–8003 (2009), doi:10.1128/JVI.00635-09.
119. Y. Ichihashi, M. Oie, The activation of vaccinia virus infectivity by the transfer of phosphatidylserine from the plasma membrane. *Virology*. **130**, 306–317 (1983), doi:10.1016/0042-6822(83)90085-5.
120. S. T. H. Liu *et al.*, Synaptic vesicle-like lipidome of human cytomegalovirus virions reveals a role for SNARE machinery in virion egress. *Proceedings of the National Academy of Sciences of the United States of America*. **108**, 12869–12874 (2011), doi:10.1073/pnas.1109796108.
121. M. J. Gerl *et al.*, Quantitative analysis of the lipidomes of the influenza virus envelope and MDCK cell apical membrane. *The Journal of cell biology*. **196**, 213–221 (2012), doi:10.1083/jcb.201108175.
122. F. Mücksch *et al.*, Quantification of phosphoinositides reveals strong enrichment of PIP2 in HIV-1 compared to producer cell membranes. *Scientific reports*. **9**, 17661 (2019), doi:10.1038/s41598-019-53939-z.

123. F. Mücksch, V. Laketa, B. Müller, C. Schultz, H.-G. Kräusslich, Synchronized HIV assembly by tunable PIP2 changes reveals PIP2 requirement for stable Gag anchoring. *eLife*. **6** (2017), doi:10.7554/eLife.25287.
124. Y. Wen, G. W. Feigenson, V. M. Vogt, R. A. Dick, Mechanisms of PI(4,5)P2 Enrichment in HIV-1 Viral Membranes. *Journal of molecular biology*. **432**, 5343–5364 (2020), doi:10.1016/j.jmb.2020.07.018.
125. E. Fahy, D. Cotter, M. Sud, S. Subramaniam, Lipid classification, structures and tools. *Biochimica et biophysica acta*. **1811**, 637–647 (2011), doi:10.1016/j.bbaliip.2011.06.009.
126. G. van Meer, D. R. Voelker, G. W. Feigenson, Membrane lipids: where they are and how they behave. *Nature reviews. Molecular cell biology*. **9**, 112–124 (2008), doi:10.1038/nrm2330.
127. T. Harayama, H. Riezman, Understanding the diversity of membrane lipid composition. *Nature reviews. Molecular cell biology*. **19**, 281–296 (2018), doi:10.1038/nrm.2017.138.
128. J. Huang, G. W. Feigenson, A Microscopic Interaction Model of Maximum Solubility of Cholesterol in Lipid Bilayers. *Biophysical Journal*. **76**, 2142–2157 (1999), doi:10.1016/S0006-3495(99)77369-8.
129. G. van Meer, A. I. P. M. de Kroon, Lipid map of the mammalian cell. *Journal of cell science*. **124**, 5–8 (2011), doi:10.1242/jcs.071233.
130. A. H. Futerman, H. Riezman, The ins and outs of sphingolipid synthesis. *Trends in Cell Biology*. **15**, 312–318 (2005), doi:10.1016/j.tcb.2005.04.006.
131. C. A. Lingwood, Glycosphingolipid functions. *Cold Spring Harbor perspectives in biology*. **3** (2011), doi:10.1101/cshperspect.a004788.
132. A. Varki, Biological Roles of Glycans. *Glycobiology*. **27**, 3–49 (2017), doi:10.1093/glycob/cww086.
133. K. N. Burger, P. van der Bijl, G. van Meer, Topology of sphingolipid galactosyltransferases in ER and Golgi: transbilayer movement of monohexosyl sphingolipids is required for higher glycosphingolipid biosynthesis. *The Journal of cell biology*. **133**, 15–28 (1996), doi:10.1083/jcb.133.1.15.
134. S. Basu, B. Kaufman, S. Roseman, Enzymatic Synthesis of Ceramide-Glucose and Ceramide-Lactose by Glycosyltransferases from Embryonic Chicken Brain. *Journal of Biological Chemistry*. **243**, 5802–5804 (1968), doi:10.1016/S0021-9258(18)91935-6.
135. H. Schulze, T. Kolter, K. Sandhoff, Principles of lysosomal membrane degradation: Cellular topology and biochemistry of lysosomal lipid degradation.

- Biochimica et biophysica acta.* **1793**, 674–683 (2009), doi:10.1016/j.bbamcr.2008.09.020.
136. Y. Ishibashi, A. Kohyama-Koganeya, Y. Hirabayashi, New insights on glucosylated lipids: metabolism and functions. *Biochimica et biophysica acta.* **1831**, 1475–1485 (2013), doi:10.1016/j.bbalip.2013.06.001.
137. N. Stahl, H. Jurevics, P. Morell, K. Suzuki, B. Popko, Isolation, characterization, and expression of cDNA clones that encode rat UDP-galactose: ceramide galactosyltransferase. *Journal of neuroscience research.* **38**, 234–242 (1994), doi:10.1002/jnr.490380214.
138. S. Ichikawa, Y. Hirabayashi, Glucosylceramide synthase and glycosphingolipid synthesis. *Trends in Cell Biology.* **8**, 198–202 (1998), doi:10.1016/S0962-8924(98)01249-5.
139. D. J. Sillence *et al.*, Glucosylceramide modulates membrane traffic along the endocytic pathway. *Journal of lipid research.* **43**, 1837–1845 (2002), doi:10.1194/jlr.m200232-jlr200.
140. K. Drews *et al.*, Glucosylceramidase Maintains Influenza Virus Infection by Regulating Endocytosis. *Journal of virology.* **93** (2019), doi:10.1128/JVI.00017-19.
141. K. Drews *et al.*, Glucosylceramide synthase maintains influenza virus entry and infection. *PLoS one.* **15**, e0228735 (2020), doi:10.1371/journal.pone.0228735.
142. E. B. Vitner *et al.*, Glucosylceramide synthase inhibitors prevent replication of SARS-CoV-2 and influenza virus. *The Journal of biological chemistry.* **296**, 100470 (2021), doi:10.1016/j.jbc.2021.100470.
143. M. J. Drake *et al.*, A role for glycolipid biosynthesis in severe fever with thrombocytopenia syndrome virus entry. *PLoS pathogens.* **13**, e1006316 (2017), doi:10.1371/journal.ppat.1006316.
144. R. L. Bratton, G. R. Corey, Tick-borne disease. *Am Fam Physician.* **71**, 800–802 (2005), doi:10.1093/med/9780190888367.003.0117.
145. S. E. Randolph, Tick-borne disease systems. *Rev sci tech Off int Epiz.* **27** (2008).
146. J. Shi, Z. Hu, F. Deng, S. Shen, Tick-Borne Viruses. *Virologica Sinica.* **33**, 21–43 (2018), doi:10.1007/s12250-018-0019-0.
147. L. Bell-Sakyi, E. Zwegarth, E. F. Blouin, E. A. Gould, F. Jongejan, Tick cell lines: tools for tick and tick-borne disease research. *Trends in parasitology.* **23**, 450–457 (2007), doi:10.1016/j.pt.2007.07.009.

148. L. Bell-Sakyi, A. Darby, M. Baylis, B. L. Makepeace, The Tick Cell Biobank: A global resource for in vitro research on ticks, other arthropods and the pathogens they transmit. *Ticks and tick-borne diseases*. **9**, 1364–1371 (2018), doi:10.1016/j.ttbdis.2018.05.015.
149. A. Al-Rofaai, L. Bell-Sakyi, Tick Cell Lines in Research on Tick Control. *Frontiers in physiology*. **11**, 152 (2020), doi:10.3389/fphys.2020.00152.
150. M. Mazelier *et al.*, Uukuniemi Virus as a Tick-Borne Virus Model. *Journal of virology*. **90**, 6784–6798 (2016), doi:10.1128/JVI.00095-16.
151. M. Crispin *et al.*, Uukuniemi Phlebovirus assembly and secretion leave a functional imprint on the virion glycome. *Journal of virology*. **88**, 10244–10251 (2014), doi:10.1128/JVI.01662-14.
152. A. K. Overby, R. F. Pettersson, E. P. A. Neve, The glycoprotein cytoplasmic tail of Uukuniemi virus (Bunyaviridae) interacts with ribonucleoproteins and is critical for genome packaging. *Journal of virology*. **81**, 3198–3205 (2007), doi:10.1128/JVI.02655-06.
153. C. H. von Bonsdorff, R. Pettersson, Surface structure of Uukuniemi virus. *Journal of virology*. **16** (1975).
154. J. Koch *et al.*, TMPRSS2 expression dictates the entry route used by SARS-CoV-2 to infect host cells. *The EMBO journal*. **40**, e107821 (2021), doi:10.15252/embj.2021107821.
155. B. Brügger, Lipidomics: analysis of the lipid composition of cells and subcellular organelles by electrospray ionization mass spectrometry. *Annual review of biochemistry*. **83**, 79–98 (2014), doi:10.1146/annurev-biochem-060713-035324.
156. A. Hoffmann, M. Mazelier, P. Leger, P.-Y. Lozach, Deciphering Virus Entry with Fluorescently Labeled Viral Particles. *Methods in Molecular Biology*. **1836**, 159–183 (2018), doi:10.1007/978-1-4939-8678-1_8.
157. V. M. Vaughn, C. C. Streeter, D. J. Miller, S. R. Gerrard, Restriction of rift valley Fever virus virulence in mosquito cells. *Viruses*. **2**, 655–675 (2010), doi:10.3390/v2020655.
158. S. E. Newton, N. J. Short, L. Dalgarno, Bunyamwera Virus Replication in Cultured *Aedes albopictus* (Mosquito) Cells: Establishment of a Persistent Viral Infection. *Am Soc Microbiol*. **38**, 1015–1024 (1981), doi:10.1128/jvi.38.3.1015-1024.1981.
159. S. Sim, G. Dimopoulos, Dengue virus inhibits immune responses in *Aedes aegypti* cells. *PloS one*. **5**, e10678 (2010), doi:10.1371/journal.pone.0010678.

160. J. T. Huiskonen, A. K. Overby, F. Weber, K. Grunewald, Electron cryo-microscopy and single-particle averaging of Rift Valley fever virus: evidence for GN-GC glycoprotein heterodimers. *Journal of virology*. **83**, 3762–3769 (2009), doi:10.1128/JVI.02483-08.
161. M. B. Sherman, A. N. Freiberg, M. R. Holbrook, S. J. Watowich, Single-particle cryo-electron microscopy of Rift Valley fever virus. *Virology*. **387**, 11–15 (2009), doi:10.1016/j.virol.2009.02.038.
162. J. Cox *et al.*, Accurate proteome-wide label-free quantification by delayed normalization and maximal peptide ratio extraction, termed MaxLFQ. *Molecular & cellular proteomics : MCP*. **13**, 2513–2526 (2014), doi:10.1074/mcp.M113.031591.
163. Z. M. Uckelely *et al.*, Quantitative Proteomics of Uukuniemi Virus-host Cell Interactions Reveals GBF1 as Proviral Host Factor for Phleboviruses. *Molecular & cellular proteomics : MCP*. **18**, 2401–2417 (2019), doi:10.1074/mcp.RA119.001631.
164. A. Abe *et al.*, Improved Inhibitors of Glucosylceramide Synthase. *J. Biochem*. **111**, 191–196 (1992), doi:10.1093/oxfordjournals.jbchem.a123736.
165. G. E. Atilla-Gokcumen, A. V. Bedigian, S. Sasse, U. S. Eggert, Inhibition of glycosphingolipid biosynthesis induces cytokinesis failure. *Journal of the American Chemical Society*. **133**, 10010–10013 (2011), doi:10.1021/ja202804b.
166. S. Alam, A. Fedier, R. S. Kohler, F. Jacob, Glucosylceramide synthase inhibitors differentially affect expression of glycosphingolipids. *Glycobiology*. **25**, 351–356 (2015), doi:10.1093/glycob/cwu187.
167. G. A. Grabowski, Phenotype, diagnosis, and treatment of Gaucher's disease. *The Lancet*. **372**, 1263–1271 (2008), doi:10.1016/S0140-6736(08)61522-6.
168. U. Andersson, T. D. Butters, R. A. Dwek, F. M. Platt, N-butyldeoxygalactonojirimycin: a more selective inhibitor of glycosphingolipid biosynthesis than N-butyldeoxynojirimycin, in vitro and in vivo. *Biochemical Pharmacology*. **59**, 821–829 (2000), doi:10.1016/S0006-2952(99)00384-6.
169. P. Alfonso *et al.*, Miglustat (NB-DNJ) works as a chaperone for mutated acid beta-glucosidase in cells transfected with several Gaucher disease mutations. *Blood cells, molecules & diseases*. **35**, 268–276 (2005), doi:10.1016/j.bcmd.2005.05.007.
170. M. Nagata *et al.*, Intracellular metabolite β -glucosylceramide is an endogenous Mincle ligand possessing immunostimulatory activity. *Proceedings of the National Academy of Sciences of the United States of America*. **114**, E3285–E3294 (2017), doi:10.1073/pnas.1618133114.

171. A. Helenius, J. Kartenbeck, K. Simons, E. Fries, On the entry of Semliki forest virus into BHK-21 cells. *Journal of Cell Biology*. **84**, 404–420 (1980), doi:10.1083/jcb.84.2.404.
172. E. Bermúdez-Méndez, E. A. Katrukha, C. M. Spruit, J. Kortekaas, P. J. Wichgers Schreur, Visualizing the ribonucleoprotein content of single bunyavirus virions reveals more efficient genome packaging in the arthropod host. *Communications biology*. **4**, 345 (2021), doi:10.1038/s42003-021-01821-y.
173. W. Schreur, Paul J., J. Kortekaas, Single-Molecule FISH Reveals Non-selective Packaging of Rift Valley Fever Virus Genome Segments. *PLoS pathogens*. **12**, e1005800 (2016), doi:10.1371/journal.ppat.1005800.
174. W. Schreur, J. Paul, R. Kormelink, J. Kortekaas, Genome packaging of the Bunyavirales. *Current opinion in virology*. **33**, 151–155 (2018), doi:10.1016/j.coviro.2018.08.011.
175. A. Arakelyan, W. Fitzgerald, L. Margolis, J.-C. Grivel, Nanoparticle-based flow virometry for the analysis of individual virions. *The Journal of clinical investigation*. **123**, 3716–3727 (2013), doi:10.1172/JCI67042.
176. R. Gaudin, N. S. Barteneva, Sorting of small infectious virus particles by flow virometry reveals distinct infectivity profiles. *Nature communications*. **6**, 6022 (2015), doi:10.1038/ncomms7022.
177. J. L. R. Zamora, H. C. Aguilar, Flow virometry as a tool to study viruses. *Methods (San Diego, Calif.)*. **134-135**, 87–97 (2018), doi:10.1016/j.ymeth.2017.12.011.
178. R. Lippé, Flow Virometry: a Powerful Tool To Functionally Characterize Viruses. *Journal of virology*. **92** (2018), doi:10.1128/JVI.01765-17.
179. Q. Niu *et al.*, Quantitative Assessment of the Physical Virus Titer and Purity by Ultrasensitive Flow Virometry. *Angewandte Chemie (International ed. in English)*. **60**, 9351–9356 (2021), doi:10.1002/anie.202100872.
180. M. Maltseva, M.-A. Langlois, Flow Virometry for Characterizing the Size, Concentration, and Surface Antigens of Viruses. *Current protocols*. **2**, e368 (2022), doi:10.1002/cpz1.368.
181. M. E. Piper, D. R. Sorenson, S. R. Gerrard, Efficient Cellular Release of Rift Valley Fever Virus Requires Genomic RNA. *PloS one*. **6** (2011), doi:10.1371/journal.pone.0018070.g001.
182. M. Bruns, S. Miska, S. Chassot, H. Will, Enhancement of Hepatitis B Virus Infection by Noninfectious Subviral Particles. *Journal of virology*. **72** (1998), doi:10.1007/s10479-021-04505-2.

183. N. Chai *et al.*, Properties of subviral particles of hepatitis B virus. *Journal of virology*. **82**, 7812–7817 (2008), doi:10.1128/JVI.00561-08.
184. A. Vaillant, HBsAg, Subviral Particles, and Their Clearance in Establishing a Functional Cure of Chronic Hepatitis B Virus Infection. *ACS infectious diseases*. **7**, 1351–1368 (2021), doi:10.1021/acsinfecdis.0c00638.
185. C. I. Real *et al.*, Hepatitis B virus genome replication triggers toll-like receptor 3-dependent interferon responses in the absence of hepatitis B surface antigen. *Scientific reports*. **6**, 24865 (2016), doi:10.1038/srep24865.
186. G. E. Rydell, K. Prakash, H. Norder, M. Lindh, Hepatitis B surface antigen on subviral particles reduces the neutralizing effect of anti-HBs antibodies on hepatitis B viral particles in vitro. *Virology*. **509**, 67–70 (2017), doi:10.1016/j.virol.2017.05.017.
187. J. H. Kim *et al.*, Circulating serum HBsAg level is a biomarker for HBV-specific T and B cell responses in chronic hepatitis B patients. *Scientific reports*. **10**, 1835 (2020), doi:10.1038/s41598-020-58870-2.
188. N. Le Bert *et al.*, Effects of Hepatitis B Surface Antigen on Virus-Specific and Global T Cells in Patients With Chronic Hepatitis B Virus infection. *Gastroenterology*. **159**, 652–664 (2020), doi:10.1053/j.gastro.2020.04.019.
189. S. Reignat *et al.*, Escaping high viral load exhaustion: CD8 cells with altered tetramer binding in chronic hepatitis B virus infection. *The Journal of experimental medicine*. **195**, 1089–1101 (2002), doi:10.1084/jem.20011723.
190. O. Hajdušek *et al.*, Interaction of the tick immune system with transmitted pathogens. *Frontiers in cellular and infection microbiology*. **3**, 26 (2013), doi:10.3389/fcimb.2013.00026.
191. D. E. Sonenshine, W. L. Hynes, Molecular characterization and related aspects of the innate immune response in ticks. *Frontiers in bioscience : a journal and virtual library*. **13**, 7046–7063 (2008), doi:10.2741/3209.
192. M. J. Lehane, S. Aksoy, E. Levashina, Immune responses and parasite transmission in blood-feeding insects. *Trends in parasitology*. **20**, 433–439 (2004), doi:10.1016/j.pt.2004.07.002.
193. P. Kopáček, R. Vogt, L. Jindrák, C. Weise, I. Safarik, Purification and characterization of the lysozyme from the gut of the soft tick *Ornithodoros moubata*. *Insect Biochemistry and Molecular Biology*. **29**, 989–997 (1999), doi:10.1016/S0965-1748(99)00075-2.
194. Y. Nakajima, A. G. van Naters-Yasui, D. Taylor, M. Yamakawa, Two isoforms of a member of the arthropod defensin family from the soft tick, *Ornithodoros moubata* (Acari: Argasidae). *Insect Biochemistry and Molecular Biology*. **31**, 747–751 (2001), doi:10.1016/S0965-1748(01)00066-2.

195. L. S. Pereira, P. L. Oliveira, C. Barja-Fidalgo, S. Daffre, Production of reactive oxygen species by hemocytes from the cattle tick *Boophilus microplus*. *Experimental parasitology*. **99**, 66–72 (2001), doi:10.1006/expr.2001.4657.
196. M. G. Rittig *et al.*, Phagocytes from both vertebrate and invertebrate species use “coiling” phagocytosis. *Developmental & Comparative Immunology*. **20**, 393–406 (1996), doi:10.1016/S0145-305X(96)00023-7.
197. S. Kurscheid *et al.*, Evidence of a tick RNAi pathway by comparative genomics and reverse genetics screen of targets with known loss-of-function phenotypes in *Drosophila*. *BMC molecular biology*. **10**, 26 (2009), doi:10.1186/1471-2199-10-26.
198. E. Schnettler *et al.*, Induction and suppression of tick cell antiviral RNAi responses by tick-borne flaviviruses. *Nucleic acids research*. **42**, 9436–9446 (2014), doi:10.1093/nar/gku657.
199. A. C. Fogaça *et al.*, Tick Immune System: What Is Known, the Interconnections, the Gaps, and the Challenges. *Frontiers in immunology*. **12**, 628054 (2021), doi:10.3389/fimmu.2021.628054.
200. M. P. Alberdi *et al.*, Detection and identification of putative bacterial endosymbionts and endogenous viruses in tick cell lines. *Ticks and tick-borne diseases*. **3**, 137–146 (2012), doi:10.1016/j.ttbdis.2012.05.002.
201. L. Bell-Sakyi, H. Attoui, Endogenous tick viruses and modulation of tick-borne pathogen growth. *Frontiers in cellular and infection microbiology*. **3**, 25 (2013), doi:10.3389/fcimb.2013.00025.
202. H. Attoui *et al.*, Complete sequence characterization of the genome of the St Croix River virus, a new orbivirus isolated from cells of *Ixodes scapularis*. *The Journal of general virology*. **82**, 795–804 (2001), doi:10.1099/0022-1317-82-4-795.
203. J. Lee, K. R. Koehler, Skin organoids: A new human model for developmental and translational research. *Experimental dermatology*. **30**, 613–620 (2021), doi:10.1111/exd.14292.
204. J. D. Jones, H. E. Ramser, A. E. Woessner, K. P. Quinn, In vivo multiphoton microscopy detects longitudinal metabolic changes associated with delayed skin wound healing. *Communications biology*. **1**, 198 (2018), doi:10.1038/s42003-018-0206-4.
205. F. Helmchen, W. Denk, Deep tissue two-photon microscopy. *Nature methods*. **2**, 932–940 (2005), doi:10.1038/nmeth818.
206. S. V. Barrass, S. J. Butcher, Advances in high-throughput methods for the identification of virus receptors. *Medical microbiology and immunology*. **209**, 309–323 (2020), doi:10.1007/s00430-019-00653-2.

207. A. Salonen, T. Ahola, L. Kääriäinen, Viral RNA replication in association with cellular membranes. *Current topics in microbiology and immunology*. **285**, 139–173 (2005), doi:10.1007/3-540-26764-6_5.
208. S. Miller, J. Krijnse-Locker, Modification of intracellular membrane structures for virus replication. *Nature reviews. Microbiology*. **6**, 363–374 (2008), doi:10.1038/nrmicro1890.
209. E. Sun, J. He, X. Zhuang, Dissecting the role of COPI complexes in influenza virus infection. *Journal of virology*. **87**, 2673–2685 (2013), doi:10.1128/JVI.02277-12.
210. T. Watanabe *et al.*, Influenza virus-host interactome screen as a platform for antiviral drug development. *Cell host & microbe*. **16**, 795–805 (2014), doi:10.1016/j.chom.2014.11.002.
211. V. Yadav, A. T. Panganiban, K. Honer Zu Bentrup, T. G. Voss, Influenza infection modulates vesicular trafficking and induces Golgi complex disruption. *Virusdisease*. **27**, 357–368 (2016), doi:10.1007/s13337-016-0347-3.
212. E. Wessels *et al.*, Effects of picornavirus 3A Proteins on Protein Transport and GBF1-dependent COP-I recruitment. *Journal of virology*. **80**, 11852–11860 (2006), doi:10.1128/JVI.01225-06.
213. E. Wessels *et al.*, A viral protein that blocks Arf1-mediated COP-I assembly by inhibiting the guanine nucleotide exchange factor GBF1. *Developmental cell*. **11**, 191–201 (2006), doi:10.1016/j.devcel.2006.06.005.
214. V. Chukkapalli, N. S. Heaton, G. Randall, Lipids at the interface of virus-host interactions. *Current opinion in microbiology*. **15**, 512–518 (2012), doi:10.1016/j.mib.2012.05.013.
215. M. Mazzon, J. Mercer, Lipid interactions during virus entry and infection. *Cellular Microbiology*. **16**, 1493–1502 (2014), doi:10.1111/cmi.12340.
216. M. Lorizate, H.-G. Kräusslich, Role of lipids in virus replication. *Cold Spring Harbor perspectives in biology*. **3**, a004820 (2011), doi:10.1101/cshperspect.a004820.
217. E. Kuismanen, K. Hedman, J. Saraste, R. F. Pettersson, Uukuniemi virus maturation: accumulation of virus particles and viral antigens in the Golgi complex. *Molecular and cellular biology*. **2**, 1444–1458 (1982), doi:10.1128/mcb.2.11.1444-1458.1982.
218. J. F. Smith, D. Y. Pifat, Morphogenesis of sandfly fever viruses (Bunyaviridae family). *Virology*. **121**, 61–81 (1982), doi:10.1016/0042-6822(82)90118-0.

219. M. Jmoudiak, A. H. Futerman, Gaucher disease: pathological mechanisms and modern management. *British journal of haematology*. **129**, 178–188 (2005), doi:10.1111/j.1365-2141.2004.05351.x.
220. A. R. P. Varela *et al.*, Pathological levels of glucosylceramide change the biophysical properties of artificial and cell membranes. *Physical chemistry chemical physics : PCCP*. **19**, 340–346 (2016), doi:10.1039/c6cp07227e.
221. S. Reza, M. Ugorski, J. Suchański, Glucosylceramide and galactosylceramide, small glycosphingolipids with significant impact on health and disease. *Glycobiology*. **31**, 1416–1434 (2021), doi:10.1093/glycob/cwab046.
222. M. C. Messner, M. C. Cabot, Glucosylceramide in humans. *Advances in experimental medicine and biology*. **688**, 156–164 (2010), doi:10.1007/978-1-4419-6741-1_11.
223. J. S. Rossman, R. A. Lamb, Influenza virus assembly and budding. *Virology*. **411**, 229–236 (2011), doi:10.1016/j.virol.2010.12.003.
224. P.-Y. Lozach, J. Huotari, A. Helenius, Late-penetrating viruses. *Current opinion in virology*. **1**, 35–43 (2011), doi:10.1016/j.coviro.2011.05.004.
225. M. Hemmersbach-Miller, P. Parola, R. N. Charrel, J. Paul Durand, P. Brouqui, Sandfly fever due to Toscana virus: an emerging infection in southern France. *European journal of internal medicine*. **15**, 316–317 (2004), doi:10.1016/j.ejim.2004.05.006.
226. T. Vilibic-Cavlek *et al.*, Clinical, Virological, and Immunological Findings in Patients with Toscana Neuroinvasive Disease in Croatia: Report of Three Cases. *Tropical medicine and infectious disease*. **5** (2020), doi:10.3390/tropicalmed5030144.
227. G. Lemke, C. V. Rothlin, Immunobiology of the TAM receptors. *Nat Rev Immunol*. **8**, 327–336 (2008), doi:10.1038/nri2303.
228. G. J. Freeman, J. M. Casasnovas, D. T. Umetsu, R. H. Dekruyff, TIM genes: a family of cell surface phosphatidylserine receptors that regulate innate and adaptive immunity. *Immunological reviews*. **235**, 172–189 (2010), doi:10.1111/j.0105-2896.2010.00903.x.
229. K. S. Ravichandran, Beginnings of a good apoptotic meal: the find-me and eat-me signaling pathways. *Immunity*. **35**, 445–455 (2011), doi:10.1016/j.immuni.2011.09.004.
230. V. A. Fadok *et al.*, Exposure of phosphatidylserine on the surface of apoptotic lymphocytes triggers specific recognition and removal by macrophages. *Journal of immunology (Baltimore, Md. : 1950)*. **148**, 2207–2216 (1992).

231. E. M. Bevers, P. L. Williamson, Getting to the Outer Leaflet: Physiology of Phosphatidylserine Exposure at the Plasma Membrane. *Physiological reviews*. **96**, 605–645 (2016), doi:10.1152/physrev.00020.2015.
232. S. Bavari *et al.*, Lipid raft microdomains: a gateway for compartmentalized trafficking of Ebola and Marburg viruses. *The Journal of experimental medicine*. **195**, 593–602 (2002), doi:10.1084/jem.20011500.
233. D. Sancho, C. Reis e Sousa, Sensing of cell death by myeloid C-type lectin receptors. *Current opinion in immunology*. **25**, 46–52 (2013), doi:10.1016/j.coi.2012.12.007.
234. P.-Y. Lozach *et al.*, DC-SIGN and L-SIGN are high affinity binding receptors for hepatitis C virus glycoprotein E2. *The Journal of biological chemistry*. **278**, 20358–20366 (2003), doi:10.1074/jbc.M301284200.
235. S. Yamasaki *et al.*, Mincle is an ITAM-coupled activating receptor that senses damaged cells. *Nat Immunol*. **9**, 1179–1188 (2008), doi:10.1038/ni.1651.
236. J. T. Monteiro *et al.*, The CARD9-Associated C-Type Lectin, Mincle, Recognizes La Crosse Virus (LACV) but Plays a Limited Role in Early Antiviral Responses against LACV. *Viruses*. **11** (2019), doi:10.3390/v11030303.
237. K. Schön *et al.*, Vector and Host C-Type Lectin Receptor (CLR)–Fc Fusion Proteins as a Cross-Species Comparative Approach to Screen for CLR–Rift Valley Fever Virus Interactions. *IJMS*. **23**, 3243 (2022), doi:10.3390/ijms23063243.
238. C. G. Park *et al.*, Five mouse homologues of the human dendritic cell C-type lectin, DC-SIGN. *International Immunology*. **13** (2001), doi:10.1093/intimm/13.10.1283.
239. I. Caminschi *et al.*, Functional comparison of mouse CIRE/mouse DC-SIGN and human DC-SIGN. *International Immunology*. **18**, 741–753 (2006), doi:10.1093/intimm/dxl011.
240. E. A. Koppel, K. P. J. M. van Gisbergen, T. B. H. Geijtenbeek, Y. van Kooyk, Distinct functions of DC-SIGN and its homologues L-SIGN (DC-SIGNR) and mSIGNR1 in pathogen recognition and immune regulation. *Cellular Microbiology*. **7**, 157–165 (2005), doi:10.1111/j.1462-5822.2004.00480.x.
241. K. Takahara *et al.*, Functional comparison of the mouse DC-SIGN, SIGNR1, SIGNR3 and Langerin, C-type lectins. *International Immunology*. **16**, 819–829 (2004), doi:10.1093/intimm/dxh084.
242. Y.-S. Kang *et al.*, SIGN-R1, a novel C-type lectin expressed by marginal zone macrophages in spleen, mediates uptake of the polysaccharide dextran. *International Immunology*. **15**, 177–186 (2003), doi:10.1093/intimm/dxg019.

243. M. O'Keeffe *et al.*, Mouse plasmacytoid cells: long-lived cells, heterogeneous in surface phenotype and function, that differentiate into CD8(+) dendritic cells only after microbial stimulus. *The Journal of experimental medicine*. **196**, 1307–1319 (2002), doi:10.1084/jem.20021031.
244. M. Lieber, B. Smith, A. Szakal, W. Nelson-Rees, G. Todaro, A continuous tumor-cell line from a human lung carcinoma with properties of type II alveolar epithelial cells. *International journal of cancer*. **17**, 62–70 (1976), doi:10.1002/ijc.2910170110.
245. I. Macpherson, M. Stoker, Polyoma transformation of hamster cell clones - an investigation of genetic factors affecting cell competence. *Virology*. **16** (1962), doi:10.1016/0042-6822(62)90290-8.
246. G. Artigas *et al.*, Glycopeptides as Targets for Dendritic Cells: Exploring MUC1 Glycopeptides Binding Profile toward Macrophage Galactose-Type Lectin (MGL) Orthologs. *Journal of medicinal chemistry*. **60**, 9012–9021 (2017), doi:10.1021/acs.jmedchem.7b01242.
247. W. S. Pear, G. P. Nolan, M. L. Scott, D. Baltimore, Production of high-titer helper-free retroviruses by transient transfection. *Proc. Natl. Acad. Sci.* **90** (1993), doi:10.1073/pnas.90.18.8392.
248. B. Snijder *et al.*, Population context determines cell-to-cell variability in endocytosis and virus infection. *Nature*. **461**, 520–523 (2009), doi:10.1038/nature08282.
249. X. Wei *et al.*, Emergence of resistant human immunodeficiency virus type 1 in patients receiving fusion inhibitor (T-20) monotherapy. *Antimicrobial agents and chemotherapy*. **46**, 1896–1905 (2002), doi:10.1128/AAC.46.6.1896-1905.2002.
250. U. G. Munderloh, Y. Liu, M. Wang, C. Chen, T. J. Kurtti, Establishment, Maintenance and Description of Cell Lines from the Tick *Ixodes scapularis*. *The Journal of Parasitology*. **80**, 533 (1994), doi:10.2307/3283188.
251. P. J. Price, E. A. Gregory, Relationship between in vitro growth promotion and biophysical and biochemical properties of the serum supplement. *In Vitro*. **18** (1982), doi:10.1007/BF02810081.
252. F. Halary *et al.*, Human Cytomegalovirus Binding to DC-SIGN Is Required for Dendritic Cell Infection and Target Cell trans-Infection. *Immunity*. **17**, 653–664 (2002), doi:10.1016/S1074-7613(02)00447-8.
253. P. Léger *et al.*, Dicer-2- and Piwi-mediated RNA interference in Rift Valley fever virus-infected mosquito cells. *Journal of virology*. **87**, 1631–1648 (2013), doi:10.1128/JVI.02795-12.

254. M. Kielian, S. Jungerwirth, Sayad, K.U., S. DeCandido, Biosynthesis, maturation, and acid activation of the Semliki Forest virus fusion protein. *Journal of virology*. **64** (1990), doi:10.1128/jvi.64.10.4614-4624.1990.
255. R. Persson, R. E. Pettersson, Formation and Intracellular Transport of a Heterodimeric Viral Spike Protein Complex. *The Journal of cell biology*. **112** (1991), doi:10.1083/jcb.112.2.257.
256. J. Veijola, R. F. Pettersson, Transient association of calnexin and calreticulin with newly synthesized G1 and G2 glycoproteins of uukuniemi virus (family Bunyaviridae). *Journal of virology*. **73**, 6123–6127 (1999), doi:10.1128/JVI.73.7.6123-6127.1999.
257. L. W. Laughlin, J. M. Meegan, L. J. Strausbaugh, D. M. Morens, R. H. Watten, Epidemic Rift Valley fever in Egypt: observations of the spectrum of human illness. *Transactions of the Royal Society of Tropical Medicine and Hygiene*. **73**, 630–633 (1979), doi:10.1016/0035-9203(79)90006-3.
258. A. Billecocq *et al.*, RNA polymerase I-mediated expression of viral RNA for the rescue of infectious virulent and avirulent Rift Valley fever viruses. *Virology*. **378**, 377–384 (2008), doi:10.1016/j.virol.2008.05.033.
259. C. Giorgi *et al.*, Sequences and coding strategies of the S RNAs of Toscana and Rift Valley fever viruses compared to those of Punta Toro, Sicilian sandfly fever, and Uukuniemi viruses. *Virology*. **180**, 738–753 (1991), doi:10.1016/0042-6822(91)90087-R.
260. R. Pettersson, L. Kääriäinen, The ribonucleic acids of Uukuniemi virus, a noncubical tick-borne arbovirus. *Virology*. **56**, 608–619 (1973), doi:10.1016/0042-6822(73)90062-7.
261. Özbalci C., Sachsenheimer T., Brügger B., Quantitative Analysis of Cellular Lipids by Nano-Electrospray Ionization Mass Spectrometry. *Methods in Molecular Biology*. **1033** (2013), doi:10.1007/978-1-62703-487-6_1.
262. F. Paltauf, A. Hermetter, Strategies for the synthesis of glycerophospholipids. *Progress in lipid research*. **33**, 239–328 (1994), doi:10.1016/0163-7827(94)90028-0.
263. J. Schindelin *et al.*, Fiji: an open-source platform for biological-image analysis. *Nature methods*. **9**, 676–682 (2012), doi:10.1038/nmeth.2019.
264. C. A. Schneider, W. S. Rasband, K. W. Eliceiri, NIH Image to ImageJ: 25 years of image analysis. *Nature methods*. **9**, 671–675 (2012), doi:10.1038/nmeth.2089.
265. B. Stockinger, T. Zal, A. Zal, D. Gray, B Cells Solicit Their Own Help from T Cells. *J. Exp. Med*. **183** (1996), doi:10.1084/jem.183.3.891.

266. S. L. Winter, P. Chlanda, Dual-axis Volta phase plate cryo-electron tomography of Ebola virus-like particles reveals actin-VP40 interactions. *Journal of structural biology*. **213**, 107742 (2021), doi:10.1016/j.jsb.2021.107742.
267. T. G. Müller *et al.*, HIV-1 uncoating by release of viral cDNA from capsid-like structures in the nucleus of infected cells. *eLife*. **10** (2021), doi:10.7554/eLife.64776.
268. J. Bruening *et al.*, Hepatitis C virus enters liver cells using the CD81 receptor complex proteins calpain-5 and CBLB. *PLoS pathogens*. **14**, e1007111 (2018), doi:10.1371/journal.ppat.1007111.
269. C. Schneider, R. A. Newman, D. R. Sutherland, U. Asser, M. F. Greaves, A one-step purification of membrane proteins using a high efficiency immunomatrix. *Journal of Biological Chemistry*. **257**, 10766–10769 (1982), doi:10.1016/S0021-9258(18)33889-4.
270. G. Gerold *et al.*, Quantitative Proteomics Identifies Serum Response Factor Binding Protein 1 as a Host Factor for Hepatitis C Virus Entry. *Cell reports*. **12**, 864–878 (2015), doi:10.1016/j.celrep.2015.06.063.
271. A. G. Bunn, A dendrochronology program library in R (dplR). *Dendrochronologia*. **26**, 115–124 (2008), doi:10.1016/j.dendro.2008.01.002.
272. S. Tyanova *et al.*, The Perseus computational platform for comprehensive analysis of (prote)omics data. *Nature methods*. **13**, 731–740 (2016), doi:10.1038/nmeth.3901.
273. J. A. Vizcaíno *et al.*, ProteomeXchange provides globally coordinated proteomics data submission and dissemination. *Nature biotechnology*. **32**, 223–226 (2014), doi:10.1038/nbt.2839.
274. J. A. Vizcaíno *et al.*, 2016 update of the PRIDE database and its related tools. *Nucleic acids research*. **44**, 11033 (2016), doi:10.1093/nar/gkw880.
275. S. Orchard *et al.*, The MIntAct project--IntAct as a common curation platform for 11 molecular interaction databases. *Nucleic acids research*. **42**, D358-63 (2014), doi:10.1093/nar/gkt1115.
276. J. Cox *et al.*, Andromeda: a peptide search engine integrated into the MaxQuant environment. *Journal of proteome research*. **10**, 1794–1805 (2011), doi:10.1021/pr101065j.
277. V. G. Tusher, R. Tibshirani, G. Chu, Significance analysis of microarrays applied to the ionizing radiation response. *Proceedings of the National Academy of Sciences of the United States of America*. **98**, 5116–5121 (2001), doi:10.1073/pnas.091062498.

278. M. Magrane, UniProt Knowledgebase: a hub of integrated protein data. *Database : the journal of biological databases and curation*. **2011**, bar009 (2011), doi:10.1093/database/bar009.
279. R. P. Huntley *et al.*, The GOA database: gene Ontology annotation updates for 2015. *Nucleic acids research*. **43**, D1057-63 (2015), doi:10.1093/nar/gku1113.
280. M. Malek *et al.*, Inositol triphosphate-triggered calcium release blocks lipid exchange at endoplasmic reticulum-Golgi contact sites. *Nature communications*. **12**, 2673 (2021), doi:10.1038/s41467-021-22882-x.
281. E. G. Bligh, W. J. Dyer, A rapid method of total lipid extraction and purification. *Can J Biochem Physiol*. **37**, 911–917 (1959), doi:10.1139/o59-099.
282. G. Liebisch *et al.*, High throughput quantification of cholesterol and cholesteryl ester by electrospray ionization tandem mass spectrometry (ESI-MS/MS). *Biochimica et biophysica acta*. **1761**, 121–128 (2006), doi:10.1016/j.bbailip.2005.12.007.
283. M. Maglinao *et al.*, A platform to screen for C-type lectin receptor-binding carbohydrates and their potential for cell-specific targeting and immune modulation. *Journal of controlled release: official journal of the Controlled Release Society*. **175**, 36–42 (2014), doi:10.1016/j.jconrel.2013.12.011.
284. S. Mayer *et al.*, C-Type Lectin Receptor (CLR)-Fc Fusion Proteins As Tools to Screen for Novel CLR/Bacteria Interactions: An Exemplary Study on Preselected *Campylobacter jejuni* Isolates. *Frontiers in immunology*. **9**, 213 (2018), doi:10.3389/fimmu.2018.00213.